University of East Anglia

Targets for DNA-based antimicrobials in *Pseudomonas aeruginosa*

By

Sandeep Bahia

Submitted for the Degree of Doctor of Philosophy

in the

Faculty of Science

School of Pharmacy

2021

Abstract

The increasing prevalence of antibiotic resistance is a global issue driving the need for the identification of novel target sites and development of new antimicrobials, in particular for Gram-negative bacteria. Rapid and comprehensive sequencing of microbial pathogens has identified control of bacterial transcription as a source of these needed targets. Transcription factor decoys (TFDs) are short oligonucleotides that competitively inhibit the bacterial transcription factors controlling genes essential for infection. To facilitate the delivery of TFD a delivery molecule, 12-bis-THA, has been developed. An analogue of the quaternary ammonium cation dequalinium, 12-bis-THA has been shown cause membrane disruption in order to delivery TFDs intracellularly. As this disruption results in a stress response likely to be driven by changes in transcription factor (TF) expression, an investigation into detection of these changes using proteomics was explored. In this thesis a proteomic workflow was developed to enrich for the detection of changes in TF expression in response to high and low dose 12-bis-THA treatment, with an aim to identify potential TFD targets. Initial experimentation utilised the model organism *E. coli* NCTC_9001. Shortcomings highlighted in these experiments informed modification in the workflow for the bacterium of interest, *P. aeruginosa.* These experiments were successful at identifying changes in TFs expression between treatment conditions. Analysis of the data identified two potential TFD targets, the biofilm resistance locus regulator, BrlR and the alginate and motility regulator, AmrZ. TFDs were then designed to target these TFs and their efficacy explored. The developed proteomic workflow has great potential for application to other bacterial organisms and as a tool for identification of TFD targets and the future development of the novel antimicrobial strategy.

Table of Contents

Table of Figures

Table of Tables

List of Abbreviations

12-bis-THA	12,12'-(dodecane-1,12-diyl) bis(9-amino-1,2,3,4- tetrahydroacridinium)
APS	Ammonium Persulfate
ATP	Adenosine Triphosphate
BCA	Bicinchoninic acid
c-di-GMP	Cyclic di-GMP
CF	Cystic Fibrosis
CFTR	Cystic Fibrosis Transmembrane Conductance Regulator
cfu	Colony Forming Units
CL	Cardiolipin
CM	Cytoplasmic membrane
CV	Coefficient of Variation
DCR	Derived count rate
DLS	Dynamic Light Scattering
DQC	Dequalinium
DTT	Dithiothreitol
EDTA	Ethylenediaminetetraacetic acid
ENP	Empty Nanoparticle
FDR	False Discovery Rate
GO	Gene Ontology
LB	Luria Broth
LC	Liquid Chromatography
LFQ	Label Free Quantification
LNP	Loaded Nanoparticle
LPS	Lipopolysaccharides
MDR	Multi-drug resistance
MHB2	Mueller Hinton cation Adjusted Broth
MIC	Minimum Inhibitory Concentration
MS	Mass Spectrometer
MW	Molecular Weight
OD	Optical Density
OM	Outer membrane
PBPs	Penicillin binding proteins
PCL	Periciliary fluid
PDI	Polydispersity index
PE	Phosphatidylethanolamine
PG	Phosphatidylglycerol
PMNs	Polymorphonuclear leukocytes
PMOs	Phosphorodiamidate morpholino oligonucleotides
PNAs	Peptide based nucleic acids
PTMs	Post Translational Modifications
QS	Quorum sensing
RND	Resistance-Nodulation-Division
SAM	Significance of analysis of microarrays
SDS	Sodium dodecyl sulfate
SILAC	Stable Isotopic Labelling of Amino Acids in Cell Culture
SPS	Synchronous Precursor Selection
TAE	Tris-acetate-EDTA
TBE	Tris-Borate-EDTA
TBS	Tris buffered saline
TBST	Tris-buffered saline, 0.1% Tween 20

TEMED	Tetramethylethylenediamine
TF	Transcription Factor
TFD	Transcription Factor Decoy
TMT	Tandem Mass Tagging
TPL	Total Protein Lysate
Z Avg	Z-average
ZP	Zeta Potential

Acknowledgements

I would like to thank the Medical Research Council (MRC) and Procarta Biosystems for funding my research.

I would like to thank my supervisors Chris Morris and Michael McArthur for all their help and support throughout my PhD, it has always been appreciated. I would also like to thank Jake Malone for hosting me at the JIC for the phenotypic knockout experiments.

Additionally, I would like to thank my lab mates both past and present for all their help, thought provoking discussions and most of all for listening to my complaining. Special thanks to Adam for all his help with the confocal work and generally being a fellow member of the grumpy northerner's club, I hope you're having a good time.

Special mention to Team Bath, who complaints about life and everything have made me feel so much better. Thanks for asking about my PhD despite not understanding it at all. Most of all Bhavika, bringer of baked goods and sender of emergency chocolate, thanks for making the 300-mile round trip to see me in Norwich.

Finally, I would like to thank my parents for always being there. You both annoy me to no end but are still some of my most favourite people.

Chapter 1: General Introduction

1.1 Cystic Fibrosis

Cystic fibrosis (CF) is an autosomal recessive disorder caused by mutations in the gene coding for the Cystic Fibrosis Transmembrane Conductance Regulator (CFTR). In 2021 it affected approximately 10600 people in the UK [1] and is predominantly found in individuals of European descent [2]. All new-borns in the UK are screened for CF using the heel-prick blood test, where blood is taken from a five-day old baby via the heel and tested for genetic diseases including CF. Additionally, CF can be diagnosed using the sweat test, where abnormally high values of chloride can be indicative of the disease state. The CFTR is a cyclic-AMP regulated chloride ion channel and is located at the apical surface of epithelial cells, the malfunction of CFTR caused by gene mutations results in the secretion of highly viscous fluids which affects many parts of the body including the pancreas and the lungs (Fig. 1.1). The effect of CFTR malfunction on the pancreas results in loss of pancreatic endocrine function leading to malnutrition and poor growth if lost enzymes are not replaced [2, 3]. However, the major cause of mortality in CF patients is driven by the effect the disease has on the patient's lungs [4]. This is primarily driven by the cycle of infection and excessive and often ineffective inflammatory response [5]. Hence, CF is a rare and life-limiting disease where the median age of survival is 41 years [1].

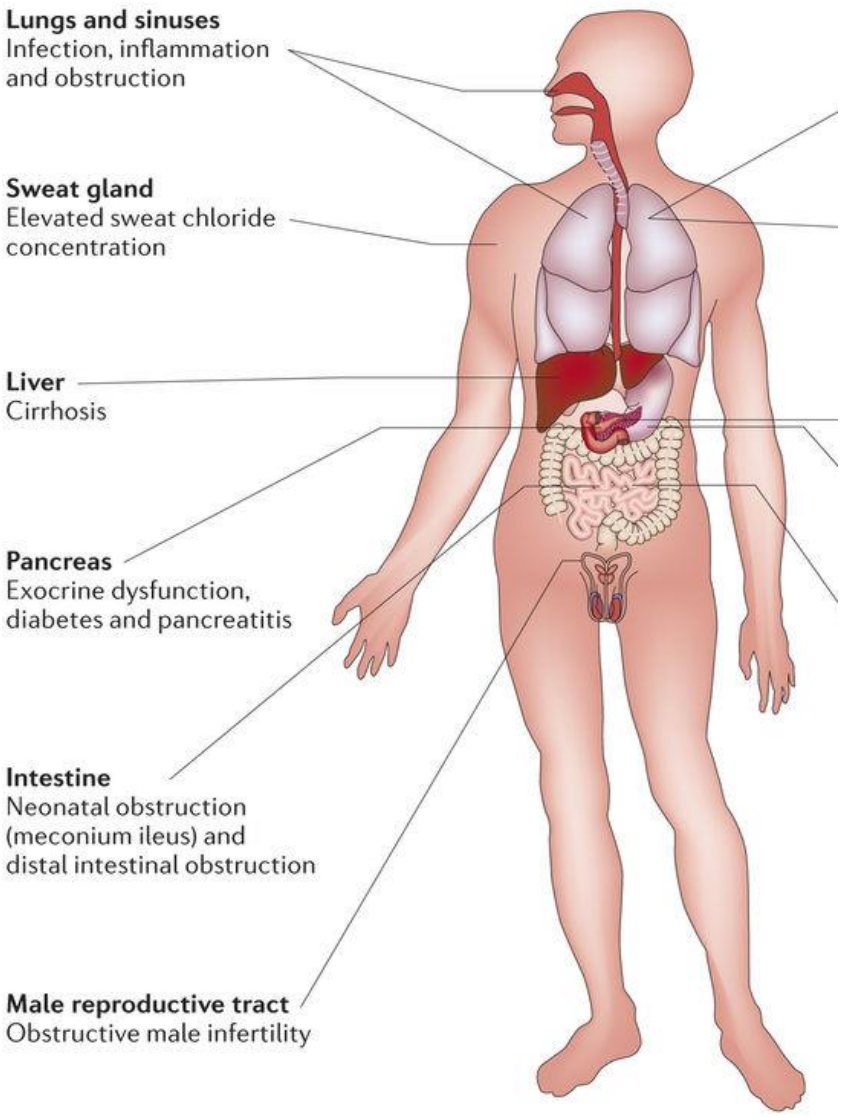

Figure 1.1 Common phenotypic features of Cystic Fibrosis. Adapted from [2]

1.1.1 The Cystic Fibrosis Airway and Microbiota

The airways of CF individuals differ from that of a regular human due to a combination of congenital differences such as increased thickness of airway walls and increased dilation [6], and structural changes caused by persistent inflammation [7]. Persistent inflammation is linked to the other anomalies in the CF airway caused directly by the CFTR dysfunction. Abnormal chloride secretion and increased sodium absorption in the lung reduces the volume of periciliary fluid (PCL) and increases the thickness of mucus [8]. This combination brings the mucus closer

to the epithelium, pressing it down into the cilia, resulting in the poor mucociliary clearance of microorganisms which may have entered the lower respiratory tract (Fig. 1.2).

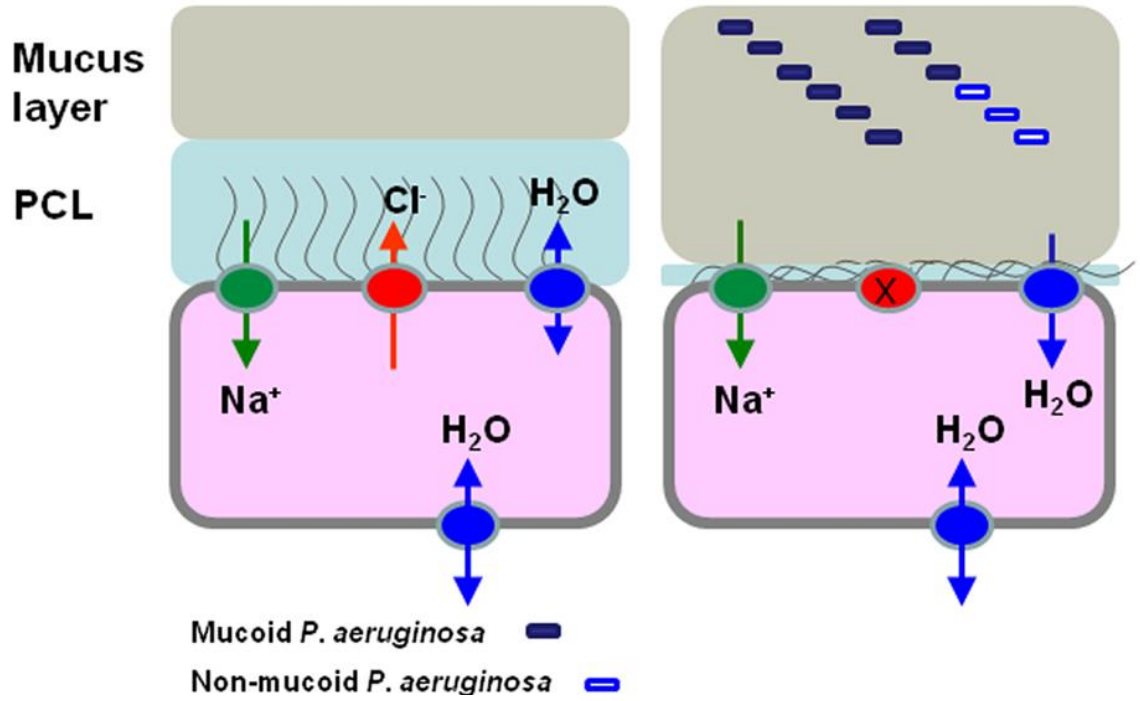

Figure 1.2 Schematic showing difference in mucociliary function in normal (left) and CF (right) airway epithelial cells. Adapted from [9]. In the CF airway, balance between chloride ion and sodium ion transport is lost, resulting in a reduced volume of periciliary fluid (PCL), thus bringing mucus into contact with the cilia, preventing clearance of microorganisms such as *P. aeruginosa*.

An additional compounding factor in the clearance of mucus in the CF phenotype is the emergence of goblet cell hyperplasia, where the increased expression of goblet cells results in increased mucus production [10]. This increased volume of mucus further hampers the clearance mechanisms.

The inability of the innate immune response to clear these microorganisms brings about the recruitment of cells triggering an inflammatory response. This involves the increased production of IL-8 [4], recruitment of polymorphonuclear leukocytes (PMNs) and production of antibodies from the specific immune system [3, 7]. This response is excessive in CF, producing high amounts of IL-8 and increased neutrophil recruitment resulting in structural damage to the lung which, in turn, increases the retention of mucosal secretions and bacteria [3, 4]. This inflammation is

ultimately ineffective against the bacteria and results in a continuous cycle of infection, inflammation and tissue destruction. Consequently, the extensive use of antibiotics in this population is required for survival. Prior to the antimicrobial era the average lifespan of a CF individual was less than two years [8]. However, CF patients eventually develop chronic infections caused by bacterial adaptation and gain of multi-drug resistance (MDR) which results in death in 80 % of CF sufferers [2, 6].

The microbiota of the CF lung is complex and differs between individuals and throughout the life-span of a patient [7, 11]. Throughout younger life individuals are predominately infected with *Staphylococcus aureus.* After the age of 25, when it is thought that the CF pathogen community is fully established, *Pseudomonas aeruginosa* and *Burkholderia cepacia* complex are the predominate species [3, 8, 11]. Other common pathogens present in the CF lung include *Stenotrophomonas maltophilia, Streptococcus ssp.* and *Haemophilus influenza* [3, 11].

Chronic infections in CF are established through the repeated colonisation, antibiotic-mediated eradication and recolonization by the same genus. Often the paranasal sinuses can provide a niche for the infecting pathogen as the thick mucus, reduced airflow and reduced antibiotic exposure provides an environment where adaptation can take place and a chronic infection become established before moving into the lower respiratory tract [7]. In 60-70 % of cases *P. aeruginosa* is the archetypal pathogen that is present in chronic infection [12].

1.2 *Pseudomonas aeruginosa*

Pseudomonas aeruginosa is a gram-negative, rod-shaped and ubiquitous environmental bacterium found in the soil, water and hospitals. As an opportunistic pathogen, it can cause a wide range of diseases from soft rot in some plants [13], infections in livestock and companion animals as well as hospital-acquired infections particularly in immunocompromised humans. Common *P. aeruginosa*-related illnesses in humans include ventilator associated pneumonia,

catheter associated infections, wound infections and surgery related infections [14]. However, the most clinically significant *P. aeruginosa* infections are in CF patients, where chronic infections and related mutations result in the formation of alginate biofilms and gains in multi-drug resistance (MDR) contributing to patient morbidity and mortality [6, 14-16]. The challenges of MDR in *P. aeruginosa* resulted in the World Health Organisation listing it as a pathogen for which the development of new antibiotics is urgently needed [17]. The problems associated with *P. aeruginosa* infections have been noted for a number of years, such that it is a member of the ESKAPE organisms. ESKAPE is an acronym for those bacteria which are the major causes of nosocomial infections across the world, many of which are multidrug resistant and includes the pathogens *Enterococcus faecium, Staphylococcus aureus, Klebsiella pneumoniae, Acinetobacter baumannii, Pseudomonas aeruginosa* and *Enterobacter* species [18].

The major challenge when tackling infections caused by *P. aeruginosa* is the extensive number of virulence factors and intrinsic antibiotic resistance found in the bacterium [16, 19] (Fig 1.3). These features permit environmental adaptation in the CF lung and aid its survival against the host defence system and a large number of antibiotics. A major source of intrinsic antimicrobial resistance is the outer membrane.

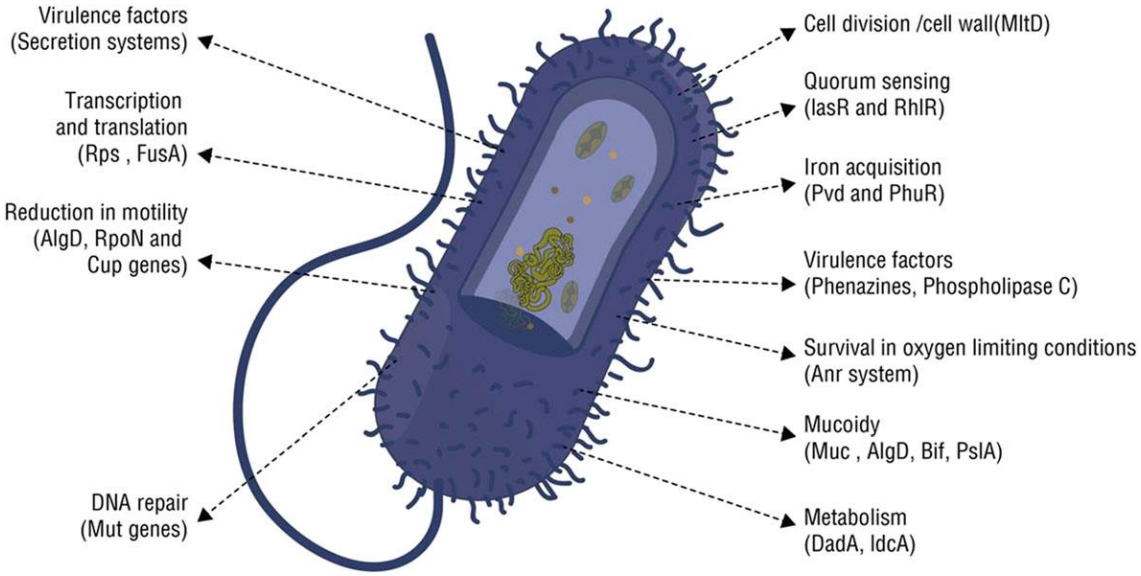

Figure 1.3 The features of P. aeruginosa relevant to its pathogenicity and adaptability. Figure taken from [6].

1.2.1 Pseudomonas aeruginosa Outer Membrane

Gram-negative bacteria are characteristically surrounded by two lipid bilayers: the cytoplasmic membrane (CM) and the outer membrane (OM). The OM acts as an additional layer of protection for the cell by working as a selective barrier through its combination of highly hydrophobic lipids and size selective porins [16, 20]. The OM is asymmetric, with lipopolysaccharides (LPS) found exclusively on the outer surface (Fig 1.4) and the inner surface having a composition similar to that of CM: approximately 80 % phosphatidylethonalamine, 15 % phosphatidylglycerol and 5 % cardiolipin [20]. The OM of *P. aeruginosa* has been described to be one hundred times less permeable than the OM of *Escherichia coli* [21]. This has been linked to the limited number of porins in the OM, the increased number of closed versus open state of these porins, and the increased stability of its LPS layer [20-22].

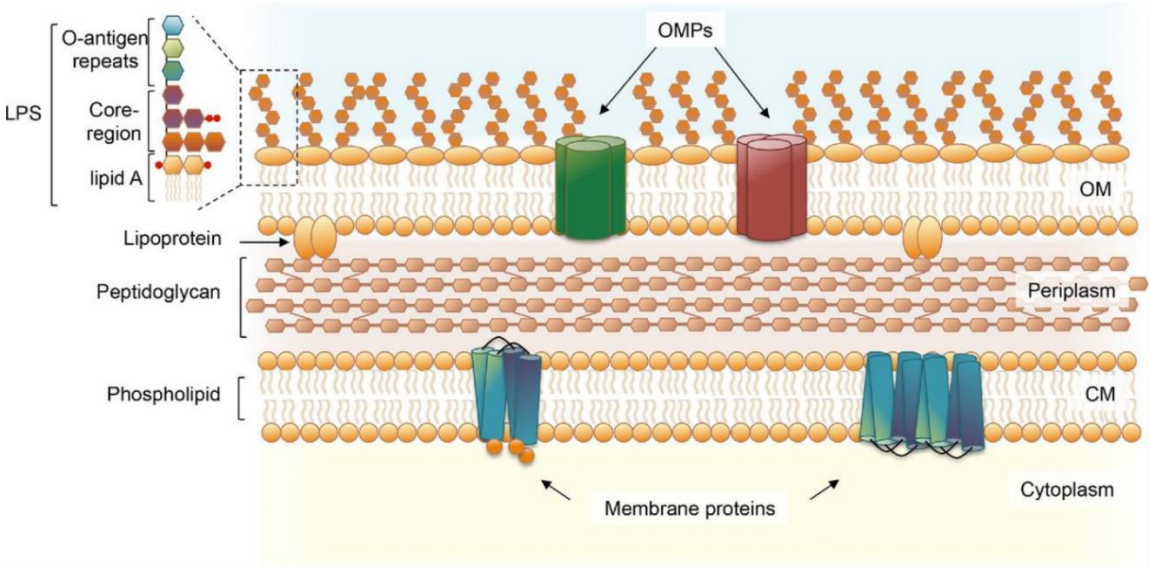

Figure 1.4 Cell envelope organisation of Gram-negative bacteria. The outer membrane is asymmetric with LPS found only on the outer leaflet. The presence of outer membrane proteins (OMPs) allows for the movement of hydrophilic molecules in and out of the cell. Figure taken from [23].

Lipopolysaccharides

Lipopolysaccharides (LPS) are a virulence factor comprised of the fatty acid lipid A, a core oligosaccharide and the immunogenic oligosaccharide O-antigen. It is the structure of LPS that makes the OM a much more hydrophobic barrier than the phospholipid bilayer of the cytoplasmic membrane [20]. In *P. aeruginosa* the lipid A component typically contains shorter fatty acids compared to *E. coli* resulting in a larger number of OH groups to compensate for loss of van der Waals interactions, stabilising the LPS interactions through increased hydrogen bonding resulting in reduced permeability to hydrophilic molecules [22]. As in most gram-negative bacteria, the LPS layer in *P. aeruginosa* is stabilised by the presence of divalent cations, typically Mg^{2+}, which promote interactions between LPS molecules through cross-linking [21]. The removal of these divalent cations can destabilise the LPS layer allowing for the penetration of certain molecules into the periplasm, such as polymyxins. However, it had been observed that in Mg^{2+} limited conditions, an upregulation of the OMP OprH can occur replacing the OM stabilising divalent cations [24].

Mutations of synthesis enzymes of LPS in *P. aeruginosa* have been observed in chronic infections, altering immune response [23, 25]. Changes observed include modifications in the O side chain, resulting in the loss of serotype [23], and protection of the cell from pyocin (toxins which target closely related species) mediated killing [25]. Additionally, changes in lipid A have been observed, such as modifications to increase the initial pro-inflammatory response [23] and addition of aminoarabinose to one of the phosphate groups, promoting resistance to cationic antimicrobial peptides [25]. Mutations of LPS can also bring about resistance to polymyxin antibiotics, of which LPS is a target. Mutations in the two component systems PhoP/PhoQ and PmrA/PmrB cause LPS modifications: mutations in PmrB have been shown in those patients with colistin resistance and result in changes to the overall charge of LPS disrupting electrostatic binding of the antibiotic [26].

Porins

Porins are β-barrel shaped proteins, usually associated as trimers which span the outer membrane, allowing for the movement of small hydrophilic molecules across the OM [16]. *P. aeruginosa* produces several types of porins with the major nonspecific porin being OprF [22]. OprF is a 'slow porin' and despite its large pore size, shows low permeability [22]. This can be attributed to the two conformers of the OprF porin: 'open' and 'closed', one which allows the permeation of sucrose and one which does not [27]. The majority of OprF porins in the *P. aeruginosa* OM exist in the closed conformer, thus making the *P. aeruginosa* OM intrinsically poorly permeable. Changes in porins have been linked to drug resistance, an example of which is a mutation in OprD. OprD is a specialised porin involved in the uptake of positively charged amino acids and loss of this protein has been linked to imipenem resistance, increasing the minimum inhibitory concentration (MIC) by eight-fold [16, 20].

1.2.2 *Pseudomonas aeruginosa* Treatment and Resistance

Due to the ubiquitous presence of *P. aeruginosa* and its ability to cause life limiting infections the need for effective treatments is required. Antibiotics used in treatment of *P. aeruginosa* infections include penicillins, cephalosporins, aminoglycosides, polymyxins, carbapenems and fluoroquinolones [14, 28-30]. Typically, in the UK, chronic *P. aeruginosa* infections in CF are managed using inhaled colistin or tobramycin with the addition of intravenous antibiotics during exacerbations [31].

1.2.2.1 Mechanism of Action of Antibiotics that Act Against *Pseudomonas aeruginosa*

In the clinical treatment of *P. aeruginosa* infections, the traditional antibiotics used generally fall into one of four classes of antibiotics: ß-lactams (e.g. penicillins, carbapenems, cephalosporins), aminoglycosides, fluroquinolones and polymyxins. β-lactams inhibit cell wall synthesis by blockading the activity of penicillin binding proteins (PBPs) which in turn results in cell lysis. Within the family of ß-lactams, three main classes are used to treat pseudomonal infections: penicillins in combination with a ß-lactamase inhibitor (e.g. piperacillin-tazobactam), carbapenems (e.g. imipenem) and cephalosporins (e.g. ceftazidime) [28, 30, 32]. Aminoglycosides (e.g. tobramycin) work by inhibiting protein synthesis, specifically by binding to the 30S ribosomal subunit resulting in misincorporation of amino acids during protein syntheses [32]. The resultant proteins misfold and incorporation of these misfolded proteins into membranes generates membrane stress which eventually leads to cell death [33]. Aminoglycosides can work synergistically with β-lactam antibiotics and be used in dual therapies [28]. Fluoroquinolones (e.g. ciprofloxacin) work by inhibiting DNA synthesis. Inhibition of the enzymes DNA gyrase and topoisomerase IV prevents the relegation reaction resulting in cell death [30, 32]. Polymyxins (e.g. colistin) disrupt the OM [30] and are often used to treat infections in CF patients [28]. Polymyxins displace the stabilising divalent cation in the LPS layer resulting in OM disruptions eventually leading to cell death [34, 35].

1.2.2.2 Mechanisms of Antibiotic Resistance in *Pseudomonas aeruginosa*

The major challenge in the treatment of *P. aeruginosa* infections is resistance. The resistance mechanisms can generally be grouped into intrinsic, acquired or adaptive. As previously discussed, the poor permeability of the OM plays an important role is the intrinsic resistance of *P. aeruginosa* to antibiotics. Loss of functional porins can result in increased tolerance to quinolones and ß-lactams, whereas LPS modifications lead to aminoglycoside and polymyxin resistance [36]. This poor permeability works synergistically with the presence of an efficient efflux system found in this species.

There are five families of efflux pump systems known in bacteria: the resistance-nodulation-division (RND) system, ATP-binding cassette superfamily, major facilitator superfamily, multidrug and toxic compound extrusion family and the small multidrug resistance family. The RND associated efflux pumps are known to contribute to antibiotic resistance [36]. In *P. aeruginosa* there are four well described RND family multidrug efflux pumps: MexAB-OprM, MexXY-OprM, MexCD-OprJ and MexEF-OprN [14, 28]. Two of these efflux pumps, MexAB-OprM and MexXY-OprM are the most clinically significant [14]. MexXY-OprM overexpression can result in the resistance of *P. aeruginosa* to aminoglycosides, fluoroquinolones, tetracycline and erythromycin [18, 37]. Whereas MexAB-OprM can efflux β-lactams, fluoroquinolones, tetracycline, chloramphenicol, macrolides and many other molecules [37]. Overexpression of these efflux pumps increases the likelihood of resistance in *P. aeruginosa* to antibiotics substrates of these pumps.

Additional causes of intrinsic resistance in *P. aeruginosa* are related to the presence of antibiotic inactivating enzymes such as β-lactamase [36]. The gene *ampC* encodes for a chromosomal β-lactamase, which can degrade antibiotics such as cephalosporins and penicillins [16, 30].

Acquired resistance is conferred through changes in gene expression, which may have been caused by horizontal or vertical gene transfer. Horizontal gene transfer involves the movement

of a plasmid from one cell to another via conjugation, transformation or transduction. Plasmid-encoded resistance in acquired via this method in *P. aeruginosa* has been reported, such as β-lactam resistance through acquirement of extended spectrum β-lactamases [14]. Vertical gene transfer occurs between a parent and offspring and when discussing in terms of antibiotic resistance the passing on of gene mutations that confer resistance is what is of interest. Exposure to antibiotic stresses and host defences can drive gene mutation resulting in a gain of resistance [14, 15]. Examples of gene mutations that result in resistance in *P. aeruginosa* include the change in *gyrB*, the DNA gyrase B subunit which is targeted by quinolones, resulting in quinolone resistance and mutations in LPS which result in polymyxin resistance [28].

Adaptive antibiotic resistance relates to resistance phenotypes gained by transient changes in gene or protein expression induced [36] by environmental factors. One example of this is antimicrobial resistance induced by biofilm formation. Biofilms consist of a number of bacterial cells which are frequently encapsulated in a self-produced matrix of extracellular polymeric substances (EPS) that are attached to each other and/or a surface. The antimicrobial resistance of biofilms can be attributed to a number of different factors. For example, poor penetration of antibiotics through the matrix, combined with an attenuated metabolic state result in higher concentrations of antibiotic needed for antimicrobial activity. Moreover, the internal biofilm milieu presents a harsh environment (e.g. reduction of oxygen permeation, increase of reactive oxygen species, increase of nitrogen oxide species) that promotes mutational changes that enhance the resistant phenotype of bacterial cells compared to their planktonic counterparts.

The intrinsic resistance of *P. aeruginosa* combined with its ability to rapidly mutate and form biofilms has resulted in multidrug resistant strains.

1.2.3 Novel Treatment Methods for *Pseudomonas aeruginosa*

The growing problem of multidrug resistance in *P. aeruginosa* drives the urgent need for the development of novel treatments for infections caused by this organism. The ability of *P.*

aeruginosa to rapidly develop resistance and the reduced metabolic state of bacteria in biofilms commonly formed in chronic infections warrants the need to move away from the traditional antibiotic targets. Much work has been done in this area, researching and developing treatments utilising novel mechanisms of action [38]. These include targeting quorum sensing, lectins, use of bacteriophages and antimicrobial cationic peptides, vaccinations and targeting the genetics.

Quorum sensing (QS) is utilized by individual bacterial cells to communicate with each other through the production and detection of small signalling molecules along a gradient [39]. QS is considered a therapeutic target as disrupting these methods of bacterial communication would interfere with colonisation. There are four quorum sensing (QS) signalling pathways in *P. aeruginosa* Las, Rhl, Pqs and IQS [14]. QS is important in the regulation of virulence factors in *P. aeruginosa* and plays a role in biofilm formation [14]. There are many approaches for the development of QS inhibitors, such as blocking molecule production, reducing molecule levels and blocking molecule detection [40]. A promising approach is targeting the acyl-homoserine lactone QS molecule [40]. Testing of a QS inhibitor C11, which is a part of this family, has shown inhibition of this molecule can prevent biofilm formation [41].

Lectin inhibitors are another potential novel therapy. Lectins are proteins involved in the cross-linking of bacteria and biofilm formation through sugar recognition. The lectins LecA and LecB are potential targets for this therapy [30, 39]. *In vitro* work has shown successful prevention of biofilm formation with lectin inhibitors, however the number and complexity of adhesins employed by *P. aeruginosa* may affect the efficacy of this approach [36].

Bacteriophages, viruses which infect bacterial cells are another non-traditional antibacterial candidate. There are 137 different bacteriophages known to target the *Pseudomonas* genus that have been characterised. Studies into phage therapies have shown successful penetration and dispersal of the *P. aeruginosa* biofilm [39, 40, 42]. However, there is more work to be done

before this becomes a viable therapy, with concerns regarding virulence and phage resistance [36, 39, 42].

Endolysins, which hydrolyse the peptidoglycan cell wall, are produced by bacteriophages and have been considered as a novel therapy [39]. Recently a novel endolysin LysPA26 has been shown to have potential against MDR *P. aeruginosa*, [43] however more work needs to done to explain the efficacy and lytic mechanism before this becomes a viable therapy.

Other research into novel therapies include use of iron chelators, targeting efflux pumps and enhancing biofilm dispersal with agents such as DNase [30, 39, 40].

In addition to the development of treatments, vaccinations against *P. aeruginosa* has been proposed [30, 39, 40, 44-46]. However, a Cochrane review in 2015 of vaccine trails has shown that none were effective and could not be recommend in CF patients currently [44], indicating the need for further work in this area.

Compromising the ability of bacteria to express or translate their genes as an antimicrobial approach is an area with great potential. Using antisense or anti-gene strategies can prevent the successful replication of bacteria cells as well as prevent the action of resistance genes [39, 47]. There is a large scope of potential targets for oligonucleotide therapeutic molecules and several classes (DNA, mRNA sRNA) interfere with bacterial gene expression at multiple stages [39, 47, 48].

Much work has been done in the area of antisense therapy, which targets mRNA. There are two main methods of blocking mRNA translation: steric blockade by binding to complementary mRNA, and; degradation through recruitment of RNase H which breakdown mRNA through enzymatic degradation [49]. Examples of antisense therapies include phosphorothioate oligonucleotides (S-oligos), analogues of phosphodiester oligonucleotides, which have sulphur atoms instead of oxygen on the non-bridging phosphate linker. S-oligos bind to complementary mRNA activating RNase H. Locked nucleic acids (LNAs) may also act through RNase H. These

are oxyphosphorothioate analogues and are stable to nucleases. They have been shown to have high DNA and RNA affinity. Phosphorodiamidate morpholino oligonucleotides (PMOs) are comprised of the four DNA bases with modified base linkages, where morpholine has been substituted for ribose. Peptide based nucleic acids (PNAs) synthesised polymers with a similar structure to DNA and RNA, and contain modified backbone comprised of polyamide. They have a neutral charge and are resistant to nucleases and proteases. Both PNAs and PMOs act via steric blockade of complementary mRNA [47, 49, 50]. Figure 1.5 shows the two mechanisms of mRNA silencing described.

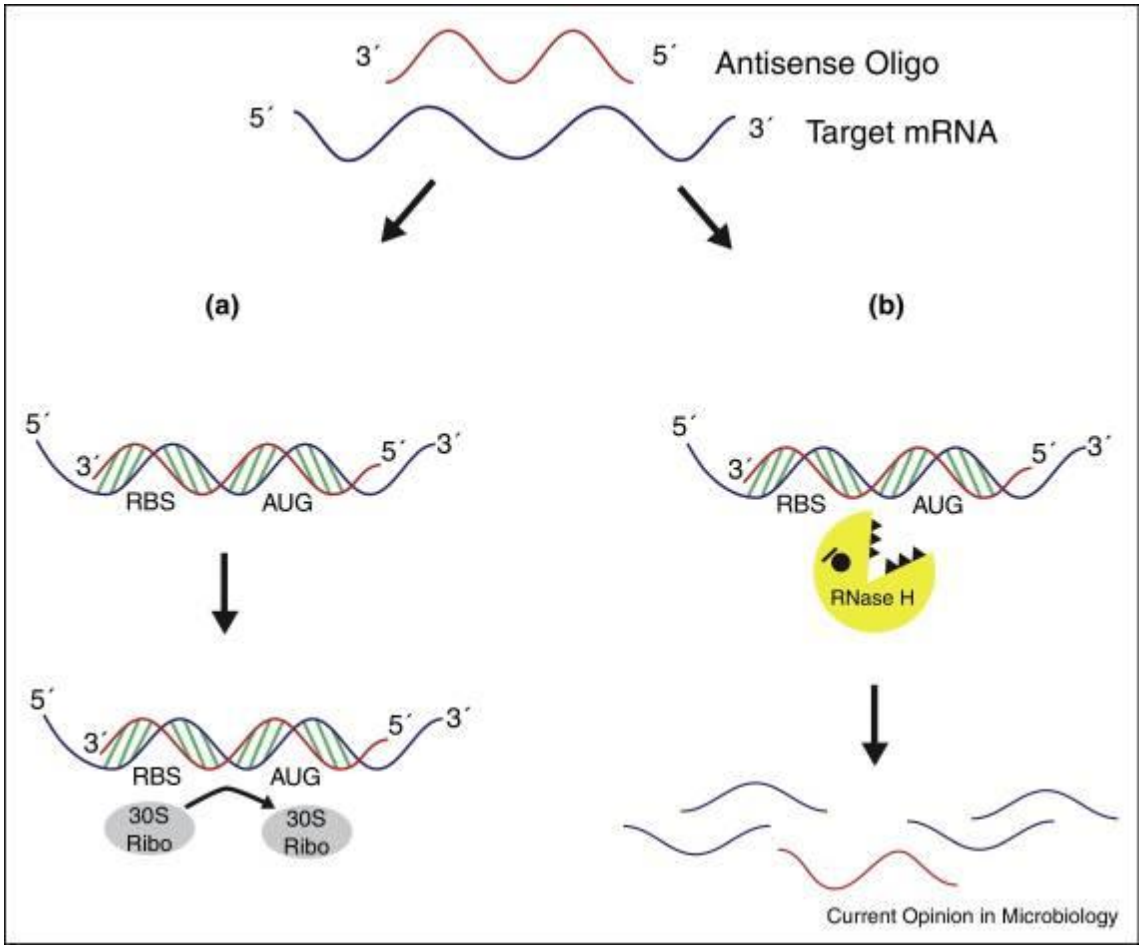

Figure 1.5 Mechanisms of antisense oligomer inhibition of gene expression. (a) The antisense oligomer binds to the target complementary mRNA, sterically blocking the 30S ribosomal subunit and initiation of translation. (b) RNase H is activated upon oligomer binding, leading to the degradation of the targeted mRNA. Taken from [49]

The barriers to delivering genetic material will prove a challenge for the development of therapies using this approach, but the development of an effective delivery system could make this a viable strategy in the clinic.

Alternative strategies targeting gene expression include acting on the process of gene transcription rather than mRNA translation as the above-mentioned therapies do. One such technology for which there is potential scope in this area is the use of transcription factor decoys (TFDs).

1.3 Transcription Factor Decoys (TFDs)

A transcription factor (TF) is a regulatory protein which binds to a specific DNA sequence to regulate expression of the targeted gene. TFs can upregulate or downregulate the extent of expression and may act alone, in combination with other transcription factors and/or nucleoid associated proteins. Generally, they directly contact the RNA polymerase complex to either enhance recruitment to the transcriptional promoter (in the case of upregulation) or block its recruitment, sometimes by steric hinderance of binding sites of other TFs that would have acted to recruit the polymerase. The binding sites of transcription factors have been discovered through numerous methods including DNA footprinting, *in vitro* selection, use of reporter assays, ChIP assays and mutational studies. Databases collate the binding sites of many well characterised TFs but the majority remain unknown. There are however bioinformatic tools to predict unknown binding sites based on alignment of co-regulated genes, as discovered by transcriptomic studies of bacteria carrying knock-outs of a TF, and comparison to homologues in well characterised strains. Additionally, the binding sites commonly exist as direct or inverted repeats of a five to seven nucleotide motif often separated by a short spacer. This is consistent with the TFs binding as dimers either in the same or opposing orientations [51].

Though the DNA-protein binding interaction is sequence specific, binding sites for a one TF can differ between target genes [52].

TFDs are oligonucleotides which interfere in the process of gene expression (Fig 1.6) via competitive inhibition. The oligonucleotide sequence of the TFDs contain the TF binding site and so when transfected into the cell can interfere with TF binding to its site in the promoter. Through this competition, the recruitment of RNA polymerase is inhibited with concomitant down regulation of the targeted gene.

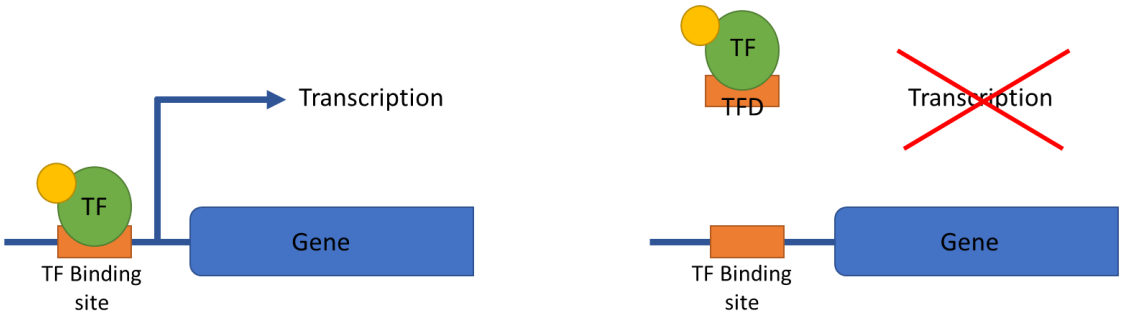

Figure 1.6 *Schematic illustrating effect of a transcription factor decoy (TFD).* Yellow sphere indicates RNA polymerase. In normal conditions (left) a transcription factor (TF) binds to its binding site within the promoter to enhance expression of the associated gene. However, in the presence of a TFD (right) the TF binds to the TFD instead of the promoter, thus transcription is blocked and mRNA is no longer produced.

As TFDs inhibit the enzymatic production of mRNA by RNA polymerase they are far more effective than antisense molecules, which commonly prevent translation of mRNA molecules by steric hinderance. This explains why TFDs have been found to be effective at very low concentrations as single events may block the production of many thousands of mRNA molecules [53, 54]. Additionally, TFs commonly control several to many hundreds of individual genes creating a plethora of adverse effects for the bacteria, whereas antisense molecules can only target a single species of antisense and are susceptible to mutation of their binding site causing resistance.

In contrast resistance to TFDs through mutations is considered less likely as they would need two independent events. Mutations to the TF to alter its affinity for its binding site may decrease the efficacy of the TFD but would also prevent the TF from binding to the promoter, effectively disrupting its function. Similarly, mutation to the TF binding site would render it refractive to TF

binding, again leading to loss of function. Instead, mutations to both the TF to alter its binding affinity and a compensatory change to the binding site would be necessary to evade TFD activity.

Another attractive property of the technology is that TFDs can be designed to target specific TFs. This allows affecting of large regulons, bacterial genes essential for pathogenicity or survival and also controlling the antimicrobial spectrum of the agents by selecting genes specific to a pathogen, ideally to leave commensal bacteria intact. Thus, giving this technology the flexibility to be designed for specific disease needs.

Challenges to the technology include the redundancy inherent in bacterial regulatory networks, so that other TFs may compensate for the loss of the targeted TF activity. Also, the identification of suitable target genes and the sequence of the correct TF binding site can be onerous and needs independent validation with *in vitro* studies. However, the largest challenge is the delivery of the TFD to the bacteria cytoplasm, or transfection. Given the high molecular weight and polyanionic nature of the TFD, the bacterial cell wall is the main barrier. The poor permeability of the OM of *P. aeruginosa* constitutes a further challenge. The ideal delivery system would have three key properties: 1) the ability to bind the TFD efficiently, 2) the ability to selectively target the bacterial cell wall and cross it without causing lysis and 3) the protection of the TFD, by condensation, to prevent degradation in biological fluids. Therefore, it is imperative that a reliable and safe delivery system is developed for this technology in order to make this a viable antimicrobial in the clinic.

1.3.1 Transcription Factor Decoy Delivery with Nanoparticles

The delivery of a TFD through bacterial membranes poses a great challenge. Previous methods of oligonucleotide delivery have utilised cationic peptides. However, the oligonucleotides need to undergo chemical modification to remove their negative charge in order to avoid precipitation when combined with the positively charged peptide [55, 56]. Therefore, an alternative approach is needed to deliver unmodified TFDs.

One such alternative is the use of nanoparticles that can condense and encapsulate the TFD, masking its charge and protecting it from nuclease degradation during the delivery process. In addition to the protective capacity of these nanoparticles, one which would aid in the intracellular delivery of TFD is desirable. One potential molecule for the use in such a nanoparticle is the bolaamphiphilic molecule, 12,12'-(dodecane-1,12-diyl) bis(9-amino-1,2,3,4-tetrahydroacridinium), (12-bis-THA) , which has been recently described (Fig 1.7) [53, 57]. This molecule is a derivative of the clinically approved antiseptic, dequalinium (DQC) (Fig. 1.8).

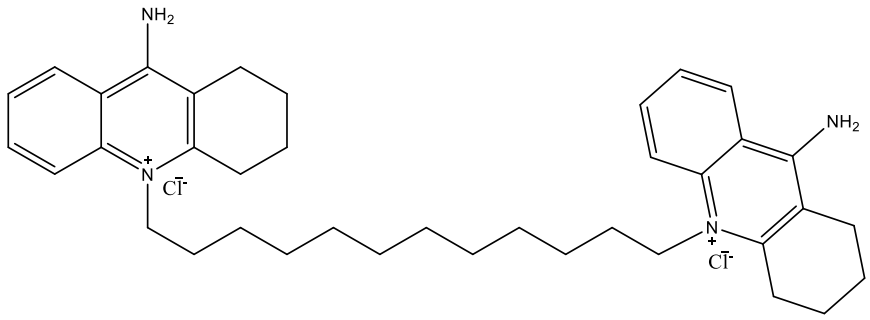

Figure 1.7 Chemical Structure of 12-bis-THA

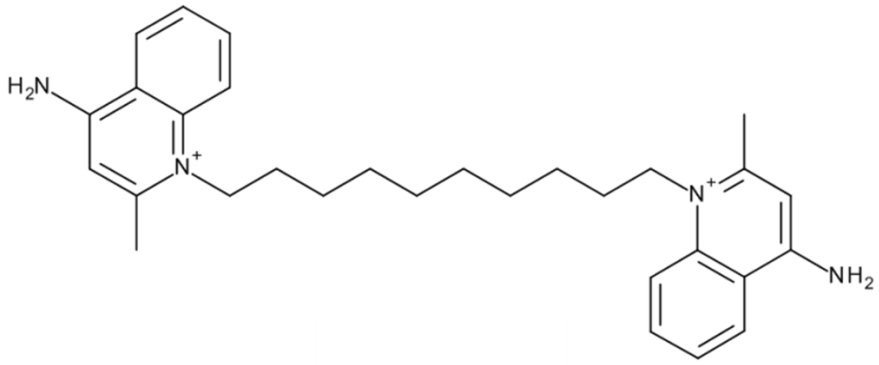

Figure 1.8 Chemical Structure of Dequalinium

In dilute aqueous solution 12-bis-THA molecules self-assembles to form colloidally unstable aggregates termed empty nanoparticles (ENPs). Upon mixing with DNA, 12-bis-THA undergoes electrostatic compensation to form TFD-loaded nanoparticles (LNPs) (Fig 1.9).

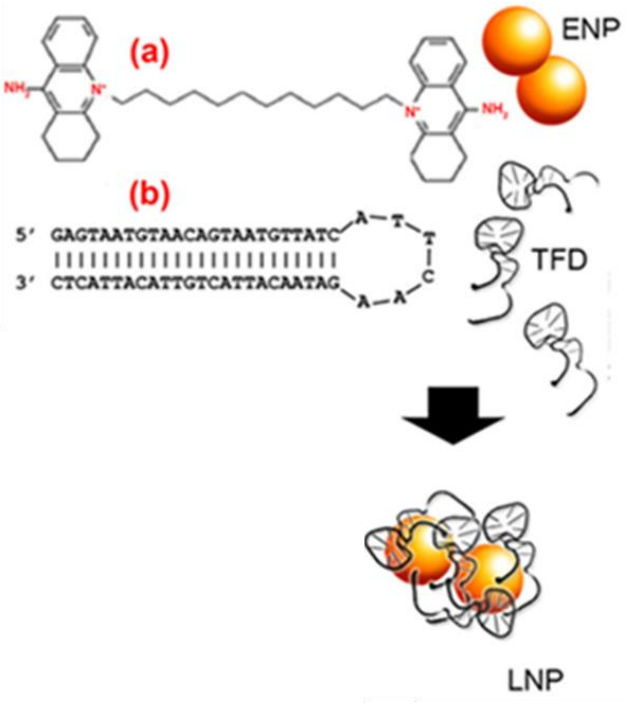

Figure 1.9 *Formation of TFD-loaded nanoparticles (LNPs). (a) chemical structure of 12-bis-THA which forms, in aqueous solution empty nanoparticles (ENPs). When mixed with a TFD such as the hairpin shown in (b), DNA is condensed to form TFD loaded nanoparticles (LNPs).* Adapted from [53].

The two tetrahydroacridinium head groups provide a net positive delocalised charge that remains on the LNPs. This is sufficient to drive electrostatic interactions with bacterial membranes.

An advantage of 12-bis-THA is that is has been shown to interact with the bacterial membrane lipid cardiolipin, destabilizing the membrane and forming transient pores, thus aiding in the delivery of the encapsulated TFD [53]. A study by Marin-Menendez et al. [53] used 12-bis-THA to deliver a SigH inhibiting TFD to *Clostridium difficile* and *Escherichia coli* and liposomes modelling membranes of varying compositions. The OM comprises of three major phospholipids: zwitterionic Phosphatidylethanolamine (PE), anionic phosphatidylglycerol (PG) and anionic cardiolipin (CL) [58]. The anionic phospholipids, PG and CL, are crucially absent from eukaryotic plasma membranes. These anionic phospholipids both interact with 12-bis-THA and the study found that there was a stronger interaction between 12-bis-THA and CL than with PG. This was hypothesised to be most likely due to the surface charge density and non-zero

spontaneous curvature of CL. The study noted that confocal laser scanning microscopy (CLSM) results of live bacterial cells treated with LNPs, displayed intact membranes despite internalisation of TFDs. Following further investigations utilising model liposomes, it was hypothesised that the delivery of TFDs by 12-bis-THA were due to the formation of transient pores. Through the electrostatic interactions of the LNPs and CL additional membrane destabilisation was attributed to the conformational pressures of CL, which resulted in the formation of these transient pores, aiding in TFD delivery. Additionally, these LNP interactions saw a decrease in LNPs concentration indicating that the binding of LNP to the bacterial membrane destabilised the molecule, releasing TFD. The CLSM results in this study also showed diffuse TFD signal inside the bacterial cells following LNP treatment, indicated that TFD release from LNPs occurred after crossing the cell wall. Recently published data has also established the role of LNP interaction with LPS in the intracellular delivery of TFDs [59]. LNP-LPS interactions were shown to induce destabilisation of the membrane and increase membrane permeability. Alongside this a LPS sequestering effect was also observed, reducing the inflammatory activity driven by LPS. The findings of Marin-Menendez et al. [53] were able to hypothesis the potential mechanism of TFD delivery driven by 12-bis-THA as a two-step process. The first step involving the interaction of LNPs with the bacterial membrane and the second involving the release of TFD into the cell's cytoplasm.

12-bis-THA has also been shown to induce DNA supercoiling [60], reducing the bulkiness of the large molecules thus aiding in the passage of the DNA molecule across the membrane and renders it resistant to nuclease degradation, as the canonical structure of the helix is collapsed.

Like its parental molecule, DQC, 12-bis-THA is known to have an antimicrobial effect on bacterial species [57] most likely due to its activity on bacterial membranes and the DNA intercalating activity of the THA headgroups [59]. LNPs formed by 12-bis-THA can affect TFD delivery without causing lysis but the action of transfection and binding to CL results in the bacteria mounting a stress response. This in turn would lead to the upregulation and induction TFs involved in

regulating the cell response to 12-bis-THA activity, e.g., those involved in membrane repair regulation. Therefore, if the action of 12-bis-THA, a delivery agent for TFDs results in an upregulation of TFs there is the potential to design TFDs to specifically target the cell response to this stressor. Hence, investigating the changes in TF levels in response to the presence of 12-bis-THA is a valid approach.

1.4 Dynamic Light Scattering and Zeta Potential

The use of a nanoparticle-based delivery system introduces the need to assess the successful association and/or encapsulation of the delivery molecule of interest. In regards to 12-bis-THA/TFD based nanoparticles, previous studies [53, 57, 61] successfully utilised dynamic light scattering (DLS) and zeta potential to prove 12-bis-THA and TFD association, thus confirming LNP formation.

1.4.1 Dynamic Light Scattering

Dynamic light scattering (DLS), also known as quasi-elastic light scattering or photon correlation spectroscopy is a non-invasive technique used to measure the size and predict stability of particles in a liquid. DLS measures Brownian motion (the random movement of particles due to solvent interactions) by measuring changes in light scattering. This can be used to determine the translational diffusion coefficient (D) and relate it so hydrodynamic diameter, d(H), using the Stokes-Einstein equation:

$$d(H) = \frac{kT}{3\pi\eta D}$$

Where d(H) = hydrodynamic diameter, D =translational diffusion coefficient, k = Boltzmann's constant, T = absolute temperature and η = viscosity.

The intensity of light scattered is dependent on the diameter of the particle to the sixth power, therefore larger particles scatter more light than smaller ones, making highly polydisperse

mixture difficult to analyse as large molecules may mask smaller ones. The fluctuations in light scattering are used to create a correlation function by comparing the signal at time t to the signal at time (t+δt). If the two signals compared are taken at very short intervals, they will be essentially unchanged, as the interval grows, the correlation between this signals decays until the signals have no correlation. Samples containing small particles will reach this point faster than larger particles. This correlation function can be used to obtain size information about the particles by applying algorithms such as Cumulant analysis which fits a single exponential curve to the correlation function to estimate the mean size (z-average) of the nanoparticles, this is suitable for analysis of monodisperse or narrow distribution populations. An alternative algorithm CONTIN (*constrained regularization method for inverting data)* fits multiple exponentials to generate a particle size distribution and is more suitable for polydisperse samples. Cumulant analysis can also generate a Polydispersity index (PDI) which describes the width of size distribution of the particles in the sample and is calculated by $(\text{width/mean})^2$. Samples with a PDI < 0.1 are said to be monodisperse [62].

In order to compare signal strength between samples the derived count rate (DCR) can be obtained. As the machinery used in DLS and Zeta-potential measurements can analyse samples of varying concentrations an attenuator if often applied to adjust the intensity of the light applied to the sample. The attenuator reduces the amount of light shone and can differ between samples. Therefore, in order to compare between samples a theoretical count rate for 100 % light intensity can be calculated, the DCR, which allows comparison between sample. It should be noted that the DCR is not a count of the number of particles within the solution but a measure of the scattering intensity.

1.4.2 Zeta Potential

Zeta potential is a measure of the surface charge of a nanoparticle at the edge of its diffuse layer (Fig 1.10). It is an indicator of the stability of a colloidal system. Particles with large positive or

negative zeta potential will repel and are unlikely to aggregate, whereas particles with low zeta potential tend to flocculate. A zeta potential more positive than +30 mV or more negative than -30 mV are generally considered to be stable, however this may not be the case in high density systems. The zeta potential may also be affected by changes in pH [63, 64].

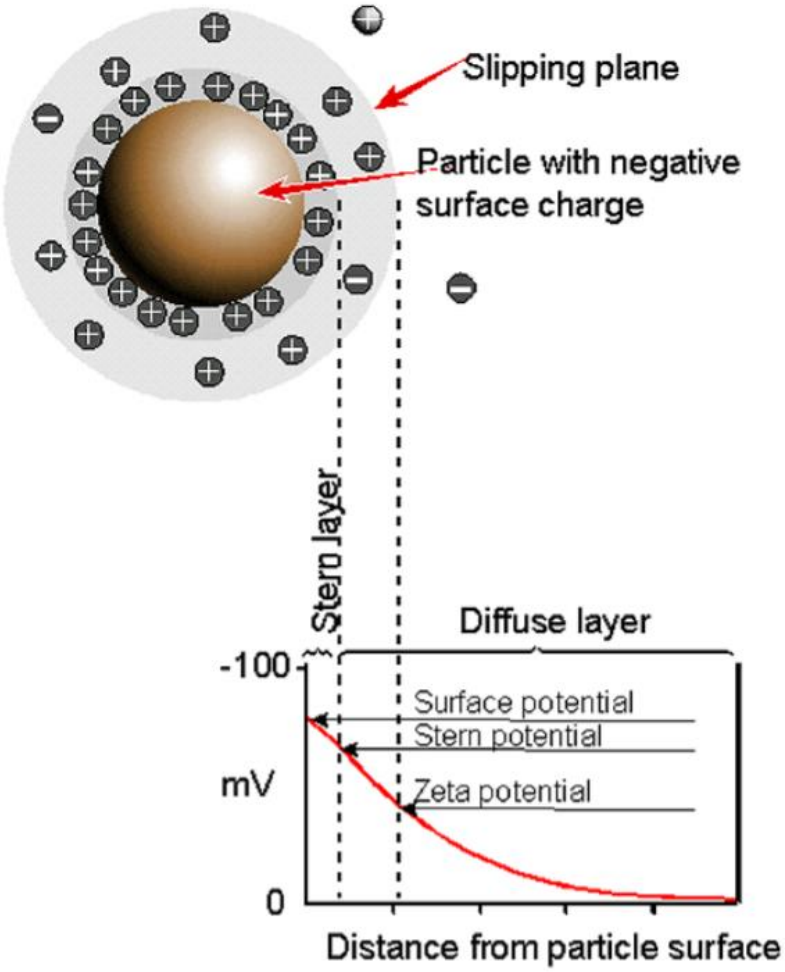

Figure 1.10 Schematic representation of zeta potential. Reproduced from Zeta potential-An introduction in 30 minutes [64]

1.5 Methods of Detecting TF Response to the Presence of 12-bis-THA

The upregulation of TFs can be monitored in many ways such as utilising transcriptomics or proteomics. Transcriptomics is the study of an organism's transcriptome which is the total of an

organism's RNA transcript repertoire under a given experimental condition. There are two main technologies used in the field of transcriptomics: microarrays, which quantify predetermined sequences, and; RNA sequencing (RNA-seq) which is a high-throughput sequencing methodology which samples the entire RNA population with less bias [65]. However, as this technology focuses on RNA it is limited in terms of TF protein quantification and activation status. TFs can exist in the inactive form within the cell and many act as repressors, hence, RNA quantification may not necessarily correlate with TF quantity. Although, many TFs regulate a limited number of genes, there are also global TFs present in an organism which regulate the expression of a large array of genes e.g., the global TF FNR in *E. coli* which has many downstream targets [66, 67]. Therefore, due to these redundancies in the TF regulatory network, changes in RNA levels may be attributed to many TFs and it can be difficult to ascertain which TF is responsible.

A method that allows direct identification of TF binding sites within bacteria is the chromatin immunoprecipitation (ChIP) assay. ChIP is an assay used for investigating protein-DNA interactions within the natural context of the cell, or when treated with an antimicrobial agent- in our case 12-bis-THA. This assay can be used to identify multiple binding sites of a particular protein or the proteins binding to a particular genomic region [67-69]. The assay involves formaldehyde fixation which preserves the DNA-protein interaction by crosslinking. Antibodies can be raised against the TF of interest and are then used to precipitate the chromatin fragments, or those of the bacterial nucleoid, following digestion or sonication. Any DNA-associated with the protein of interest will co-precipitate and can be purified following cross-link reversal. Following purification, PCR may be used to identify the region of genome associated with the proteins of interest and DNA sequence. This method can be used to investigate TF binding and has been used to determine FNR binding sites in *E. coli* [66, 67]. Therefore, ChIP can be utilised to identify TF binding sites and aid in informing TFD design,

however, it is limited as it is specific to a particular protein or binding region making it an inappropriate choice in the discovery stage.

Proteomics is an alternative, more comprehensive approach that can be utilised. Proteomics is the large-scale analysis of the proteins found within an organism. Some applications of proteomics include the relative or absolute quantification of proteins, mapping protein-protein interactions, determining protein modification and localisation of proteins within the cell [70, 71]. Proteomics involves the use of high throughput technologies for the identification and/or quantification of proteins, such as Liquid chromatography-tandem mass spectrometry (LC-MS/MS) which is one of the most commonly used technologies in modern proteomics [70].

Proteomics has been shown to have a role in antimicrobial studies and its use has been well documented in the literature such as investigations into the proteomic response to vancomycin in *S. aureus* and proteomic response to tobramycin in *P. aeruginosa* [72-74]. Studies have utilised proteomics as a tool in TF studies in both prokaryotic and eukaryotic organisms [75, 76] indicating that this methodology is an appropriate tool for the investigation of TF response to 12-bis-THA induced stress.

1.6 Proteomics

The most common modern proteomic analyses utilise mass spectrometry for the accurate and precise quantification and identification of proteins in a biological sample. Mass spectrometry measures the mass-to-charge (m/z) ratio of gas-phase ions. Mass spectrometers ionize protein or peptide samples resulting in fragmentation and separates them based on their m/z ratio. In tandem MS/MS the first MS (MS1) ionizes, accelerates and separates the sample, the second MS (MS2) then fragments these MS1 ions to generate fragment spectra. These fragments are matched with a database of the masses of possible peptides generated by the genetic sequence of the organism begin investigated, to predict the identity of the protein and calculate

confidence [70, 71, 77]. Liquid chromatography (LC) is typically used alongside tandem MS/MS to further fractionate the sample prior to ionisation. This reduces the complexity of the sample as it enters the MS, reducing the impact of peak capacity resolution on protein identification [77].

Mass spectrometry based proteomics can be either top-down, where whole proteins are ionised and analysed by MS, or bottom-up, where proteins are subjected to an enzymatic digest (typically by trypsin or lysC) prior to MS analysis. In discovery proteomics, also known as shotgun proteomics, a bottom-up approach is most commonly used [77].

In bottom-up proteomics, daughter peptides are identified during LC-MS/MS rather than proteins. Using a reference proteome generated from genomic data and software such as MaxQuant, SEQUEST and MASCOT identified peptides are mapped to a parental protein, allowing for protein identification [72]. This process is often the most challenging part of proteomics as not all peptides generated can be correctly assigned to their parental protein. Missed cleavage sites and lack of consideration in regards to peptide modifications may result in misidentification of peptide, resulting in inaccurate data. The knowledge of peptide modifications and MS settings are key to accurate assignment of proteins.

Limitations of bottom-up proteomics include the preferential detection of high abundance peptides and loss of protein information, such as secondary and tertiary structural information, during conversion to daughter peptides [77]. When using proteomics for quantification a label-free or labelled approach may be used.

1.6.1 Label Free Proteomics

Label-free quantification (LFQ) is the simpler of the two approaches and is therefore a more rapid approach suited to applications such as shotgun proteomics [78]. Two main approaches can be used in LFQ: MS1 full-scan filtering and spectral counts. Relative quantification by spectral count compares the number of identified spectra between samples for the same

protein. The theory behind this method is more abundant proteins will generate more proteolytic peptides. However, this method requires normalization and robust statistical analysis to verify accuracy [78].

MS1 filtering involves direct comparison of the peak intensities of each peptide ion in multiple data sets (e.g. comparison of the peptide ion peak from different experimental conditions). However, there are limitations to this approach as spectral peaks must be aligned for accurate quantification and normalization is required [78]. Software that can align the peaks from multiple runs and measure relative abundance is available, one such example being Skyline [79].

LFQ is a relative quantification technique and requires each sample to analysed separately. Therefore, this technique is greatly impacted by run-to-run variation and missing quantification values [80]. To avoid the impact of these variations a label-based approach may be used.

1.6.2 Label Based Proteomics

Label based methods include the use of isobaric tags such as tandem mass tagging (TMT) or stable isotopic labelling of amino acids in cell culture (SILAC) can be used to combine samples for analysis and quantify protein abundance relatively [70].

SILAC involves growing bacteria on 'heavy' and 'light' media containing isotopes of one element (e.g. ^{14}N and ^{15}N) and combining the two differentially labelled protein samples. The 'heavy' and 'light' peptides detected by subsequent MS analysis can be compared to determine relative abundances via comparison of peak intensities [70]. Although considered one of the most accurate approaches the number of sample conditions that can be analysed in one MS run is limited to three (heavy, medium and light isotopes). Additionally, over sequencing of isotope variants, driven by the complexity of the MS1, can result in reduced numbers of identified peptide [80]. Furthermore, this is one of the costliest quantification approaches.

Isobaric mass tagging involves peptides and proteins from different samples being tagged with different chemical tags which have the same total mass, allowing the peptides to co-elute during LC. These tags have been designed with different cleavage sites, therefore upon entering the MS/MS, ionization cleaves these tags at these cleavage sites resulting in different labelling reporter ions being generated. In the MS2 spectral output the intensities of the spectral peaks of theses tags can be used to determine relative abundances [79, 81] (Fig 1.11).

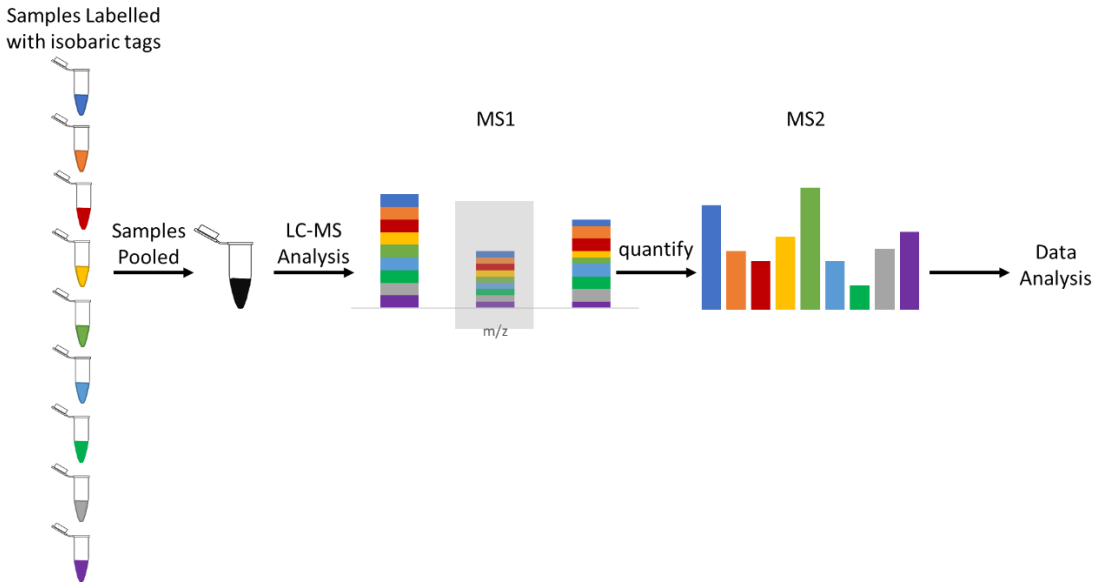

Figure 1.11 Schematic of TMT (isobaric) MS2 Workflow.

Limitations of isobaric quantification when compared to LFQ include the reduced identification rates of peptides as the presence of multiple precursor ions in the MS1 scan can result in redundancies during MS/MS scanning of the same peptide labelled with different tags [80, 82]. Additionally, there is lowered accuracy at the MS2 level as a result of signal compression at the MS1 level caused by co-isolation of precursor ions. In order to circumnavigate this issue a MS3 approach is utilised (Fig. 1.12) [80].

Synchronous Precursor Selection (SPS) MS3 allows for increased accuracy of isobaric based quantification. The targeted fragment ions in the MS2 are co-isolated and co-fragmented in the MS3 resulting in significantly increased sensitivity [80, 82, 83].

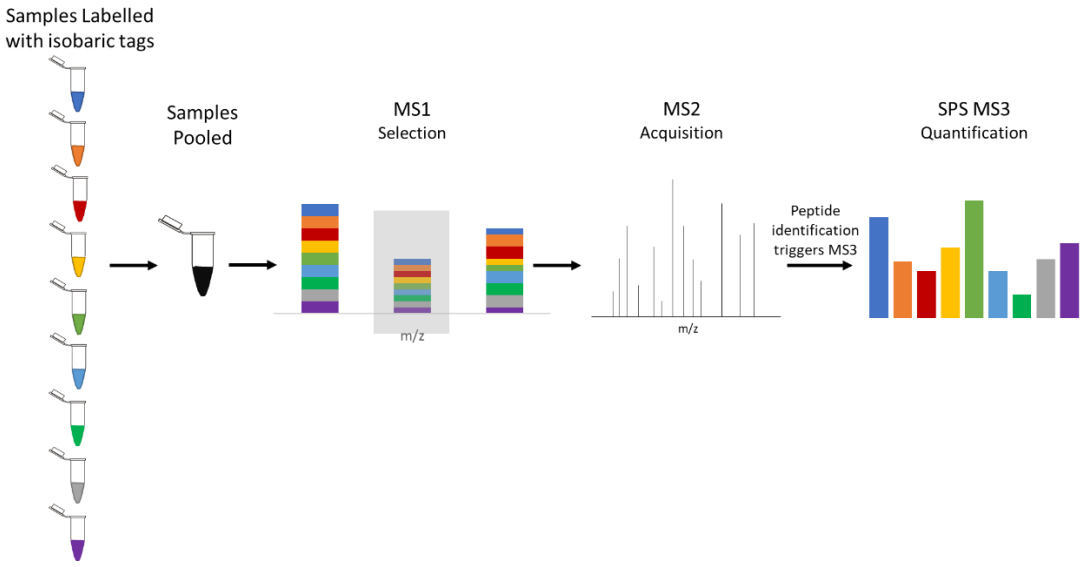

Figure 1.12 Schematic of TMT (isobaric) based SPS MS3 workflow.

1.6.3 Applying Quantitative Proteomics to TFs

A quantitative proteomic approach to determining changes in TF levels in response to 12-bis-THA induced stress warrants a shotgun approach. By design, this bottom-up technique preferentially detects and quantifies more abundant proteins. This is due to smaller signals being masked by limited resolution capacities and signal compression. Previous TF studies that have utilised quantitative proteomics have purified for TFs using a variety of approaches such as immunoprecipitation, pull down using biotin tagged oligonucleotides and separation by mass [76]. The quality of proteomic samples is key to obtaining quality proteomic data. Thus, as TFs are low copy the sample preparation method and purification of TFs in this design is a key consideration for the success of this approach.

1.7 Aims of the Project

The aim of this project is to identify and investigate targets for novel TFD/12-bis-THA antimicrobial system in *P. aeruginosa.*

Main objectives:

1) Utilising the model organism *Escherichia coli*, develop a proteomic sample preparation protocol for the identification of TF changes in response to 12-bis-THA induced stress
2) Once a proteomic protocol was developed for successful TF identification, apply this the organism of interest, *Pseudomonas aeruginosa*
3) Identify TF changes in *Pseudomonas aeruginosa* induced by 12-bis-THA treatment at both a low and high doses
4) Identify suitable TF targets for TFD development and design TFDs for *in vitro* testing using the 12-bis-THA delivery system
5) Conduct *in vitro* testing of these TFDs to establish if TFD by 12-bis-THA occurs in *P. aeruginosa* and investigate whether expected phenotypic changes occur in response to successful TFD delivery

Chapter 2: General Materials and Methods

2.1 Culturing Bacteria

2.1.1 Culturing Media

All media were obtained from Sigma Aldrich (Gillingham). The bacterial media used were all dissolved in ultrapure (MilliQ) water and autoclaved at 121 °C for 15 min. The composition of the media are described as follows:

Luria Broth (Miller) (LB) media: NaCl 10 g/L, Tryptone 10 g/L, Yeast extract 5 g/L.

Mueller-Hinton cation adjusted Broth (MHB2): Acid hydrolysate of casein 17.5 g/L, beef extract 3 g/L, starch 1.5 g/L supplemented with appropriate salts to provide 20-25 mg/L of calcium and 10-12.5 mg/L of magnesium.

Luria Agar (Miller) (LB Agar): Agar 15 g/L, NaCl 10 g/L, Tryptone 10 g/L, Yeast extract 5 g/L.

2.1.2 Bacterial Strains and Growth Conditions

The strains used in this study were *Escherichia coli* NCTC_9001, characterised by serotype O1:H1:K7 and was kindly provided by James Mason (Kings College London). *Pseudomonas aeruginosa* PA14 was kindly donated by Professor Craig Winstanley (Liverpool University). PA14 is characterised as highly virulent, non-mucoidal, having type IVb class pili, highly conserved b-type flagella, high pyocyanin and low pyoverdine production [84, 85]. *P. aeruginosa* Δ*brlR*PAO1 and its parental strain were kindly provided by Dr Lichuan Gu (Shandong University, China). The parental strain PAO1 is characterised as moderately virulent, non-mucoidal, having type IVa class pili, highly conserved b-type flagella, low pyocyanin and low pyoverdine production [84, 85].

All bacterial strains were grown aerobically at 37 °C with 200 rpm shaking. All *P. aeruginosa* strains were grown in MHB2 and *E. coli* NCTC_9001 was grown in LB. All strains were stored at -80 °C in 50 % glycerol. All strains were freshly streaked onto LB agar 18 h prior to any experimentation.

Optical densities were measured with a UV-Vis spectrophotometer (Spectramax M2) at a wavelength of 600 nm using Kartell semi-micro cuvettes (ThemoFisher). For each measurement 500 µL of bacterial culture was taken and diluted 1:2 into the equivalent growth media.

2.1.3 Minimum Inhibitory Concentration Testing

Minimum inhibitory concentration (MIC) testing was conducted using the broth microdilution method as described by Wiegand et al [86]. All 12-bis-THA solutions were prepared from the chloride salt dissolved in MilliQ water. Concentrations of 12-bis-THA tested for *E. coli* ranged from 155-0.225 µg/mL and 125-0.244 µg/mL for *P. aeruginosa,* using the doubling dilution method. Microtiter plates were laid out as shown in figure 2.1.

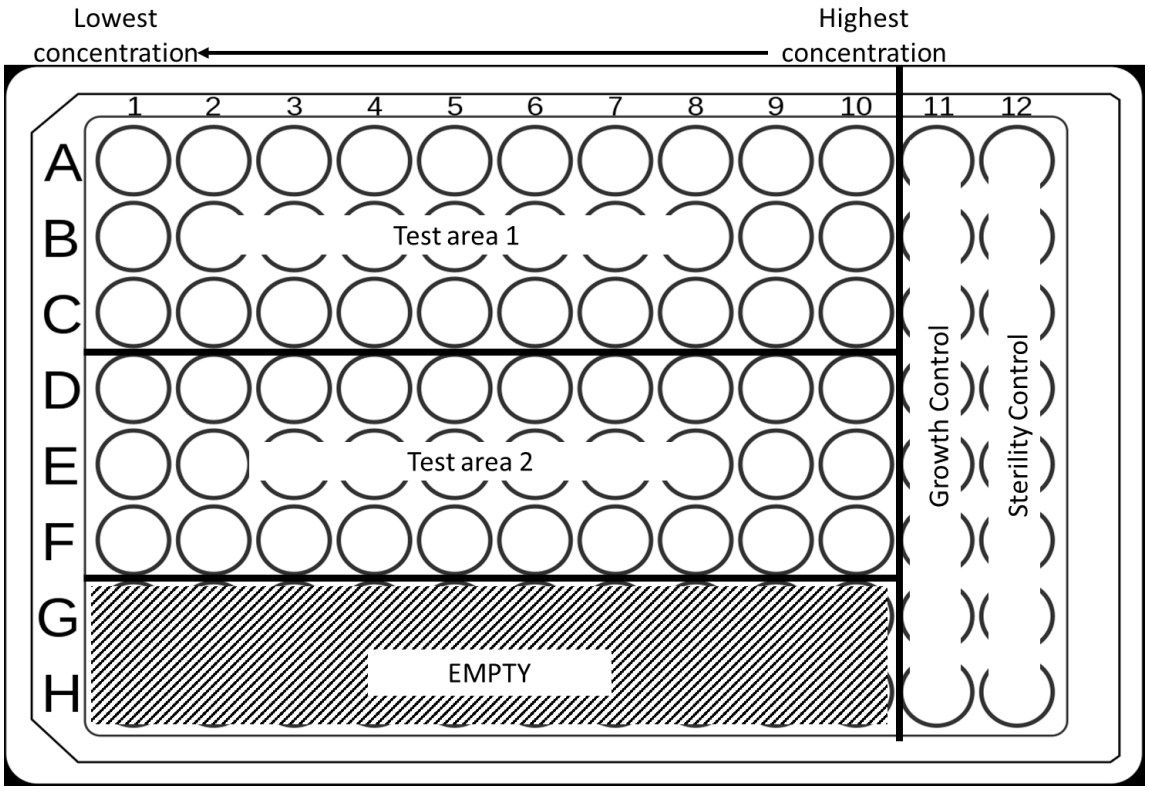

Figure 2.1 Layout of microtiter plates used for MIC testing. All wells not labelled as empty contained a final volume of 100 µL. Each test well contained 50 µL of 12-bis-THA and 50 µL of bacterial suspension. Growth control wells contained 50 µL of bacterial suspension and 50 µL of ultrapure water. Sterility control wells contained 50 µL of ultrapure water and 50 µL of double strength growth media.

For each 12-bist-THA concentration, 50 µL was added to three wells. Bacterial colonies were suspended in sterile water to a McFarland standard of 0.5 (Pro-Lab Diagnostics, Merseyside) and diluted 1:100 into double strength LB for *E. coli* NCTC_9001 or double strength MHB2 for *P. aeruginosa* PA14. 50 µL of bacterial suspension was added to each well in columns 1-11, to column twelve, 50 µL of double strength media and 50 µL of ultrapure water was added to act as a sterility control. To column eleven 50 µL of ultrapure water was added to the bacterial suspension to act as a growth control. From one growth control well 10 µL was taken and diluted 1:100 and 1:1000 and 20 µL spot plated onto LB agar to confirm cfu/mL of the bacterial suspension. All microtiter plates were incubated at 37 °C, and 200 rpm shaking for 16-18 h. Visual MICs were taken as the first non-turbid column. All MICs determinations were performed in triplicate.

In order to calculate cfu/ml, cultures were spot plated onto LB agar plates in triplicate as described above. Agar plates were incubated at 37 °C for 16-18 h and colonies counted. The formula used to calculate cfu/mL is as follows:

$$N = \frac{(C \times 50)}{10^{-D}}$$

Where N=cfu mL/1; C=number of colonies per plate, D=order of the 1:10 dilution.

2.1.4 Defining a Nanoparticle in the Context of this Thesis

Nanoparticles are a wide class of materials and are typically considered to be less than 100 nm in one dimension [87]. Although, this definition has expanded to include particles with dimensions less than 1000 nm, such as lipid nanoparticles which are typically 10-1000 nm in diameter. The exact definition of nanoparticle can differ from researcher to researcher, with some determining that the exact composition of the nanoparticles in question need to be determined before claiming it as such. As 12-bis-THA is a novel molecule, much is still yet to be determined regarding its interactions with TFDs. Currently it is yet to be proven the exact

number of molecules of 12-bis-THA that associate with each TFD molecule to form loaded nanoparticles (LNPs). Additionally, it is still yet to be determined if this 12-bis-THA/TFD interaction involves a true encapsulation (i.e. fully enclosed) of the TFD or just an association. However, as 12-bis-THA forms a measurably stable colloidal system on the nanoscale these aggregates will be referred to as nanoparticles in this thesis. Additionally, as previously published work [53] has referred to TFDs associated with 12-bis-THA as encapsulated, this term will be used within the thesis to describe this interaction.

2.1.5 Nanoparticle Treated Growth Curves

Microtiter plates were seeded as per 2.1.3 and in the layout shown in figure 2.2. Nanoparticle concentrations are stated as the 12-bis-THA component. Doubling dilutions of nanoparticles were used ranging from 100 µg/mL in column 10 to 0.195 µg/mL in column 2, column 1 contained no nanoparticle.

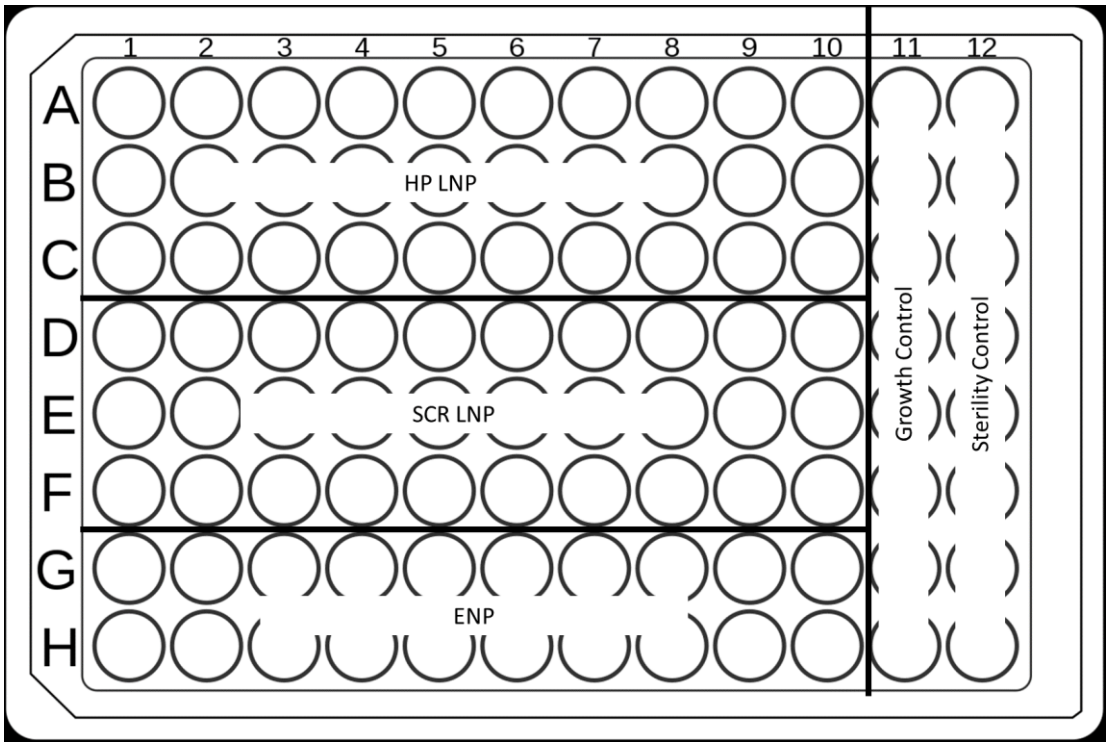

Figure 2.2 Layout of microtiter plates used for nanoparticle growth curves. HP = targeted. SCR = non-targeted, LNP=loaded nanoparticle, ENP=empty nanoparticle

2.2 SDS-PAGE

Polyacrylamide gel electrophoresis (SDS-PAGE) allows for the separation of proteins based primarily on molecular mass. The presence of sodium dodecyl sulfate eliminates the effects of charge and structure on separation and acrylamide provides a restrictive matrix for migration [88].

2.2.1 Materials

Isopropanol, Tris base, glycine, ammonium persulfate (APS) and sodium dodecyl sulfate (SDS) were obtained from ThermoFisher (Loughborough). 40 % acrylamide solution and tetramethylethylenediamine (TEMED) were obtained from Sigma (Gillingham). Precision Plus Protein Dual Colour Standards ladder, 12 % and 7.5 % pre-cast SDS-PAGE Mini-PROTEAN TGX gels, and gel casting system were obtained from BioRad (Watford). SDS loading dye (3x) and dithiothreitol (DTT) were obtained from New England Biolabs (Hitchin).

2.2.2 SDS-PAGE Gel and Buffer Recipes

Table 2.1 shows the recipes of the hand-cast gels used in this thesis. Gels percentages that would preferentially separate proteins with a molecular weight ≥ 50 kDa were selected for testing.

Table 2.1 Composition of Hand-cast SDS PAGE resolving gels

	6 %	7 %	7.5 %	8 %
Ultrapure Water	3.50 mL	3.30 mL	3.25 mL	3.20 mL
40 % Acrylamide	0.90 mL	1.05 mL	1.13 mL	1.20 mL
1.5 M Tris pH 8.8	1.5 mL	1.5 mL	1.5 mL	1.5 mL
10 % SDS	60 µL	60 µL	60 µL	60 µL
10 % APS	60 µL	60 µL	60 µL	60 µL
TEMED	6 µL	6 µL	6 µL	6 µL

Recipe is for 6 mL

A 4 % stacking gel was prepared for all PAGE gels according to the following recipe: 0.5 mL 40 % acrylamide, 3.1 mL ultrapure water, 1.25 mL 0.5 M Tris pH 6.8, 50 µL 10 % APS, 50 µL 10 % SDS, 5 µL TEMED.

A tris-glycine SDS running buffer was used for all experiments and was comprised of 6.06 g Tris, 28.8 g Glycine, 2 g SDS in ultrapure water adjusted to a pH of 8.3 and final volume of 2 L. For proteomic samples HPLC grade water was used (ThermoFisher).

2.2.3 Hand-Casting Polyacrylamide Gels

Gels were cast in two stages, first the resolving gel solution was added to the casting system and 100 µL of isopropanol added onto to smooth the surface and eliminate bubbles. The resolving gel was left to polymerise at room temperature for 60 min. The isopropanol was then removed and the top of the gel washed once with ultrapure water. An appropriate volume of stacking gel solution was then added, comb inserted and left to polymerise at room temperature for 30 min. Set gels were wrapped in moist paper and stored at 4 °C.

2.2.4 SDS-PAGE Protocol

All polyacrylamide gels were resolved using a Mini-PROTEAN Tetra Vertical Electrophoresis Cell (BioRad). All protein samples were reduced by 1 µL of 30x DTT (1.25 M) without boiling. The maximum total volume loaded onto gels was 20 µL, containing 5 µL of 3x SDS loading dye. 5 µL of protein ladder was loaded for each experiment. All SDS PAGE experiments were run at 100 V for 20-25 min for fractionated samples and until ladders were fully resolved for 12 % fully resolved gels, typically 1 h 10 min. Stained gels were imaged using BioRad Chemidoc XRS.

2.3 Native PAGE

2.3.1 Materials

O'Range 5 bp ladder and SYBR safe were obtained from ThermoFisher (Loughborough). The gel casting system was obtained from BioRad (Watford). SDS free loading dye (6x), and low molecular weight ladder were obtained from New England Biolabs (Hitchin).

2.3.2 Native PAGE Gel and Buffer Recipes

The recipe for 5x Tris-Borate-EDTA (TBE) used was: 5.4 g Tris, 27.5 g boric acid, 20 mL 0.5 M EDTA (pH 8) in ultrapure water to a final volume of 1 L. 5x TBE was diluted 20 mL in 1000 mL to make 1x TBE running buffer used in native PAGE experiments.

The recipe for 20 % gel used is as follows: 6 mL 40 % acrylamide, 3.6 mL ultrapure water, 2.4 mL 5x TBE, 200 µL APS, 10 µL TEMED

2.3.3 Hand-Casting Polyacrylamide Gels

The gel solution was added to the casting system, comb inserted and was left to polymerise at room temperature for 60 min. Set gels were wrapped in moist paper and stored at 4 °C.

2.3.4 Native PAGE Protocol

Gels were resolved using a Mini-PROTEAN Tetra Vertical Electrophoresis Cell (BioRad). For each TFD 0.5 µL of 1 mg/mL TFD was loaded with 6x loading dye in a final volume of 10 µL. 1 µL of low molecular weight ladder and 2 µL of O'Range 5 bp ladder were loaded for each experiment. Gels were electrophoresed at 110 V at 100 min for and post stained with 5 µL SYBR safe in 100 mL 1x TBE for 30 min. Gels were imaged on Syngene G:Box Chemi XRS.

2.4 Western Blot

2.4.1 Materials

Tris, sodium chloride, hydrochloric acid, glycine, methanol, nitrocellulose membrane, polyvinylidene difluoride membrane and Tween 20 were obtained from ThermoFisher (Loughborough). Skimmed milk powder was obtained from Sigma Aldrich (Gillingham). Anti-RpoB (ab191598) was obtained from Abcam (Cambridge). Anti-rabbit HRP-linked IgG was obtained from Cell Signalling Technologies (Netherlands). Western blot transfers were conducted using a Mini-PROTEAN Tetra Vertical Electrophoresis Cell (BioRad).

2.4.2 Buffer Recipes

Transfer buffer: 6.06 g tris, 28.8 g glycine, 400 mL methanol, distilled water to 2 L, pH 8.3.

10x Tris buffered saline (TBS): 24 g tris and 88 g NaCl dissolved in 900 mL distilled water. pH to 7.6 with 12 N HCl and make up to 1 L with distilled water.

Washing buffer (TBST): 100 mL of 10x TBS, 900 mL distilled water, 1 mL Tween 20 make up to 1 L with distilled water.

Blocking buffer: 5 % (w/v) skimmed milk powder in TBST.

2.4.3 Western Blot Protocol

SDS PAGE gels were resolved as described above and proteins were transferred from the gel to a 0.2 µm nitrocellulose membrane at 100 V for 1 h at 4°C. The membrane was incubated in blocking buffer at room temperature for 1 h with rocking.

A 1 in 2000 dilution of rabbit anti-RPOB antibody (Abcam) was prepared in 1 % skimmed milk powder in TBST. The membrane was incubated, with rocking, in this solution overnight at 4°C then for a further 1 h at room temperature. The membrane was washed (3x) TBST. A 1 in 2000 solution containing the secondary anti-rabbit IgG HRP-linked antibody (CST) in 1 % milk in TBST

was added. The membrane was incubated in this solution for 1 h at room temperature with rocking. After this the membrane was washed with TBST and imaged (BioRad Chemidoc XRS) and 30 seconds of exposure. Western blot densitometries were analysed by importing tiff images into the NHI open-source software ImageJ.

2.5 Agarose Gel Electrophoresis

2.5.1 Materials

Agarose, glacial acetic acid and ethylenediaminetetraacetic acid (EDTA) were obtained from ThermoFisher (Loughborough).

2.5.2 Recipes

The recipe for 50x Tris-acetate-EDTA (TAE) used was: 242 g Tris base, 57.1 mL of glacial acetic acid, 100 mL of 0.5 M EDTA (pH of 8.0), distilled water to 1 L. 50x TAE was diluted 20 mL in 1000 mL distilled water to make 1x TAE used as running buffer in agarose gel electrophoresis experiments.

The recipe for 1.8 % agarose gel used is as follows: 1.8 g agarose melted into 100 mL 1x TAE. To pre-stain the gel 10 µL of SYBR safe was added to 100 mL of molten agarose gel.

2.5.3 Agarose Gel Electrophoresis Protocol

Cast gels were loaded with 10 µL of PCR product with 6x loading dye and 2 µL of LMW ladder. Gels were electroporated in 1x TAE at 80 V until the loading dye had travelled two thirds down the gel. Gel were imaged using Syngene G:Box Chemi XRS.

2.6 Proteomics

2.6.1 Reference Proteomes used in Proteomic Analysis

Reference proteomes used in the proteomic analysis were obtained from Uniprot [89]. For *E. coli* NCTC_9001 analysis the reference proteome used was *Escherichia coli* K12, proteome ID UP000001478. For *P. aeruginosa* PA14 analysis the reference proteome used was *Pseudomonas aeruginosa* UCBPP-PA14, proteome ID UP000000653.

2.6.2 Determination of s0 for Proteomic Data Analysis

In order to determine significance of quantitative data in proteomics, data is subjected to two filtering thresholds. The horizontal threshold (FDR) and vertical threshold (fold change). These thresholds are often combined and smoothed into curves to form a volcano plot. The parameter that drives this smooth thresholding is s0 which is known as the 'fudge factor'. First defined by Tsuher et al in 2001 [90], s0 is derived from the SAM (significance of analysis of microarrays) test (a variation of the t-test) and is a constant added to estimated standard deviations to reduce the overestimation caused by small standard deviations. As s0 can greatly bias data if used incorrectly it is important to carefully consider this value before proceeding with analysis [91]. For *E. coli* proteomics s0 was left at the default of 2 as no data was near the threshold of significance and fine-tuning was superfluous. In the case of *P. aeruginosa* data analysis s0 was set at 0.2 to mimic the thresholds of fold change of >0.5 and FDR=0.5. Figure 2.3 illustrates how this was implemented.

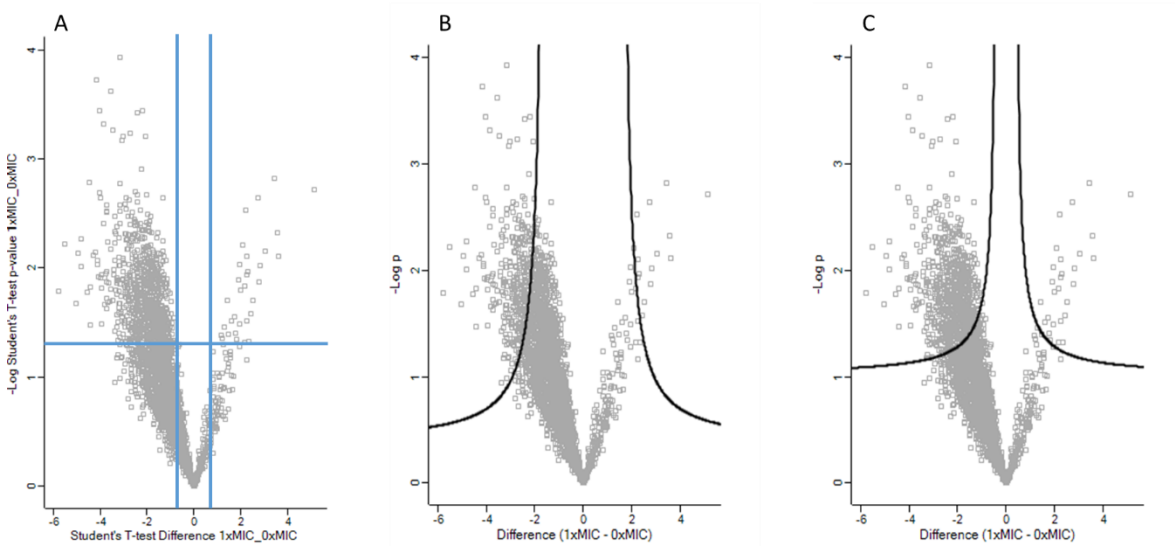

Figure 2.3 Determination of s0 for P. aeruginosa proteomic data analysis (A) scatter plot with horizontal and vertical thresholds shown independently, (B) volcano plot with FDR=0.5 and default s0=2 (C) volcano plot showing s0 adjusted to mimic thresholds in (A). Solid lines indicate boundary of significance. For (C) s0=0.2 and FDR=0.5

2.6.3 Use of R in Proteomic Data Analysis

In order to analyse the rich data sets produced by LC-MS/MS analysis, the programming language R was utilised [92]. All R scripts were written in RStudio and utilised the himsc and gdata packages alongside the himsc library. The scripts written and used for this thesis are available in the appendix. Initially the scripts were written for use in the *E. coli* proteomic data analysis and were later repurposed for use in *P. aeruginosa* proteomic data analysis. The repurposing involved changes of relevant import and export file names while maintaining the basic functions written in the code. All datafiles used in the R analysis were in .csv format to prevent corruption during the file importing process.

For transcription factor (TF) focused analysis, R scripts utilised a TF reference list, which was imported into the workspace. Gene names were used as a unique identifier for cross-referencing and extraction of TF focused data from the proteomic output. These focused extracts were outputted as .csv files to be used in further analysis.

For dataset comparison once again gene names were used as the unique identifier. Scripts were able to determine what was common and not between datasets and export this data as .csv files.

Chapter 3: Development of Proteomic Methods to Enrich for *Escherichia coli* Transcription Factors

3.1 Introduction

A transcription factor (TF) is a regulatory protein which binds to a specific DNA sequence upstream or downstream of a target gene, regulating the transcription of the target DNA into messenger RNA and through this, gene expression. TFs can work independently or complex with other proteins in promoting or blocking the recruitment of RNA polymerase to their target genes. Though the DNA-protein binding interaction is sequence specific, binding sites for one TF can differ between target genes [52]. In *Escherichia coli* transcription factors are typically low copy [93, 94] and the majority are below 50 kDa in size [95] which can make detection of these proteins difficult in MS-based proteomics, as these signals can be masked by more abundant and larger proteins.

The use of 12-bis-THA to deliver TFDs induces the expression of stress response genes, therefore, this chapter aimed to develop and optimise a proteomic method for identifying the change in transcription factor levels in response to this stress. This chapter utilised the completely annotated model organism *E. coli* for this method development. Initial objectives involved determining the optimal size fractionation technique for enriching for TFs in 12-bis-THA treated proteomic samples. Following the determination of the most suitable enrichment technique the aims focused on use of a label-free LC-MS/MS proteomic approach to determine successful TF enrichment. A secondary method for determining the equal loading of protein samples sent for proteomic analysis using RpoB Western blot analysis was also investigated.

3.2 Materials and Methods

Materials

Skimmed milk powder, Luria broth agar and Luria broth were obtained from Sigma Aldrich (Gillingham). Coomassie blue, silver stain kit, BCA kit, HPLC grade water, acrylamide, Tris, SDS, N,N,N',N'-tetramethylethylene-diamine (TEMED) ammonium persulfate (APS), methanol, glycine, urea, sodium hydrogen carbonate, Kartell cuvettes, blades, 96-well polystyrene plates and petri dishes were obtained from Fisher Scientific (Loughborough). SDS loading dye (3x) and DTT were obtained from New England Biolabs (Hitchin). Precision Plus Protein Dual Color Standards ladder, 12 % and 7.5 % SDS-PAGE gels were obtained from BioRad (Watford). Anti-RpoB (ab191598) was obtained from Abcam (Cambridge). Anti-rabbit HRP-linked IgG was obtained from Cell Signalling Technologies (Netherlands).

MIC Determination

The MIC of 12-bis-THA against *E. coli* NCTC_9001 was determined as described in 2.1.3.

Escherichia coli NCTC 9001 Growth Curves

Overnight cultures of *E. coli* NCTC_9001 were diluted to an OD_{600nm} of 0.05 in 100 mL LB and grown to an OD_{600nm} of 0.5 at 37 °C and shaking at 200 rpm. At this point the culture was split and 12-bis-THA was added at 0, 0.1 and 1x MIC. Culturing continued, monitoring every 20 min, reducing to 10 minutes as OD_{600nm} increased until an OD_{600nm} of 1.4 at which point they were harvested. All optical densities were determined using a Spectramax M2 reader.

Protein Extraction

E. coli NCTC_9001 cultures were harvested and washed 2x with PBS and pelleted at 4200 x*g* for 25 minutes at 4°C. Cells were then lysed in 1 mL 8 M urea, 25 mM $NaHCO_3$ lysis buffer (urea lysis buffer) using sonication on wet ice. Sonication (Soniprep 150) was conducted using bursts of 10 seconds on at 10 mA, 30 seconds off, repeated 10 times.

Following sonication, samples were centrifuged for 40 minutes at 4°C at 16100 x*g*. The supernatant was then taken off and retained and pellet discarded. The protein concentration of the supernatant was determined using the Pierce BCA assay kit from ThermoFisher.

Size Fractionation Investigations

Size Fractionation by Filtration

Fractionation of TPL using size fractionation filters was investigated. Total protein lysate (TPL) was adjusted to a concentration of 1 mg/mL in order to not overload the filters. Briefly, a sample of TPL containing 1 mg protein was loaded onto 50 kDa Amicon filters and centrifuged at 4000 *xg* for 10 minutes at room temperature in a swing bucket centrifuge (Eppendorf 5810R). Filters were washed with 3 mL sterile water after centrifugation and a BCA assay conducted on both retentate and filtrate. The proportion of the total protein present in the retentate and filtrate was then determined and 10 µg total protein (9 µg retentate and 1 µg filtrate) were loaded onto a 12 % SDS page gel and the gel was run as described in 2.2.4. before Coomassie staining. Briefly, gels were stained with Coomassie stain for 30 minutes, then washed with distilled water and destained for 18 h.

In-Gel Fractionation

Additional experiments involved conducting SDS-PAGE experiments at 100 V using 6 %, 7 %, 7.5 % and 8 % hand cast gels and 7.5 % gels from BioRad. Initial optimisation experiments used fixed volumes of TPL rather than standardised concentrations.

Gels were loaded with 20 µL of a denatured TPL and electrophoresed until the 50 kDa ladder marker (BioRad, Precision Plus Protein Dual Colour) had resolved from the dye front. Bands containing the dye front were then cut at 50 kDa using sterile razor blades. Bands were minced and passively eluted overnight in 1 mL of transfer buffer (25 mM Tris, 192 mM glycine, 20% methanol, pH 8.3) at 30 °C and 200 rpm shaking. Protein was then precipitated using the acetone method [96]. Briefly, 400 µL of ice-cold acetone was added to 100 µL of eluted protein

and incubated at -20 °C for 1 h. The mixture was then centrifuged at 10000 x*g* for 15 minutes at 4°C. Pellets were air dried and resuspended in 20 µL of urea lysis buffer. SDS-PAGE was performed as detailed in 2.2.4.

Gels were silver stained as per the manufacturer's instructions (Fisher). Briefly, gels were washed with ultrapure water for 5 minutes, fixed in 30 % ethanol:10 % acetic acid solution for 30 minutes, with one change of the fixing solution. Then washed 2x in 10 % ethanol and 2x in ultrapure water for 5 minutes each. Gels were then incubated in Sensitizer Working Solution for exactly 1 minute, then wash with two changes of ultrapure water for 1 minute each. Then gels were incubated in Stain Working Solution for 30 minutes. Following this 2x 20 second washes of ultrapure water were carried out. Working solution was then added and gels incubated for 2-3 minutes until bands had developed. A 5 % acetic acid solution was added to stop stain development.

Western Blot

Following filtration of total *E. coli* NCTC_9001 lysate a western blot for the presence of RpoB was conducted. An SDS-PAGE was run as described above loading 10 µg total protein on a 12 % SDS-PAGE gel. Western blots were then preformed as described in 2.4.3

Proteomic Sample Preparation

All samples were sent to the Oxford Advanced Proteomics Facility for analysis. At the facility samples were subjected to a trypsin digest followed by LC-MS/MS analysis using a 2-hour gradient and Q Exactive mass spectrometer (Thermo Scientific) with HPLC. Unfortunately, due to the closure and change in staff at the Oxford Advanced Proteomics Facility, further details into the exact sample preparation that occurred at the facility during this analysis was not provided in time for inclusion into this thesis.

The final set of biological repeats and total protein lysate samples were subjected to an additional C18 column clean up (desalting) as per Rappsilber et al., 2007 procedure 1A, C18-

stage tips for clean-up and concentration [6]. Briefly, disks were wetted with 20 µL of methanol, once the methanol was passed through the stage tip 20 µL of a 0.5 % acetic acid and 80 % acetonitrile solution was passed through the tip. This was then followed by passing 20 µL of 0.5 % acetic acid through the tip. The sample acidified by an acetic acid 5 % stock was then loaded and washed with 20 µL of acetic acid. The sample was then eluted with two applications of 10 µL acetic acid 0.5 % and acetonitrile 80 % solution. Once again due to the situation described above at the proteomics facility, the C18 column specifications and the exact volume of 5 % acetic acid used to acidify the samples were not provided.

Fractionated Samples

Proteomic analysis was carried out on fractionated samples treated with 0.1 and 1x MIC 12-bis-THA (a high and low dose) and an untreated control. Proteomic samples were prepared by loading 20 µg of TPL for each treatment condition onto a 7.5 % SDS-PAGE gel. Gels were run as described for in-gel fractionation above. Bands containing the dye front were then excised at 50 kDa using sterile blades and placed into low protein binding tubes (Eppendorf) and sent to Oxford Advanced Proteomics Facility for analysis. The top half of the gel was used for Western Blot analysis to detect the presence of RpoB and verify equal loading of samples. For each condition three biological repeats were sent for analysis over a period of 8 months.

Total Protein Lysate Samples

In addition to the ≤50 kDa fractionated samples, one set of TPL samples (0, 0.1 and 1x MIC) were also sent for analysis. These were the unfractionated lysates of the final fractionated biological replicate. To prepare the samples 20 µg of DTT denatured total protein lysate for 0, 0.1 and 1x MIC was loaded onto 12 % SDS-PAGE gels. Gels were run at 100 V until the dye front had travelled 10mm into the gel. The 10mm band was then excised and sent for analysis.

Proteomic Data Analysis

Mass Spectra Analysis

The spectra generated by the Oxford Advanced Proteomics Facility were then analysed using the MaxQuant program (version 1.6.3.3) and label-free quantification (LFQ) algorithm [97, 98]. Only one parameter group was set for the analysis. The group specific parameters used for spectral analysis were as follows: type was set as standard with a multiplicity of 1, modifications were set as the default of a maximum of 5 per peptide. The default variable modifications of oxidation and acetyl (protein N-term) and fixed modifications as carbamidomethyl were used. The digestion mode was specified as trypsin and the maximum number of missed cleavage sites as 2. The default LFQ settings were used. The match type was set as from and to, and re-quantification was turned on. The instrument was set as orbitrap and default settings used. The reference spectral database used was generated using a proteome FASTA file for *E. coli K12* obtained from UniProt [89]. Global parameters were set as: contaminates to be included and minimum peptide length set at 8, all other peptide parameters were set at the default. For global LFQ, the default options were selected with the addition of iBAQ and separate LFQ by parameter groups. Unique and razor peptides were used for protein quantification. The FDR was 0.01. All For all other settings default parameters were used.

Computational Data Analysis

Analysis of the resulting datasets was conducted using Perseus (version 1.6.7.0) [99]. The data were processed in Perseus by normalizing using a log2 transformation. Then proteins detected in only one replicate were removed from the data set and missing data was replaced using normal distribution with a width of 0.3 and down shift of 1.8. For the generation of volcano plots a pairwise student's t-test was used with S0 set to 2 and FDR set to 0.01. Permutation-based FDR was used for truncation.

Scripts written in R were used to extract TF only data for focused analysis. Additional R scripts were used to determine commonality of TFs detected in each biological repeat (see Appendix and 2.6.3).

Uniprot ID mapping [89] was used to generate gene ontology (GO) annotations with regards to the cellular locations of the proteins identified in each dataset. Protein identifiers were uploaded to the Uniprot retrieve/ID mapping tool and mapping from UniprotKB AC/ID and mapping to UniprotKB were selected as the search parameters.

3.3 Results and Discussion

3.3.1 MIC Determination

The MIC of 12-bis-THA against *E. coli* NCTC_9001 was determined to be 0.88 µg/mL±0 from three replicates. The MIC of 12-bis-THA against *E. coli* NCTC_9001 was found to be 0.88 µg/mL, which is similar to the lowest MICs of DQC reported in the literature [100], where one study found the DQC MIC in MHB to be 2 µg/mL in *E. coli* NCTC_10418 [101].

3.3.2 Growth Impact Investigations

The growth of NCTC 9001 in the presence of varying concentrations of 12-bis-THA was examined in order to standardise the samples sent for proteomic analysis. Initial investigations focused on growth in the presence of 0, 0.1, 1 and 5x MIC (Figure 3.1). These concentrations were chosen to represent sub-MIC, MIC and above MIC conditions. This would allow for analysis of the proteomic data to be related to the effects of varying the concentrations used. Both the untreated control and 0.1x MIC treatment reached the target OD_{600nm} of 1.4 at 3.5h. The 1x MIC treatment delayed growth with the target OD reached at 4h. At 5x MIC it was observed that the bacteria were unable to grow to the desired optical density (Fig 3.1) and therefore this condition was excluded from the proteomic analysis.

The delayed growth observed at 1x MIC was likely due to stressors brought about by 12-bis-THA activity. The causes of these stressors are likely the outer membrane disruptions and subsequent increased permeability of membranes caused by 12-bis-THA binding [53]. The parental molecule DQC is known to affect bacterial metabolism alongside effects on membrane permeability [100]. DQC has been shown to affect metabolism via inhibition of mitochondrial ATP synthesis, inhibition of protein synthesis at the ribosomal level and by the denaturing of proteins [100]. Therefore, it is likely that 12-bis-THA may also affect metabolism and these effects combined with membrane disruptions resulted in the observed growth delay.

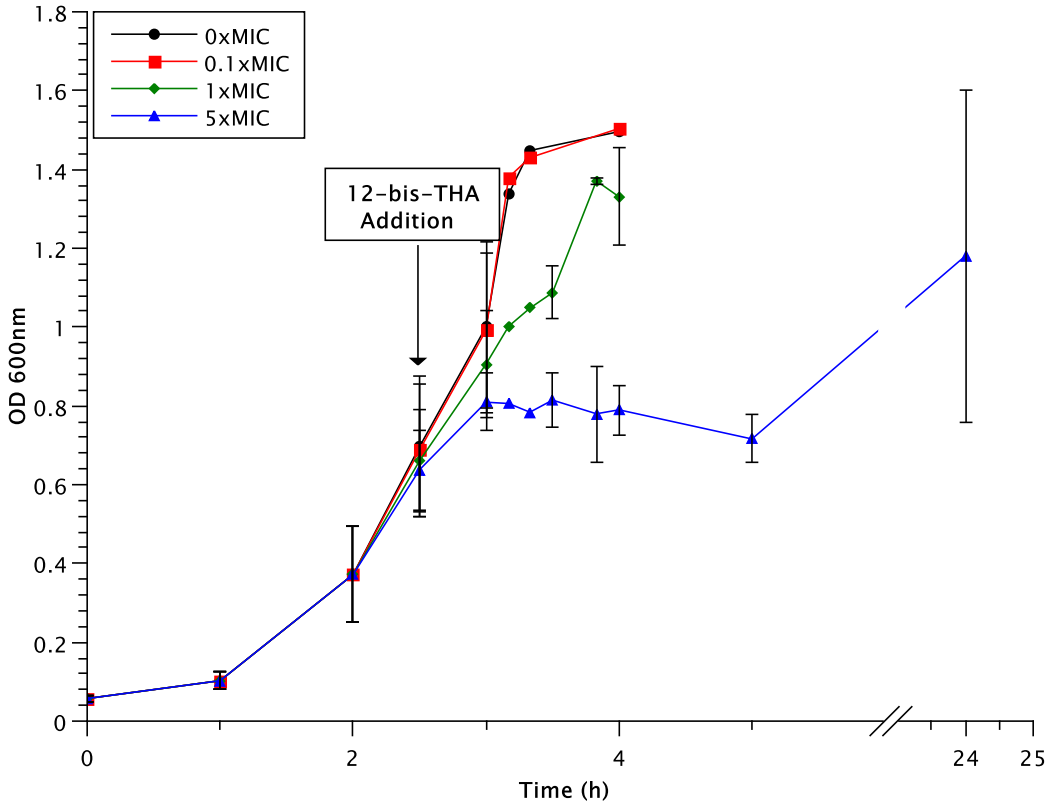

Figure 3.1 Growth Curves of E. coli NCTC_9001 treated with 12-bis-THA. Cultures were grown to OD_{600nm} 0.5 then split and 0, 0.1, 1 and 5x MIC 12-bis-THA was added to the culture. Bacteria were grown at 37°C and 200 rpm. n=3±SD.

A target OD_{600nm} of 1.4 was chosen based on a previous proteomic study investing the effects of vancomycin induced stress on the *Staphylococcus aureus* proteome [74]. This study generated a rich insight into the *S. aureus* proteome utilising a method involving treating samples at 0.5 OD_{600nm} and harvesting samples at 1.4 OD_{600nm}.

3.3.3 Size-Fractionation Techniques

Sample preparation is a critical aspect of proteomics experimental design as the quality and composition of the sample analysed greatly impacts the quality of the resulting data [94, 97, 102]. The limitations of LC-MS/MS technology can result in the masking of low signal proteins by proteins with higher peak intensities, causing potentially important data to be lost. As TFs are typically low copy it is likely that if the total protein lysate (TPL) was analysed some TF signals may not be detected due to the masking effect. Therefore, to optimise for the detection of TFs

by LC-MS/MS samples were size fractionated prior to analysis as better resolution can be obtained with less complex samples. As TFs are typically <50 kDa [89, 95, 103] this mass was targeted as the desired cut-off. This thesis will describe two size-fractionation methods investigated to generate this sub 50 kDa fraction for analysis.

Size Fractionation by Filtration

Initial sample fractionation experiments were conducted using 50 kDa Amicon filters. Mass balancing of the retentate and filtrate in relation to the loaded total protein lysate (TPL) amount showed a total protein loss of 22.8 % ± 7.3 during filtration. Bicinchoninic acid assay (BCA) results also indicated that 88.3 ± 1.2% of protein mass remained in the retentate and 11.7 ± 1.2% entered the filtrate (Table 3.1).

Table 3.1 Protein mass recovered from filtration of 1mg TPL

Treatment Condition	Filtrate (µg)	Retentate (µg)	Total Recovered (µg)
0 x MIC	90	598	688
0.1x MIC	76	685	761
1 x MIC	105	761	866

The filtrate, retentate and TPL samples were loaded onto a reducing 12 % SDS gel in order to visualise whether fractionation at 50 kDa had been successful. Due to the low concentration of protein present in the filtrate protein samples were load as per the percentage fractionation determined above. Figure 3.2 shows the result of a Coomassie stained gel loaded with 10 µg TPL, 9 µg retentate and 1 µg filtrate. Little difference can be seen between the distribution of protein banding of TPL and retentate, indicating that proteins with masses ≤50 kDa remained in the retentate. Due to the low amount of protein present in the filtrate, protein bands were poorly visualised with Coomassie staining, however faint protein bands can be observed above

and below the 50 kDa cut-off (highlighted in Figure 3.2 by red boxes). A duplicate gel was silver stained to confirm the presence of proteins in the filtrate.

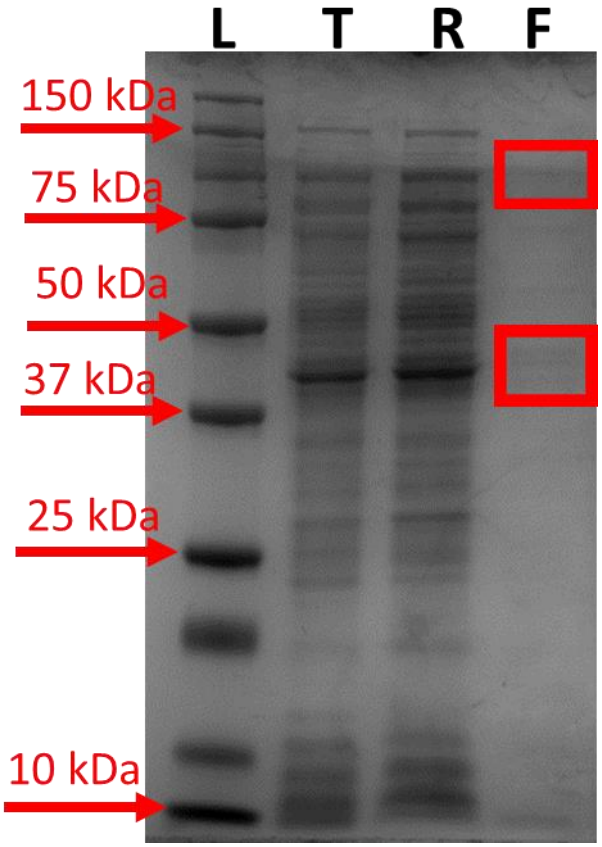

Figure 3.2 SDS-PAGE Coomassie stained gel showing proteins present in the TPL (T), protein retentate (R) and filtrate (F) L indicates protein ladder. 10 µg of TPL, 9 µg of retentate and 1 µg of filtrate was loaded onto the gel.

Figure 3.3 shows the results of the silver-stained gel. To permit visualisation of the filtrate, the retentate was overstained. Bands below 50 kDa are detected in all three retentate samples. Protein bands at 100-75kDa were observed for all three filtrate samples. These results indicate that this technique failed to efficiently fractionate the sample at 50 kDa.

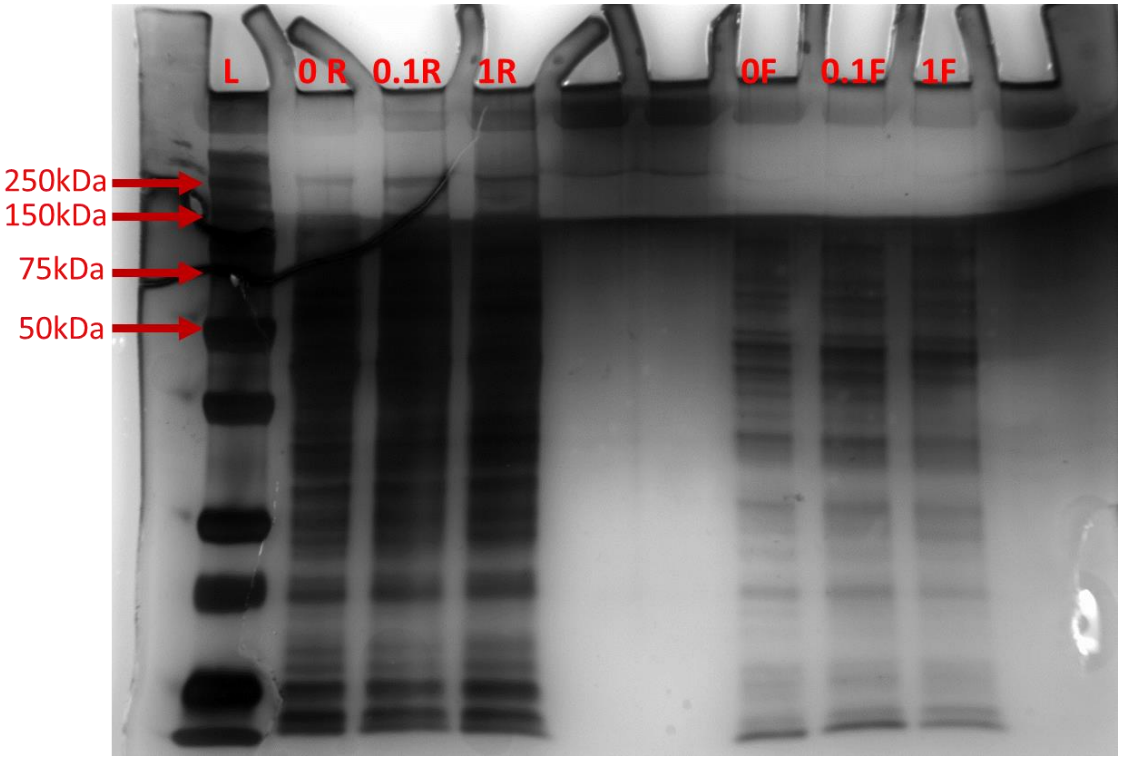

Figure 3.3 Silver stain of protein retentate (R) and filtrate (F) following SDS-PAGE. 9 µg of retentate and 1 µg of filtrate was loaded onto the gel. To visualise the filtrate, the retentate was overstained. L: protein ladder; 0, 0.1 and 1 refer to samples obtained from bacteria treated with 0, 0.1 and 1x MIC 12-bis-THA.

A 20-30 % protein loss was observed during the filtration process, indicating the likelihood that protein adsorption to the filter was occurring. This phenomenon has been previously reported, with one study finding adsorption followed time-dependent saturation kinetics [104, 105]. Although the issue of protein loss via adsorption to the filter could be tackled by coating with compounds such as PEG [106], this would introduce complications in the MS analysis. PEG is very efficiently ionised in mass spectrometers and is widely used as a calibrant for MS analysis. The inclusion of PEG would greatly interfere with protein analysis due to signal masking [107].

The issue of contaminants from surface coating is naturally seen with the filter separation method, as the filters we used were coated with glycerol. This coating is added by the manufacture to aid in the preservation of the filter during its shelf life. However, glycerol has been shown to interfere in the MS analysis of the proteome [108] resulting in reduced protein detection. Although it could be argued that the amount of glycerol entering the sample via

filtration is minimal it is best to reduce any possibilities of contamination introduction. Additionally, the option of washing the filters to remove the glycerol prior to protein filtration is available. In order to prevent the introduction of contaminants high purity water will be required and several washes would be needed to remove the glycerol. Although a good option care would need to be taken that the filter did not dry out during these wash steps as this could lead to loss of filter integrity.

Analysis of the protein molecular weight profile of the filtrate and retentate on SDS-PAGE gel showed that the filtration method had failed to give accurate separation of the protein sample. Proteins with masses above 50 kDa were detected in the filtrate and proteins below 50 kDa were detected in the retentate. These results indicate a lack of molecular weight resolution for this product.

Separation of complex protein mixtures based solely on hydrodynamic radius can result in artefactual retention of proteins that are present in oligomerised states. Transcription factors, for example, are often functional in homo- and hetero-oligomeric states. Bottom-up proteomics identifies proteins based upon the component peptide detected in the final MS step and therefore, TFs are identified in their monomeric form. As many TFs can exist in a multimeric from *in vivo* using filtration without reduction can result in TF loss in the final sample resulting in potential loss of important results and missing identifications of potential TFD targets [67, 109]. Preparation of the *E. coli* samples for proteomic analysis involved lysis into a urea buffer to denature and aid in solubilising the proteins prior to analysis. Care was taken not to heat the urea as doing so could lead to carbamylation of the proteins, leading to incomplete enzymatic digestion which would greatly affect the MS analysis [110]. Reduction using DTT was then applied to eliminate dimers and multimers linked by disulphide bridges. However this was not compatible with the filtration fractionation method due to the incompatibility of reducing agents with the BCA assay make colorimetric protein quantification difficult [111]. Although

there are BCA assays available that are compatible with DTT and other agents, there are limits to the concentrations that can be used with these compatible assays, therefore they are not always appropriate [111]. Although not shown in the results of this chapter, an experiment involving protein reduction using DTT prior to filtration was conducted. Unfortunately, accurate quantification the amount of protein in the retentate and the filtrate was not possible due to the incompatibility of DTT with the BCA assay. The interaction of the DTT with the copper based working reagent used in the BCA assay resulted in an excessive colour shift. This resulted in the samples being unable to be assigned an absorbance value by the spectrometer and therefore unable to be analysed. Hence, these results were excluded from this chapter.

Although sample fractionation via filtration is a valid method in proteomic sample preparation, the failure to achieve accurate separation with the filters tested, loss of proteins via adsorption and potential for contaminate introduction indicated this method was less desirable for this study. Additionally, as an in-gel trypsin digestion was commissioned to prevent protein loss via aggregation via in-solution digestion [96], filtered samples would have to be loaded and run into SDS-PAGE gels, introducing another processing step. Given these factors, investigations moved focus to developing an in-gel fractionation technique to achieve the desired <50 kDa protein fraction of interest with minimal protein loss.

In-Gel Fractionation

An alternative method of protein size fractionation using an in-gel method was investigated. This method would involve merely excising the dye front to fractionate the sample for proteomic analysis. This is a routine approach used in the preparation of LC-MS/MS protein samples and optimised protocols exists to aid protein extraction from the gel. Samples of TPL were electrophoresed on 6, 7, 7.5 and 8 % SDS-PAGE gels. Once the 50 kDa ladder marker has begun resolving the dye front was excised, proteins extracted and analysed separately on a 12 % gel. Figure 3.4 shows a silver-stained 12% PAGE gel after analysis of the extracted gel bands.

Fractionation of the samples at 50 kDa can be seen for 6, 7 and 7.5 % gels with no significant protein bands observed above the 50 kDa marker. For proteins extracted from the 8 % gel, protein bands were detected between 75 and 50 kDa, indicating inefficient poor size fractionation.

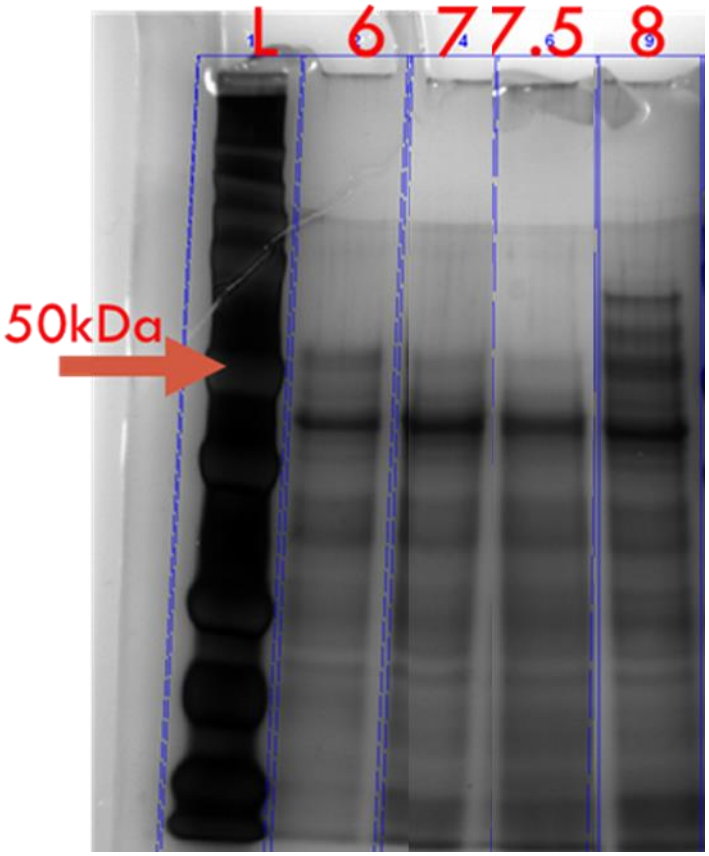

Figure 3.4 Silver stained SDS-PAGE gel for protein eluted from the dye front bands excised from 6, 7, 7.5 and 8 % SDS-PAGE gels. L=ladder, 6=6 % gel samples, 7=7 % gel sample, 7.5=7.5 % gel sample and 8=8 % gel sample

Due to the availability of a commercially produced 7.5 % gel this percentage was chosen for use in the finalised sample preparation protocol. The use of commercial 7.5 % SDS-PAGE gels eliminates the risk of protein loss due to protein cross-linking with non-polymerized gel components as well as reduced contamination from dust particulates that would greatly impact on MS analysis through keratin signal interference.

3.3.4 Proteomic Sample Preparation

Fractionated Samples

The commercial availability of pre-cast 7.5 % SDS-PAGE gels prompted their use in the preparation of the proteomic samples. Total protein lysates were quantified using a BCA assay and 20 µg loaded. Equal loading of protein samples into the gel lanes was assured by precise quantification of total protein using a BCA assay and further confirmed by examining the presence of the 150 kDa constitutively expressed protein, RpoB. This was achieved by Western blotting the top half of the gel from which the dye front samples had been excised.

Gel fractioned protein samples were sent for LC-MS/MS analysis over a period of eight months. A total of five batches of samples were sent to the Oxford Advanced proteomics facility. Only three batches met the criteria for computational analysis. One batch was excluded on the basis of a poor Western blot result that indicated highly unequal loading. Another batch was excluded due to the inability to remove proteins from the gel.

3.3.5 Proteomic Sample Quality Control

Figure 3.5 shows the various stages of sample preparation for all three data sets that were sent for analysis. The growth curves for all 3 sets shows that the target OD_{600nm} of 1.4 was reached within an average of 210 min ± 6.2 min for 0 and 0.1x MIC treatment conditions and 240 min ± 14 min for 1x MIC treatment condition (Fig. 3.5Ai-Aiii). All SDS-PAGE gels were run at the same voltage until the 50 kDa band had begun to emerge, although this is difficult to see in Fig. 3.5iii due to the quality of the photograph (Fig. 3.5Bi-Biii). Figure 3.5Ci-Ciii shows the results of the Western blot analysis of RpoB retained in the top half of the gels sent for analysis. Western blot bands were often uneven or fragmented due to the challenges associated with the transfer of small, fragile gel fragments to the blotting apparatus (Fig3.5Cii). Due to technical difficulties of the protein transfer it was difficult to quantify the bands using imaging software, however they did provide a rough snapshot into whether equal sample loading had occurred. The results of

the densitometric analysis can be seen in table 3.2. The average densiometric value across all nine bands was determined to be 170±8.9, concluding that comparable sample loading had occurred for all tested conditions across all three sample Sets sent for LC-MS/MS analysis.

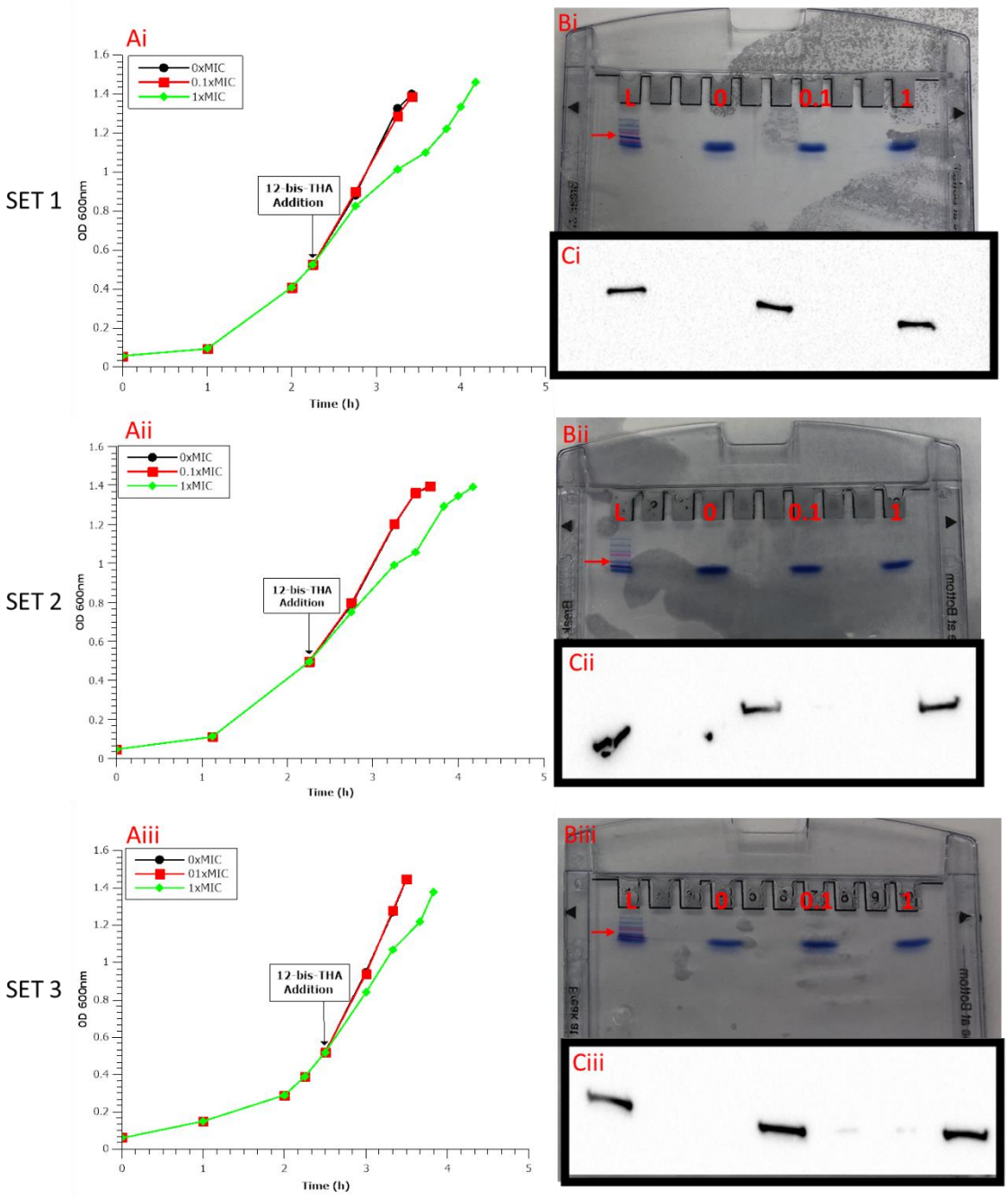

Figure 3.5 Sample preparation for proteomic analysis for all three data Sets (1-3). (Ai-iii) Growth curves generated, (Bi-ii) SDS-PAGE gel run for fractionation, (Ci-ii) Western Blot of RpoB in top half of resolving gel. L: protein ladder; 0, 0.1 and 1 refer to samples obtained from bacteria treated with 0, 0.1 and 1x MIC 12-bis-THA. Red arrow: 50 kDa ladder marker. Western blots exposure time was 1 s.

Table 3.2 Densiometric Analysis of RpoB Western blot bands

	Set 1	Set 2	Set 3
0 x MIC	163	170	186
0.1 x MIC	161	184	162
1 x MIC	173	163	174
Standard Deviation	5.25	8.73	9.80
Coefficient of Variation (%)	3.17	5.07	5.63

Densitometric analysis of RpoB Western blots indicated that consistent gel loading occurred in all 9 fractionated samples sent for analysis with the coefficient of variation <10 %. Therefore, confirming that the data could be accurately compared across all replicates.

The use of the Western blots as a verification tool allowed for confidence when comparing changes in protein quantities not only within each dataset but across all biological repeats. Although Western blotting was a quick and cost-effective way of ensuring the critical equal loading of samples this method did have drawbacks. The difficulty in loading the gel samples into the Western blotting apparatus resulted in some blots being challenging to interpret as some gels would tear and distort during the process producing uneven bands. Furthermore, this method could not be used with the TPL sample as the total proteome was sent for analysis. Alternative methods to equal loading verification were considered, such as addition of "heavy labelled" internal control proteins such as ^{15}N-labelled recombinant proteins. However, this method also had its limitations as several heavy labelled proteins would need to be spiked into the samples across a mass range in order to generate a gradient which could then be used to standardise the samples. This option was cost prohibitive in this study.

3.3.6 Proteomic Data Analysis

For each MaxQuant analysis the spectra of 0, 0.1 and 1x MIC samples from the same experiment were compared to generate a singular dataset for each biological repeat. These datasets will be referred to as Set 1, 2 and 3 respectively i.e., when referring to proteins found in a particular Set the combination of all unique proteins detected in each treatment condition is being described.

Initial data analysis focused on determining the quality and reproducibility of the proteomic outputs. Changes in protein intensities for the full detected proteome in response to 12-bis-THA treatment were then analysed before focusing on TFs.

Analysis of Proteome Coverage

The mass spectra generated by the Oxford Advanced Proteomics Facility were analysed using MaxQuant. Analysis of the raw MaxQuant data showed differences in total numbers of proteins detected but an overall similar coverage of molecular weight ranges (table 3.3). Set 3 had the lowest total number of unique proteins detected overall: 1212 *vs*. 1524 and 1427 in Set 1 and 2 respectively. In comparison to the reference proteome [89] (4310 proteins) Set1 detected 34 %, while Set 2 and 3 detected 33 % and 28 % of the total proteome, respectively. The percentage coverage of the ≤ 50 kDa proteome of *E. coli* each dataset covered a similar percentage. Set 1 detected 34 %, Set2, 32 % and Set 3, 26 % of the ≤ 50 kDa proteome.

Table 3.3 Number of Unique Proteins Identified in each Sample

Molecular Weight (kDa)	Set 1	Set 2	Set 3	Reference Proteome [1]
<10	48	42	28	448
10-20	255	227	162	831
20-30	385	358	277	921
30-40	342	312	277	823
40-50	221	206	195	581
50-60	116	110	102	236
60-70	67	59	56	163
70-80	41	37	37	93
80-90	24	25	26	79
90-100	17	25	23	53
100-150	6	23	25	68
>150	2	3	4	14

[1]Referance Proteome *E. coli* K12 obtained from Uniprot [89]

Figure 3.6 shows the percentage breakdown of molecular weight range of the proteins detected in each dataset and reference proteome. Between 20-40 kDa a higher percentage of proteins were recovered compared to what is present in the reference proteome. In this mass range *E. coli* proteins have a primary sequence of approximately 180-450 amino acids in length. For all three datasets the proteins detected were mostly found in the 10-50 kDa molecular weight range (approximately 80-450 amino acids in length), with over 50 % of proteins identified in this range. The largest protein present in the *E. coli* reference proteome has a primary sequence length of 2358 and molecular weight of 248 kDa. *E. coli* TFs in the molecular weight range <50 kDa have a primary sequence length of 70-444 amino acids.

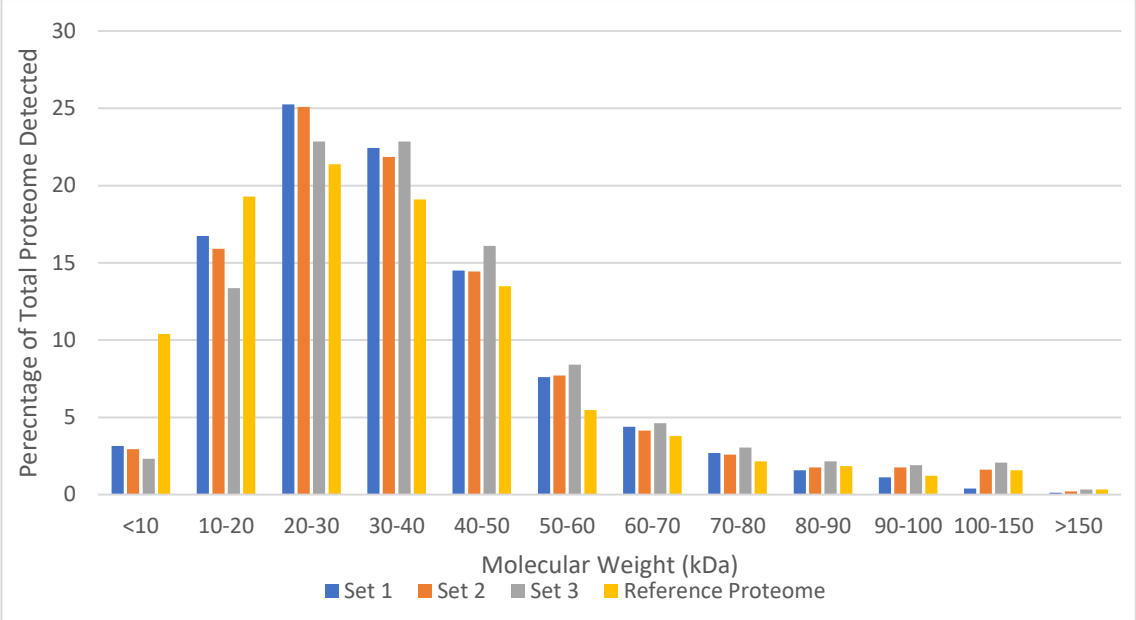

Figure 3.6 Percentage breakdown of total unique E. coli NCTC_9001 proteins detected by molecular weight range in each dataset compared to the reference proteome.

Comparison of Replicate Proteomic Datasets

The overlap between the protein identities detected in each dataset can be seen in figure 3.7. 61.7 % of to the total unique proteins detected were found in all three datasets and 82.3 % of total unique proteins were found in at least 2 datasets.

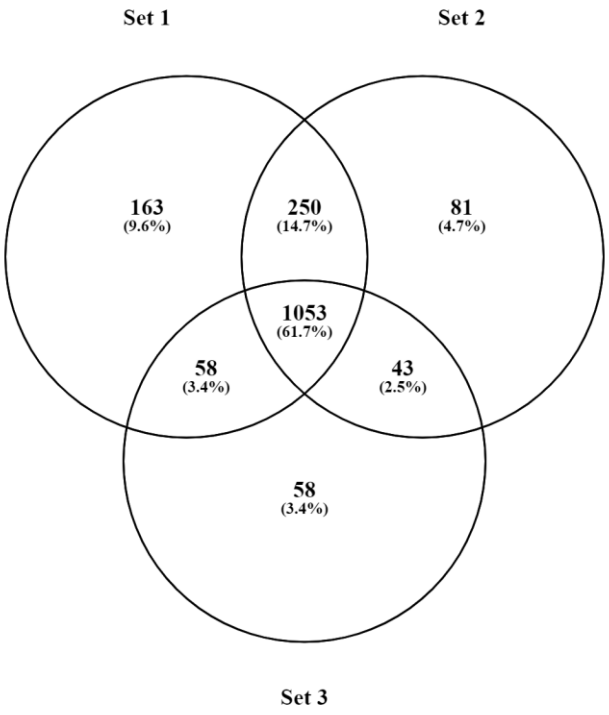

Figure 3.7 Venn diagram illustrating the commonality of unique proteins detected in each experimental dataset

The protein lists for each data set were also subjected to a Gene Ontology annotation search which determined a similar percentage breakdown of protein coverage in relation to function and origin. Figure 3.8 shows an example of the molecular function GO annotations generated by UniProt for each dataset. All three datasets showed similar detection rates in regards to molecular function despite the different number of proteins identified in each dataset. For all three datasets, the majority of identified proteins were found to be in the "binding" category and only set 3 finding no protein with toxin activity.

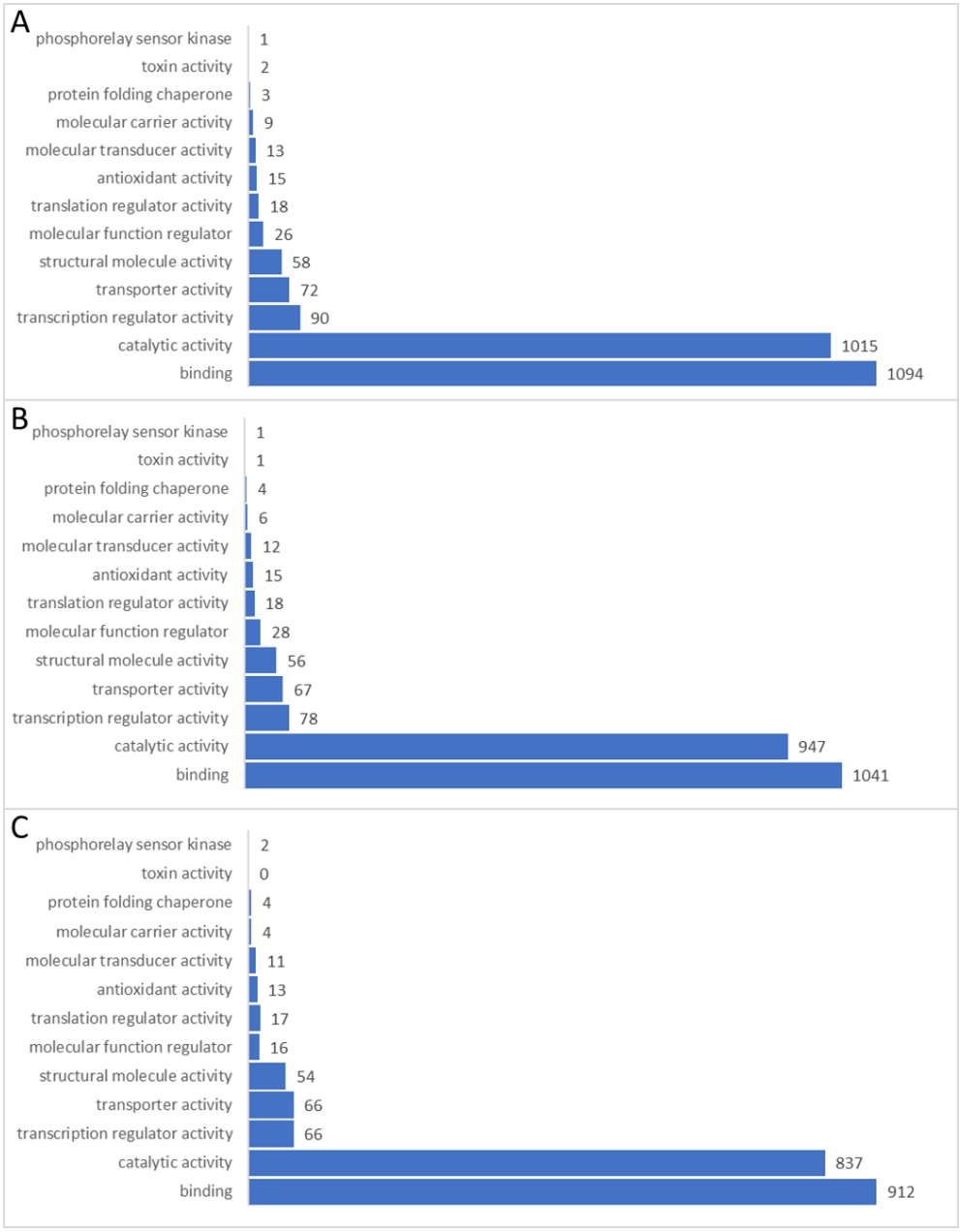

Figure 3.8 GO Molecular Function Annotation breakdown for Set 1 (A), 2(B) and 3 (C).

Analysis of Changes in Protein Intensities

The three MaxQuant outputs generated from the three biological replicates were combined and imported into Perseus for statistical analysis. Following the quality control processing of the combined datasets in Perseus a total of 875 unique proteins detected met the criteria for statistical analysis this was a loss of 178 proteins (1053 proteins common in all datasets *vs.* 875

statistically analysable proteins). Using the hierarchical clustering function in Perseus, a heatmap for the all three datasets was generated (Fig 3.9). The heatmap indicates the relative intensities of each unique protein in each sample allowing for visual comparison of the relative intensities across all nine samples analysed.

Of the three datasets, Set 3 displayed the lowest overall intensities across all three treatment conditions when compared to Set 1 and 2. Set 3 showed little changes in intensities for each protein when compared across the three tested conditions. Set 2 showed a general trend of lower protein intensities at 1x MIC in comparison to Set 1 for the same treatment condition. Set 2 showed increasing downregulation of proteins in the lower half of the hierarchical cluster when comparing 0 to 0.1 and 0.1 to 1x MIC. In Set 1, for the lower half of the cluster at 1x MIC down regulation of proteins can be seen. In general, for all three datasets less protein upregulation is seen compared to downregulation when comparing treatments to the control.

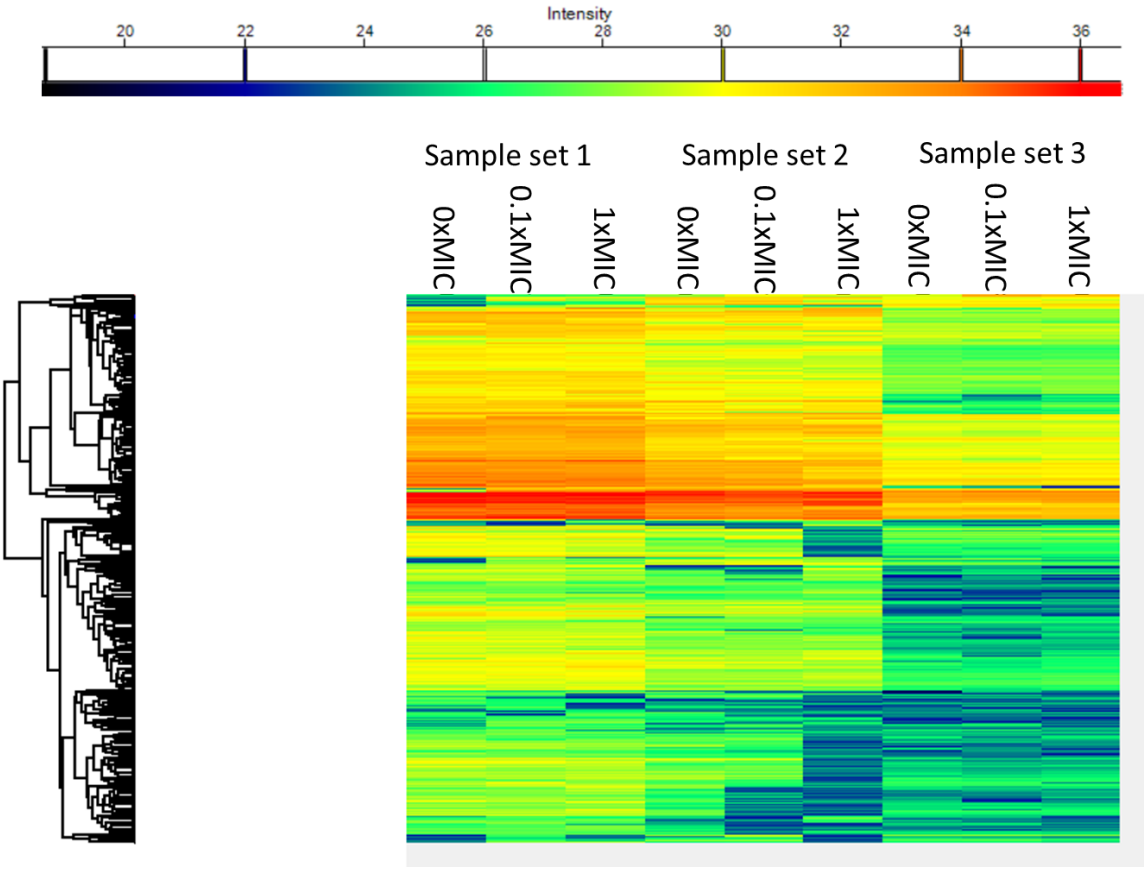

Figure 3.9 Heatmap of All Three Datasets using Normalized Intensities. Each row indicates a unique protein and each column indicates a sample. Samples are grouped by replicate sets. Cool colours represent a low abundance of detected protein and warmer colours indicate a high abundance of protein. Horizontal clustering is due to imputation order of protein in the file and not functionality

Pairwise students t-test were conducted to compare each treatment to the control and each other. The resulting data was represented using volcano plots and the significance boundaries determined by setting the false discovery rate (FDR) to 1 % and S0 to 2.

Figure 3.10 is a Volcano plot displaying the P-value for each protein against its respective change in intensity in paired comparisons of 0x and 0.1x MIC (panel A), 0x and 1x MIC (panel B) and 0.1x and 1x MIC (panel C). The boundary line indicates the threshold of statical significance (FDR=0.01, S0=2). The lack of proteins present above the boundary lines indicates that none of the detected proteins were significantly changed in intensity between any conditions.

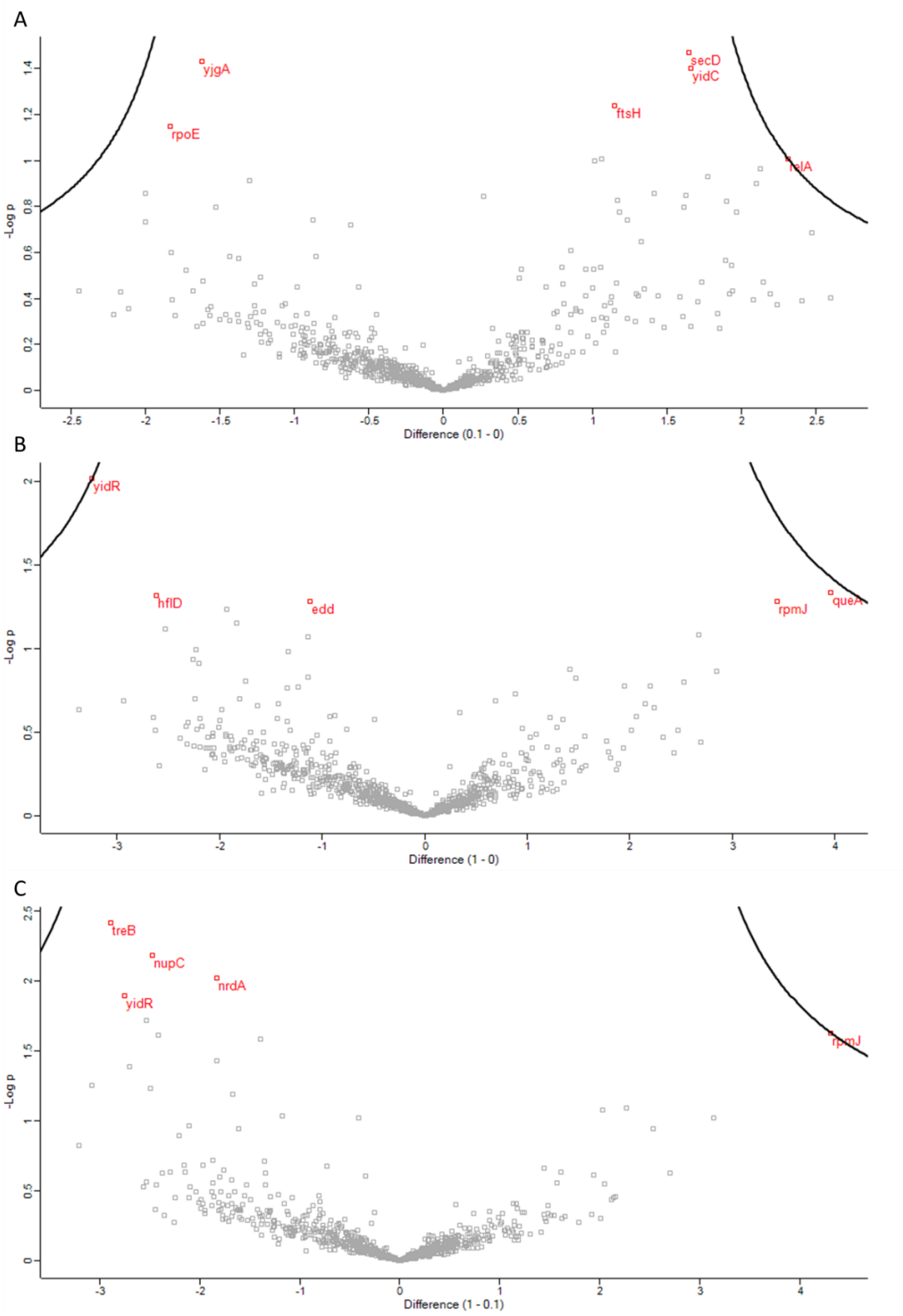

Figure 3.10 Volcano Plots Displaying Protein Comparisons between (A) 0x MIC and 0.1x MIC, (B) 0x MIC and 1x MIC and (C) 0.1x MIC and 1x MIC. The y-axis represents the -$\log_{10}$(P) value and the x axis represent the t-test difference. Solid lines indicate the statisitcal boundaries. Proteins highlighted are those present on the boundry and those with the five highest -logP values. n=3

Treatment of 0.1x MIC displayed an even distribution of up and down regulated proteins when compared to the untreated control (Fig 3.10a), with the majority of proteins showing little fold change. When comparing 1x MIC treatment to the untreated control and 0.1x MIC treatment the distribution of proteins skewed towards downregulation, with fewer proteins displaying upregulation. Many proteins showed little fold change at 1x MIC when compared to the other two treatment conditions. The five proteins with the highest -logP values from each t-test were taken forward for String analysis (Fig 3.11) [112]. Table 3.4 gives a brief description of each protein and their function.

Table 3.4 Description of Functions for Proteins with the highest statistical significance in Treatment Comparison t-tests

Protein Name	Gene Name	Protein Description [89, 103]
Phosphogluconate dehydratase	*edd*	Catalyzes the dehydration of 6-phospho-D-gluconate to 2-dehydro-3-deoxy-6-phospho-D-gluconate
ATP-dependent zinc metalloprotease FtsH	*ftsH*	Acts as an ATP-dependent zinc metallopeptidase for cytoplasmic and membrane proteins. Role in quality control of integral membrane proteins
High frequency lysogenization protein HflD	*hflD*	Negative regulator of phage lambda lysogenization, plays a role in CII phage regulatory protein degradation
Ribonucleoside-diphosphate reductase 1 subunit alpha	*nrdA*	Provides precursors required for DNA synthesis. Catalyses biosynthesis of deoxyribonucleotides from ribonucleotides
Nucleoside permease NupC	*nupC*	Transports nucleosides with a high affinity, with the exception of guanosine and deoxyguanosine
S-adenosylmethionine:tRNA ribosyltransferase-isomerase	*queA*	Transfers and isomerizes the ribose moiety
GTP pyrophosphokinase	*relA*	Mediator of the stringent response which coordinates a variety of cellular activities in response to changes in nutritional abundance. Role in biofilm formation in response to translational stress
50S ribosomal protein L36	*rpmJ*	Component of 50S subunit of ribosome
ECF RNA polymerase sigma-E factor	*rpoE*	Controls the envelope stress response in response to periplasmic protein stress, increased periplasmic LPS levels, heat shock and oxidative stress
Protein translocase subunit SecD	*secD*	Role in protein translocation. Interacts with DecYEG preprotein conducting channel
PTS system trehalose-specific EIIBC component	*treB*	Component of a major carbohydrate active transport system. Catalyses the phosphorylation of incoming proteins via this pathway

Uncharacterized protein YidR	*yidR*	Potential role in gluconate/galacturonate metabolism
UPF0307 protein YjgA	*yjgA*	Found to associate with the 50S ribosomal subunit

Figure 3.11 shows that there is no interaction between the proteins with the highest -log P values for the 0 *vs.* 1x MIC and 0.1 *vs.* 1x MIC comparisons. For the 0.1x MIC comparison to the control, only yidC and secD showed any known associations at a significance level <0.1.

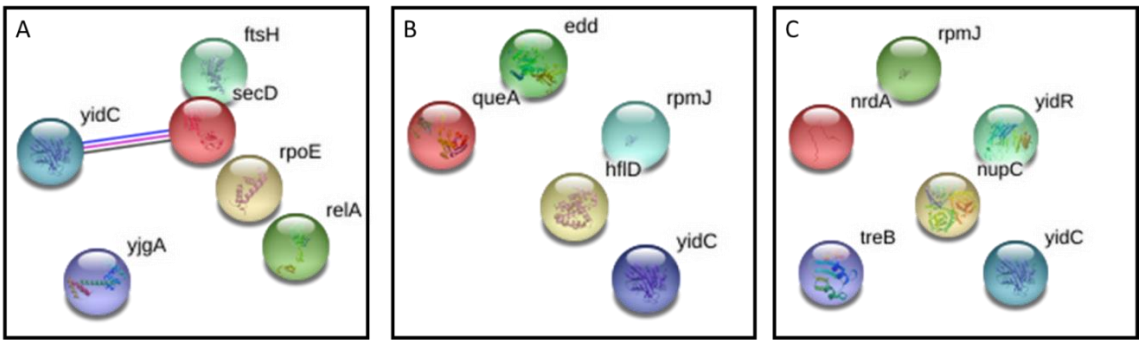

Figure 3.11 StringDB analysis of top 5 most statistically significant proteins for t-tests conducted between (A) 0 vs. 0.1x MIC. 0 vs. 1x MIC and (C) 0.1 vs. 1x MIC. The significance level was set at <0.1. Lines indicate interaction between proteins, no line indicate no interaction

The FtsH protein (ATP-dependent zinc metalloprotease FtsH) was upregulated at 0.1x MIC when compared to the control, but little change at 1x MIC compared to the control was detected. FtsH is a membrane-bound ATP dependent protein involved in LPS degradation and is the only essential metalloprotease present in *E. coli* [113, 114]. FtsH is linked with two other proteins found to have the greatest significant change, the envelope stress response protein RpoE and the TF, CpxR [115, 116]. The sigma factor RpoE works alongside the two-component system CpxRA, of which CpxR is a member [115] in a complementary manner. RpoE and CpxRA regulate proteins involved in response to envelope misfolding stresses, such as LPS alterations. The detection of these proteins is of great interest because 12-bis-THA has been shown to interact with the outer membrane of Gram-negative bacteria and is thought to bind to LPS [53, 57].

However, when investigating the LFQ intensities of RpoE and CpxR, both were downregulated after 0.1x MIC treatment. When the increase in FtsH levels for at 0.1x MIC is taken into account, the observed downregulation complements reports in the literature. Reduced levels of FtsH have been shown to induce CpxR production [116]. As FtsH plays a role in LPS degradation, its increased levels in the presence of 12-bis-THA is a finding of interest. Furthermore, the interaction of 12-bis-THA nanoparticles with the cell membrane has been shown to affect the potential of these membranes [53]. FtsH is ATP dependent and its proteolytic activity is stimulated by protonmotive force [117]. Therefore, the interplay of any changes in membrane potential caused by 12-bis-THA and FtsH activity may be of further interest.

RelA (GTP pyrophosphokinase) was another protein found to have one of the greatest significant upregulations when 0.1x MIC treatment was compared to the control. RelA is a key enzyme in the synthesis of ppGpp and is driven by NtrC in low nitrogen conditions [118]. NtrC is a TF that also plays a role in ppGpp synthesis in nitrogen starved *E. coli* [118, 119]. NtrC, encoded by *glnG* was found to have been one of the TFs with the largest statistical significance (downregulation, -logP 0.3) in the *E. coli* datasets. When taking into account the upregulation of RelA at 0.1x MIC the downregulation of the TF NarL for the same conditions is of interest. NarL is a nitrate/nitrite reductase and acts as a fumarate repressor under signals from NarQ or NarX [89, 120]. In anaerobic conditions NarL plays a role alongside the global TF, FNR and NarP [121]. These three proteins play a role in nitrate regulation via the *napF* operon in anaerobic conditions. This interplay in nitrate regulation in response to 12-bis-THA treatment and involvement with a global TF may be of further interest.

Analysis of Detected Transcription Factors

Analysis of the proteomic datasets then focused on TFs. The TFs detected from each dataset were extracted using an algorithm written in R[1] and a TF reference list generated from

[1] See supplementary document for reference source used to generate TF output

RegulonDB [95] and analysed in Perseus. *E. coli* had 212 TFs identified in its proteome, with 18 having a molecular weight greater than 50 kDa in the monomeric form. Set 1 detected the largest percentage of TFs at 45 % (96), Set 2 detected 39 % (82) and Set 3 included 33 % (69) of all known TFs. Figure 3.12 shows overlap of TFs detected between datasets. The overall number of TFs detected shows a correlation to the total number of proteins detected in each dataset. The overlap between the TFs detected in each dataset was similar to the overlap seen between the total protein results (Fig 3.8).

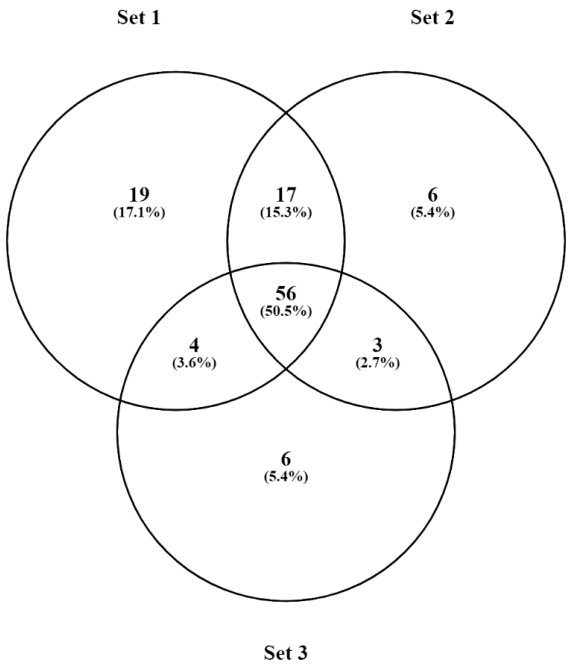

Figure 3.12 Venn diagram illustrating overlap of detected Transcription Factors in each dataset

The three TF data extracts were combined and analysed in Perseus. Following processing steps required for statistical analysis, a total of 40 proteins met the quality criteria, making 16 TFs ineligible for analysis. Using the hierarchical clustering function in Perseus the intensity for each of the 40 TFs was visualised for each experimental condition and biological replicate (Fig 3.13). As observed in the total proteome analysis, Set 3 displayed an overall lower intensity for each

TF. Set 2 showed an overall lower protein intensity at 0.1 and 1xMIC when compared to the same treatment conditions in Set 1.

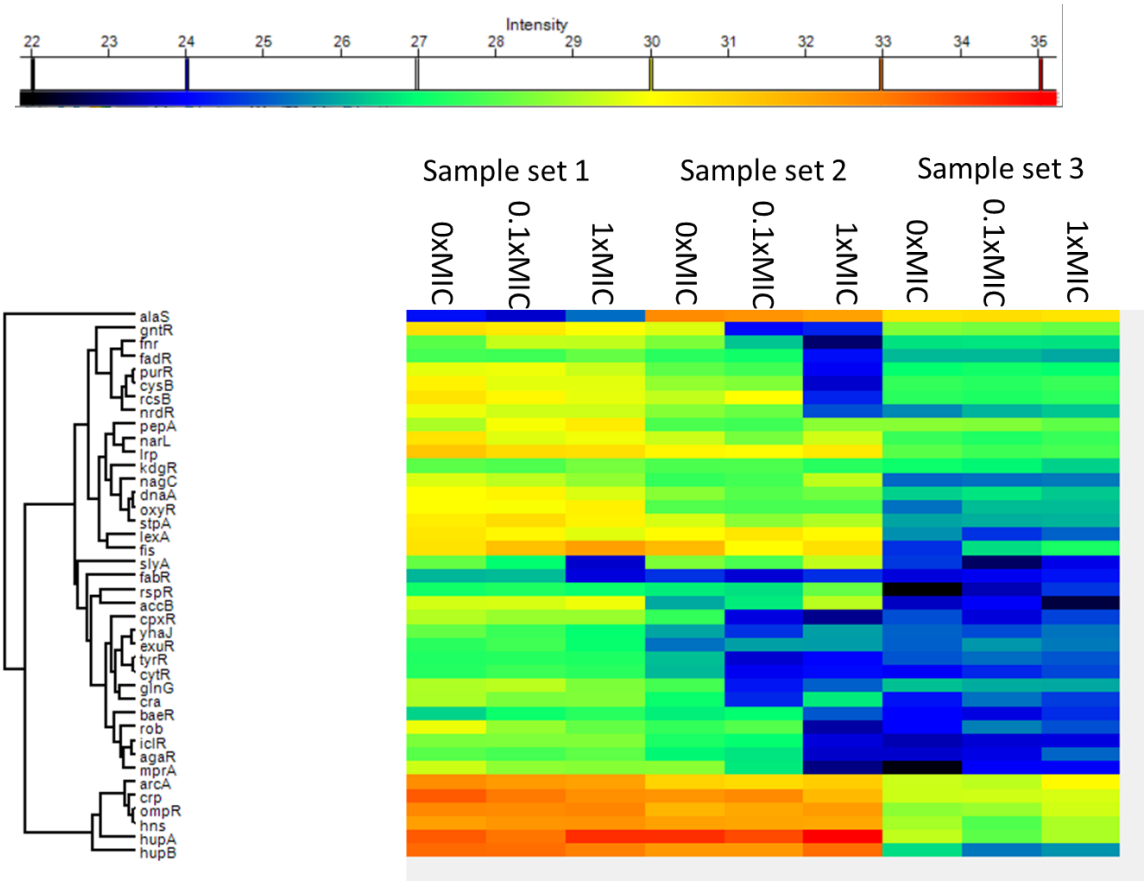

Figure 3.13 Heatmap of All Three Dataset TF extracts using Normalized Intensities. Each row indicates a unique protein and each column indicates a sample. Samples are grouped by replicate sets cool colours represent a low abundance of detected protein and warmer colours indicate a high abundance of protein.

Pairwise students t-test were conducted to compare each treatment to the control and each other. The resulting data was represented using volcano plots and the significance boundaries determined by setting the false discovery rate (FDR) to 1 % and S0 to 2. Figure 3.14 shows that none of the detected TFs displayed a significant change in intensity between any conditions. The distribution of TFs skewed towards a downregulation following treatment. This distribution is more greatly skewed towards down-regulation at 1x MIC compared to 0.1x MIC.

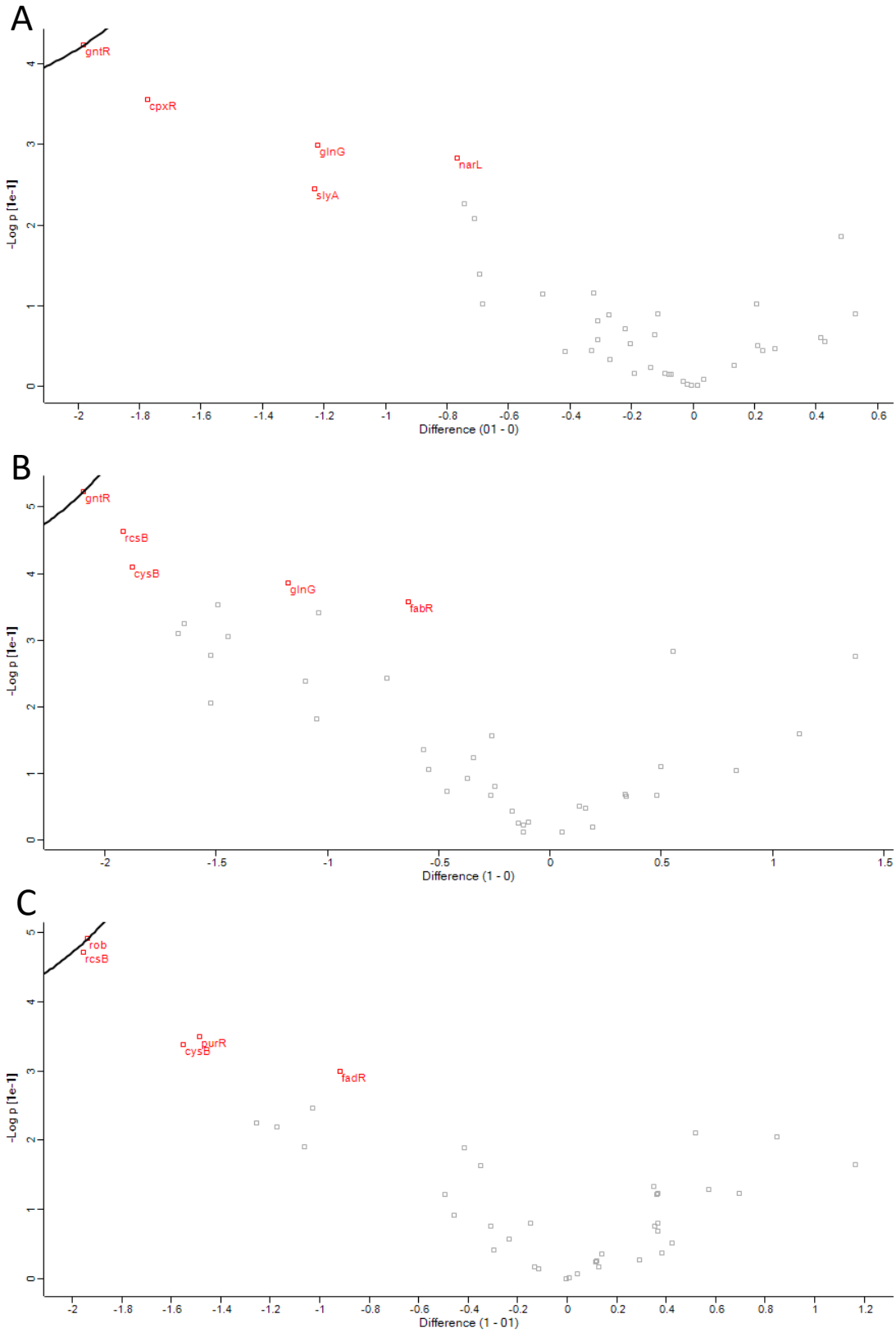

Figure 3.14 Volcano Plots Displaying TF Comparisons between (A) 0x MIC and 0.1x MIC, (B) 0x MIC and 1x MIC and (C) 0.1 xMIC and 1x MIC. The y-axis represents the -$\log_{10}$(P) value and the x axis represent the ttest difference. Boundary line inidcates the threshold of significance. Proteins highlighted are those with the highest staistical significance. n=3

As no TF was determined to have undergone a significant change in expression when treated with 12-bis-THA, the five TF with the highest -logP values from each t-test were taken forward for string analysis [112]. No interactions between any of the TF were found.

Table 3.5 gives a brief description of each TF and its function.

Table 3.5 Description of Functions for Proteins with the highest -log P values in Treatment Comparison t-tests

Protein Name	Gene Name	Protein Description *[18, 23, 25]*
Transcriptional regulatory protein CpxR (conjugative plasmid gene expression)	*cpxR*	Response regulator member of two component system CpxA/CpxR: envelope stress response. Controls 100 operons. Also involved in conjugative plasmid gene expression pilus assembly, secretion, motility and chemotaxis, biofilm development, multidrug resistance and efflux
HTH-type transcriptional regulator CysB (cysteine B)	*cysB*	Regulates positive expression of cysteine regulon. Induced by N-acetylserine. Also controls transcription of operon involved in novobiocin resistance. Negative autoregulation
HTH-type transcriptional repressor FabR (fatty acid biosynthesis regulator)	*fabR*	Represses fabA and fabB genes essential for monosaturated fatty acid biosynthesis
Fatty acid metabolism regulator protein (fatty acid degradation regulon)	*fadR*	Multifunctional dual regulator of fatty acid metabolism. Negative control over fatty acid degradative regulon and acetate metabolism. Responsible for maximal expression of unsaturated fatty acid biosynthesis
DNA-binding transcriptional regulator NtrC	*glnG*	Member of the two-component regulatory system NrtB/NrtC. Controls the expression of nitrogen regulated genes in response to nitrogen limitation. Activates transcription of genes involved in minimizing growth rate reduction under nitrogen-limiting conditions
HTH-type transcriptional regulator GntR (gluconate repressor)	*gntR*	Negative regulator of gluconate catabolism operon (gluconate utilization system GNT-I0

Nitrate/nitrite response regulator protein NarL	*narL*	Transcriptional dual regulator of many anaerobic electron transport and fermentation genes. Activates the expression of the nitrate reductase and formate dehydrogenase-N operons and represses the fumarate reductase operon in response to nitrate or nitrite signals
HTH-type transcriptional repressor PurR	*purR*	Main repressor of several genes involved in purine nucleotide biosynthesis. Also plays a role in regulating genes involved in de novo synthesis of pyrimidine nucleotides. Autoregulated
Right origin-binding protein	*rob*	Transcriptional dual regulator. Binds to the right arm of the replication origin oriC of the chromosome. Activates genes involved in antibiotic resistance, superoxide resistance and tolerance of organic solvents and heavy metals.
Transcriptional regulator SlyA	*slyA*	Activate or repress expression of target genes. Activates genes such as molecular chaperones, proteins involved in acid resistance and the starvation lipoprotein slp. Represses gene expression of those involved in histidine biosynthesis

3.3.7 Comparison of In-Gel Fractionation Method to Total Lysate Analysis

To validate the in-gel fractionation approach a series of experiments was performed in which a TPL sample was analysed for each test condition alongside a gel-fraction. These TPL samples were from the same biological source as the fractionated Set 3 described above. The resulting LC-MS/MS data were analysed in MaxQuant using the same settings and label-free quantification algorithm used for the gel-fractioned datasets.

Figure 3.15 shows the shows the molecular weight range of the proteins detected in each fractionated sample set and the TPL sample. Both Set 3 and TPL were subjected to a C18 column clean up (desalting) step as proteins had adhered to the HPLC column during analysis. As expected, the TPL dataset comprised of a larger number of higher molecular weight proteins and less of the proteins with lowest molecular weight, in comparison to the fractionated samples. Set 3 and TPL were derived from the same biological samples and had the most similar pattern of molecular weight distribution. At 10-20 kDa, TPL showed lower number of proteins compared to Set3 and the inverse was observed at 50-60 kDa. When comparing TPL to datasets not subjected to C18 clean up (Set1 and 2) TPL showed a lower percentage coverage at <30 kDa range.

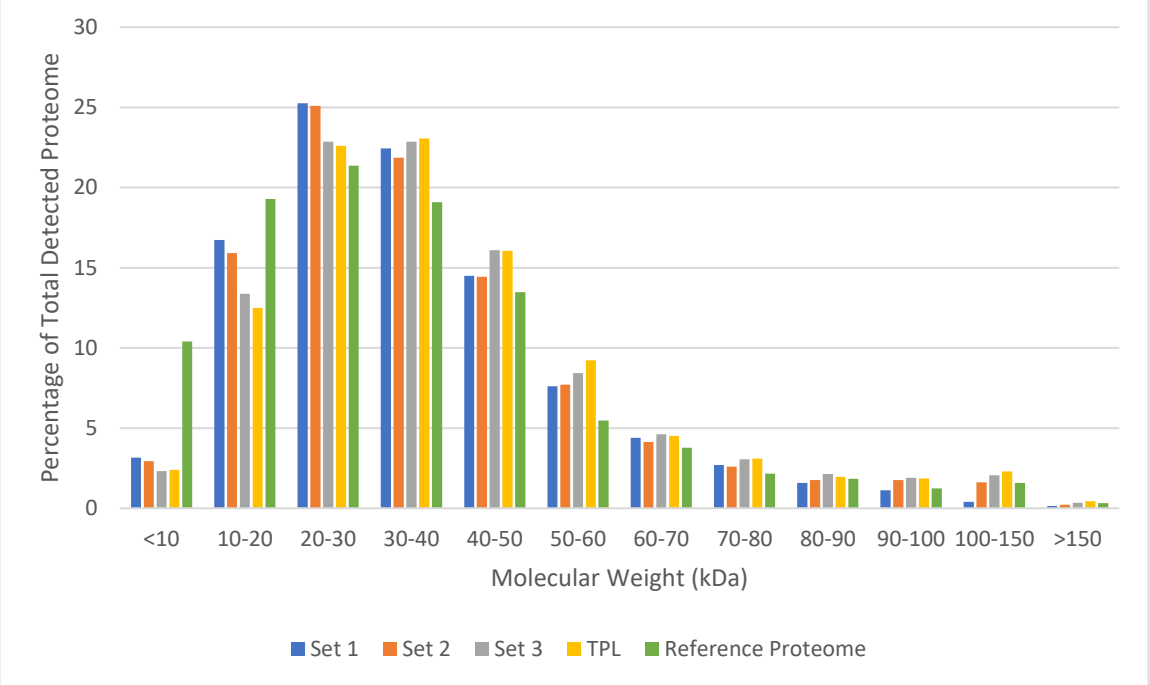

Figure 3.15 Comparison of Proteins detected across different Molecular Weights for each dataset. TPL indicated non-fractionated sample. Note: Set 3 and total protein lysate samples underwent C18 sample clean up

TPL had the lowest number of proteins detected overall, 1128 (26 % of the total *E. coli* proteome), followed by Sample Set 3, 1212 proteins (28 %). Set 1 and 2 had *vs.* 1524 (35 %) and

1427 (33 %) proteins detected respectively. TPL also detected the lowest overall amount of ≤50 kDa proteins, with only 24 % of the ≤50 kDa proteome detected.

TPL shows the lowest number of TFs detected overall (65, 31 % of all TFs), however this is only 4 fewer than Set 3 (69, 33 % of all TFs) which is representative of the same biological replicate as TPL. Of the 65 TFs detected in TPL, 60 (81 %) were found to be in common with Set 3.

Comparison of TF detection and overlap between TPL and Sets 1-3 is shown in Figure 3.16. TPL detected no TFs unique to its dataset, with all TFs detected present in one or more other datasets.

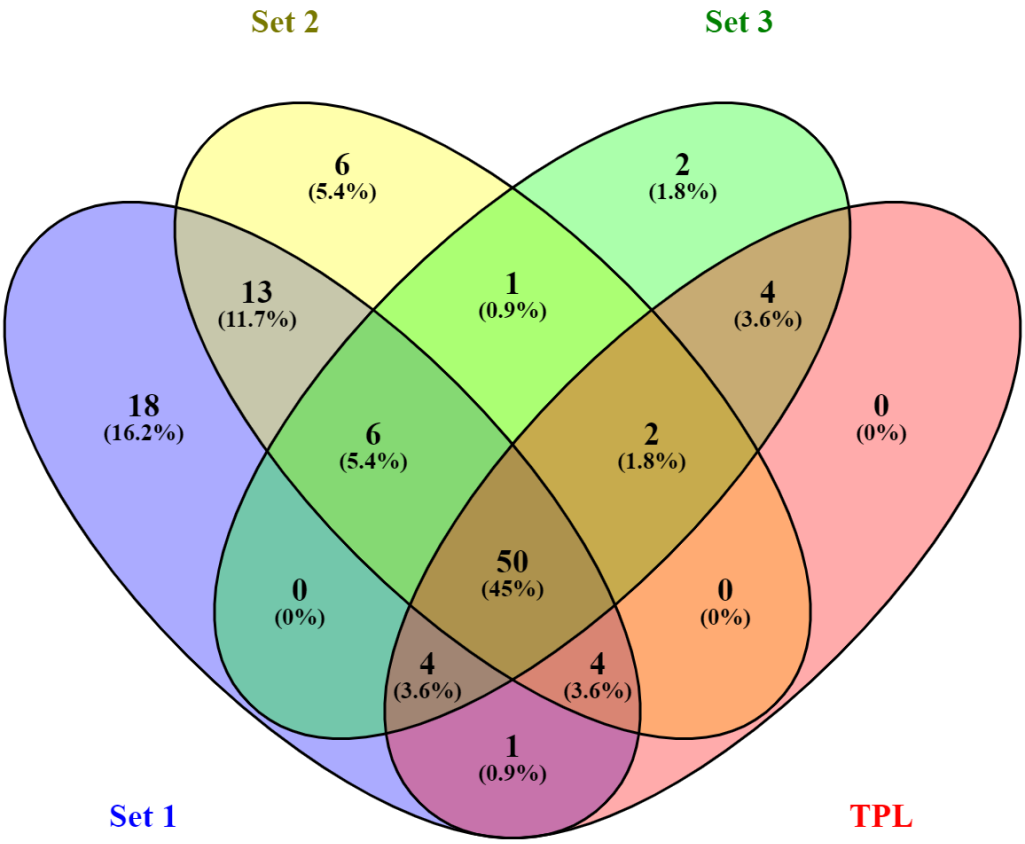

Figure 3.16 Venn diagram illustrating overlap of detected Transcription Factors between each fractionated dataset and the total protein lysate (TPL) dataset. Note: TPL and Set 3 are from the same biological sample and both underwent a C18 clean up procedure during analysis.

When comparing the proteins between the fractionated sample Set 3 and unfractionated TPL dataset there are mismatches in observed protein up- and down-regulation, despite these two datasets being from the same biological source. The protein Elongation factor Tu 2; Elongation factor Tu 1 (tufB;tufa) was shown to be one of the top 10 proteins up-regulated in Set 3 however in the TPL dataset it was shown to be one of the top 10 down-regulated proteins. The inverse relationship was seen for rpoC where it was one of the top down-regulated proteins in Set 3 and one of the top 10 up-regulated proteins in the TPL dataset.

A single TPL sample was analysed by LC-MS/MS to validate the in-gel fractionation methodology as way of improving TF detection. The samples used from this dataset were from the same biological source as Set 3 such that direct comparisons could be made. The data showed an improvement of 2 % ≤50 kDa protein detection between the TPL and Set 3. This may be explained by the extra C18 desalting step that both samples were subjected to. As previously stated, Set 3 was an overall smaller dataset and low copy proteins may have been lost during the adhesion to the column which necessitated the additional desalting step, therefore potentially affecting the number of TFs detected. Indeed, when comparing TPL to Set 1 and 2 a large reduction in the number TFs detected was seen. When focusing in on TFs alone all three fractionated samples displayed an average increased detection rate of 8 % compared to the TPL, indicating that fractionation did enrich TFs in the sample. This may indicate that the fractionation method does indeed select for better TF detection. However, the increased number of TFs detected in these two sets may also be attributed to the fact these Sets 1 and 2 were overall larger than TPL in terms of overall proteins identified. As only one TPL dataset was produced we are unable to conduct statistical testing to confirm whether this is the case. Financial constraints prevented multiple TPL samples from being sent for analysis.

3.4 General Discussion

The aim of this chapter was to develop and optimise a proteomic method for identifying changes in TF levels in response to stresses brought about by 12-bi-THA treatment.

Choice of How and When to Harvest Proteomic Samples

The sample preparation methodology used in this chapter involved harvesting all samples at the same OD_{600nm}. Multiple bacterial proteomic studies have utilised a fixed optical density harvesting point and have generated rich datasets where changes in protein expression caused by induced stress have been observed [74, 75, 84]. By harvesting at a set optical density, the amount of protein extracted for analysis is similar across all samples. Although these samples will have to be normalised prior to LC-MS/MS analysis, the difference in the load amount is in the order of a tenth of a microlitre. Therefore, the impact of any pipetting error is less likely to have a significant impact in the quantification step of the proteomic analysis and would be most likely adjusted for in the normalisation process that occurs during the MaxQuant and Perseus analysis.

An alternative to a fixed OD harvesting method is sampling after a fixed exposure time. It may be argued that this gives a better insight into 'real time' changes in protein expression caused by varying treatment exposures. However, this method will result in protein samples with greater differences in concentration and amount compared to the fixed OD sampling method. Though these samples can be normalised via methods such as the BCA assay, any error in calculations and pipetting is likely to have a greater impact during relative abundance comparisons. As this chapter utilised a label free approach where changes in relative peak intensities have a large impact on the final analysis a fixed OD harvesting point method was used.

Proteomic Data Quality and Analysis

Shotgun proteomics utilises the peak intensities of peptide fragments to identify proteins and the range of fragment peaks that are used in identification are heavily biased by higher abundance proteins. This is due to the fact that the MS-MS detection range is based on the intensity of ions. Therefore, to detect low abundant proteins samples are often separated by size or charge prior to MS-MS. As the proteins of interest in this chapter, TFs, are low in abundance samples underwent fractionation prior to analysis in order to increase the detection rate of these proteins. Fractionation of the sample at 50 kDa theoretically excluded 18 of the 212 TFs found in *E. coli* from the sample, but in reality, manual excision of the gel bands precludes precise exclusion of proteins of >50 kDa molecular mass. Indeed, of the 18 TFs >50 kDa in mass, 10 have molecular weights between 50-60 kDa and would likely have been included in the gel bands sent for analysis, indeed within the combined proteomic output ten TFs of MW >50 kDa were detected. When analysing all three fractionated datasets the coverage of the total proteome ranged from 35-28 % and for the ≤50 kDa fraction the percentage proteome coverage was similar to these values with the majority of identified proteins being in the desired molecular weight bracket. Although proteins of molecular weights much greater than 50 kDa were detected, this would have been unlikely due to a failure to fractionate but rather the presence of <50 kDa fragments. As bottom up proteomic requires only one unique peptide, a razor peptide, to successfully identify a protein of interest, these high molecular weight proteins were found in the samples. When focusing on TFs alone, the three datasets identified 45, 39 and 33 % of all know TFs in *E. coli*, these are much greater values when compared to the ≤50 kDa coverage of 34, 33 and 26 % respectively. These findings indicate that this sample preparation protocol did indeed result in great TF detection rates.

Although some of the proteins discussed above may be of interest to the 12-bis-THA delivery technology and TFD target identification, the lack of statistical significance cannot be forgotten. When regarding the hierarchical clustering heatmaps the source of the lack of statistical significance becomes clear. There is a disparity between the intensities of Set 3 and the other

two sets which becomes even more obvious when focused in on TFs. Analysis of samples from Set 3 resulted in the detection of 33 % and 25 % fewer TFs than Set 1 and 2 respectively. Both Set 3 and TPL were both subject to an extra C18 desalting [122] for reasons that were not fully disclosed to us by the proteomics facility. As the facility closed the samples could not be resubmitted. As desalting is a common procedure in HPLC-MS/MS Set 3 was included in the statical analysis, as the studies in this chapter focused more on the detection at <50 kDa rather than fold change. This process has had a clear impact on the results with these two datasets returning the smallest number of total proteins detected from all the samples. It is likely that protein aggregation and adhesion had occurred on the C18 column prior to the HPLC step and that proteins were lost during the recovery. However, we are unable to determine how this might have occurred as all samples for all 3 datasets were processed the same way prior to submission to the proteomics facility. This reduction in intensity detection in Set 3 has resulted in a widening of the standard deviation range for the data. This in turn has impacted the statistical analysis and normalization of the data in Perseus and most likely skewed the data. Although run to run variations are an accepted and expected source of error in proteomic studies [70, 71, 77, 78] the disparity between Set 3 and the other two datasets is unlikely to be from this alone. All samples were prepared according to the same protocol; however, they were prepared across a period of 12 months which may have had an impact upon the results through the aforementioned run-to-run variations and the changing state of the facility to which the samples were sent. Furthermore, the gel bands sent for analysis were not fixed and therefore proteins may have been lost from the sample as they were waiting to be processed by the facility.

Unfortunately, due to the closing of the proteomics facility we were unable to resubmit these samples for analysis. Although another facility may be used to analyse Set 3 the variations between mass spectrometers, hardware users and facility conditions would still impact and raise questions about the results [70, 71, 78, 123].

This proteomic methodology utilised a label-free shotgun approach [78, 124, 125]. This was chosen as previous work on *E. coli* NCTC_9001 response to 12-bis-THA treatment [126] was conducted with this analytical methodology. Although label-free proteomics is considered a valid method for relative quantification, it is one of the least robust quantification methods in MS based proteomics [78, 98, 124, 125]. This methodology utilises peptide peak intensities for protein quantification. The impact of run-to-run variation is therefore greater than that seen with isobaric tagging and SILAC labelling where samples can be combined and analysed by MS together [70, 124, 127]. Therefore, the use of this methodology may be a source of error for the comparative analysis conducted in this chapter. Considering these factors, a reassessment of the MS approach is required for the proteomic analysis of the organism of interest *P. aeruginosa*, where the timescale of sample analysis is reduced.

Conclusion

This chapter investigated and established a sample preparation method for the detection of transcription factors from bacteria treated with 12-bis-THA and controls. The impact of 12-bis-THA on *E. coli* NCTC_9001 protein levels has been investigated with a focused analysis on TFs. Although no significant findings were made, these investigations allowed for the development of a sample preparation method and analysis strategy that can be applied to similar investigations in *P. aeruginosa*. Critical technical shortcomings including the time between sample preparation will be addressed and a switch to isobaric mass tagging was incorporated into the experiments described in chapter 4.

Chapter 4: Proteomic Analysis of *Pseudomonas aeruginosa* Transcription Factors for the Identification of TFD Targets

4.1 Introduction

In chapter 3 a methodology was developed to prepare proteomic samples for the identification of changes in transcription factor levels in response to 12-bis-THA-induced stress. Despite the success in utilising in gel fractionation to enrich for ≤50 kDa proteins the results of proteomic analysis did not generate any significant results in the model organism *E. coli*. It was concluded that the lack of significant results was in part due to the impact of variations between sample runs which cannot be avoided using a LFQ approach. Therefore, in this chapter a change in the LC-MS/MS methodology was introduced to eliminate run-to-run variations. Isobaric mass tagging allows for samples to be mixed together and run through the mass spectrometer at the same time, eliminating the impact of these variations, resulting in more precise data [80, 128]. One of the most common forms of isobaric tagging is tandem mass tagging (TMT) [128]. TMT tags are available in a 10 plex format, allowing for the simultaneous MS analysis of up to ten samples.

The aims of this chapter were to use a TMT SPS-MS3 approach to detect changes in the proteome of *P. aeruginosa* PA14 in response to 12-bis-THA treatment. There was a specific focus on changes in transcription factor expression in order to identify potential candidates for TFD development.

4.2 Materials and Methods

Materials

Dey Engley neutralizing broth, Luria broth agar and Muller-Hinton cation adjusted broth were obtained from Sigma Aldrich (Gillingham). BCA kit, HPLC grade water, Tris, glycine, urea, sodium hydrogen carbonate, Kartell cuvettes, blades, 96-well polystyrene plates and petri dishes were obtained from Fisher Scientific (Loughborough). SDS loading dye 3x and DTT were obtained from New England Biolabs (Hitchin). Precision Plus Protein Dual Color Standards ladder, 12 % and 7.5 % SDS-PAGE gels were obtained from BioRad (Watford).

MIC Determination

The MIC of 12-bis-THA against *P. aeruginosa* PA14 was determined as described in 2.1.3.

Pseudomonas aeruginosa PA14 Growth Curves

Overnight cultures of *P. aeruginosa* PA14 were diluted to an OD_{600nm} of 0.05 in 100 mL MHB cation adjusted and grown to an OD_{600nm} of 0.5 at 37 °C and 200 rpm. At this point the culture was split and 12-bis-THA was added at 0, 0.1 and 1x MIC. Culturing continued until an OD_{600nm} of 0.8 at which point they were harvested. All optical densities were determined using a Spectramax M2 plate reader.

Protein Extraction and Processing

P. aeruginosa PA14 cultures were added to Dey Engley neutralizing broth in a 1:9 ratio, to neutralise the activity of 12-bis-THA. The bacteria were then harvested and washed 2x with PBS and pelleted at 4200 *xg* for 25 minutes at 4°C. Cells were then lysed in 1 mL of 8 M urea, 25 mM $NaHCO_3$ lysis buffer using sonication on wet ice. Sonication (Soniprep 150) was conducted using bursts of 10 seconds on at 10 mA, 30 seconds off repeated 10 times. Following sonication samples were centrifuged for 40 minutes at 4°C at 16100 *xg*. The supernatant was then taken

off and retained and pellet discarded. The protein concentration of the supernatant was determined using the Peirce BCA assay kit (ThermoFisher).

Proteomic Sample Preparation

To prepare the samples for LC-MS/MS analysis, 100 µg of TPL for each sample were loaded onto 7.5 % SDS-PAGE gels and gels run as described in 3.2 fractionated samples. The excised bands were then fixed using 2 x 30 min incubations in 50 % methanol and 7 % acetic acid. Bands were then placed in low bind Eppendorf tubes and sent to the Bristol Proteomics facility for analysis.

All nine samples (3 biological repeats for each treatment condition) were subjected to in-gel trypsin digestion followed by peptide tagging using TMT-10plex kit (ThermoFisher). The samples were then pooled and subjected to high pH RP chromatography and the resulting four fractions were then further fractionated and analysed using a SPS-MS3 workflow on a Orbitrap Fusion Lumos (Thermo Scientific).

Western Blot

Western Blots were carried out as described in 2.4.3 with PVDF membranes (Fisher) activated in 100 % methanol and equilibrated in transfer buffer.

Proteomic Data Analysis

Mass Spectra Analysis

Analysis of the MS3 spectra was conducted by the Bristol Proteomics Facility using Proteome Discoverer (v2.1, ThermoFIsher). Briefly, SEQUEST searches were conducted against the Uniprot *P. aeruginosa* strain UCBPP-PA14 [89] and contaminants database. Peptide precursor mass tolerance was set at 10 ppm, and MS/MS tolerance was set at 0.6 Da. Search criteria included oxidation of methionine (+15.9949) as a variable modification and carbamidomethylation of cysteine (+57.0214) and the addition of the TMT mass tag (+229.163) to peptide N-termini and lysine as fixed modifications. Searches were performed with full tryptic digestion and a

maximum of 2 missed cleavages were allowed. The reverse database search option was enabled and all data were filtered to satisfy a false discovery rate (FDR) of 5 %.

Additionally, the MS3 files provided by the Bristol Proteomics Facility were subjected to a MaxQuant analysis (version 1.6.3.3). The .raw Tandem mass spectra were searched against *P. aeruginosa* UCBPP-PA14 reference proteome obtained from Uniprot [89]. Reporter ions were set to MS3 with TMT mass tag set to addition at peptide N-termini and lysine fixed modification with a mass tolerance of 0.003 Da. Variable modifications were set as oxidation (M), acetyl (Protein N terminus) and fixed modifications were set as carbamidomethylation (C) with a maximum number of modifications set to 5. The instrument was set a Orbitrap and default settings used. Digestion was set as trypsin/P with maximum missed cleavage sites set to 2. FDR was set as 0.01 and minimum peptide length set to 8 for general and unspecific, all other setting were set as the default.

Computational Analysis

Analysis of the resulting dataset was conducted using Perseus (version 1.6.7.0) [99]. The data were processed in Perseus by normalizing using a log2 transformation. Then proteins detected in only one replicate were removed from the data set and missing data was replaced using normal distribution with a width of 0.3 and down shift of 1.8. For the generation of volcano plots, a pairwise student's t-test was used with S0 set to 2 and FDR set to 0.05. Permutation-based FDR was used for truncation.

Scripts written in R were used to extract TF hits for focused analysis (2.6.3 and Appendix). Additional R scripts were used to determine commonality of TFs detected in each biological repeat. Uniprot ID mapping [89] was used to generate gene ontology (GO) annotations with regards to the cellular locations of the proteins identified in each dataset. Protein identifiers were uploaded to the Uniprot retrieve/ID mapping tool and mapping from UniprotKB AC/ID and

mapping to UniprotKB were selected as the search parameters. The String database was used to map protein association networks [112].

Generation of a Transcription Factor Reference List

Unlike with *E. coli* there is no readily available reference source for transcription factors in *P. aeruginosa*. Therefore, a reference list needed to be constructed to extract the TF hits from the Proteome Discoverer output. Several potential lists were investigated. The contents of these lists were investigated using String db and Uniprot ID mapping searches to determine how many proteins in the list had been annotated.

Pseudomonas.com generated Transcription Factor List

Pseudomonas.com is a continuously updated genome database [129]. Of the many annotated genomes available through this website, PA14 is included. To generate a potential TF reference list a text search of PA14 genes was conducted. The term 'transcription' was used to extract all proteins with "transcription" present in their description

Pseudomonas.com GO annotation-based Transcription Factor List

Another method employed to generate a potential TF reference list was a search of GO (gene ontology) annotation terms on Pseudomonas.com using the search term 'transcription'. The list was further processed in Excel to remove proteins described as "sigma factors".

KEGG Ontology Transcription Factor List

A transcription factor list was generated by a KEGG database [130] search for the term 'transcription' in 2018.

Finalised Transcription Factor Reference List

Initial analysis of the proteomics dataset used the pseudomonas.com generated TF list as this was determined to be the most valid list. To validate the list the TFs extracted from the proteomic dataset and the total proteomics dataset were compared to the literature. In 2019

Filho et al. published a paper investigating the gene regulatory network of multi-drug resistant *P. aeruginosa* [131]. Within this paper they identified and listed 30 of the most influential hubs present in the *P. aeruginosa* network, 4 of which were sigma factors. Comparison of this list to the TF extract generated using the pseudomonas.com TF reference list revealed that 14 of these hubs were detected. However, with comparison to the total proteomic dataset a further 5 of these TFs were detected. Therefore, a second search of pseudomonas.com was then conducted. An advanced text search was used. The resulting list was then subjected to a UniprotKB ID search to generate a list with gene name/locus and accession number assigned to each protein. This resulting list was then used in the TF focused analysis for this chapter.

4.3 Results and Discussion

4.3.1 MIC Results

The MIC of 12-bis-THA against *P. aeruginosa* PA14 was determined to be 31.25 µg/mL, which is more than 30-fold higher than that against *E. coli* NCTC_9001. The MIC reported was found to be in the range of those reported for the structurally related molecule, dequalinium of 5-400 µg/mL [100]. The much larger MIC in *P. aeruginosa* compared to that of *E. coli* was not wholly unexpected when the decreased permeability of the outer membrane (OM) of *P. aeruginosa* is taken to account [21]. The decreased permeability of *P. aeruginosa* is partially linked to the increased stability of the LPS layer [20-22]. This increased stability can partly explain the increased MIC as the mechanism of action of 12-bis-THA is thought to involve LPS binding [53, 57]. Alongside the decreased OM permeability, the role of an efficient efflux system may also play a role in the increased 12-bis-THA MIC. Resistance-nodulation-division (RND) system associated efflux pumps are known to play a role in resistance to traditional antibiotics [36] and some RND associated proteins were found to be upregulated in the proteomic results.

4.3.2 Growth Impact Investigations

Figure 4.1 demonstrates that at 1x MIC *P. aeruginosa* PA14 was unable to reach the target OD_{600nm} of 1.4 and plateaued at OD_{600nm} 0.8. Once an OD_{600nm} of 1.4 samples were harvested for further experimentation, therefore the growth curve does not show the stationary phase. At 0 and 0.1x MIC the target OD_{600nm} of 1.4 was reached after 4.5 h, whereas for 1x MIC reached a maximum OD_{600nm} of 0.9 after six hours. This is likely due to the increased stress caused by 12-bis-THA at this concentration, as previously stated the parental molecule has been shown to affect cell metabolism [100]. When considering the proteomic data, a large number of proteins involved in biosynthesis and ATP dependent proteins were found to be downregulated at 1x MIC indicating that this was likely the case.

An initial target OD_{600nm} of 1.4 was chosen to maintain continuity with the protocol developed using the model organism *E. coli* discussed in chapter 3.

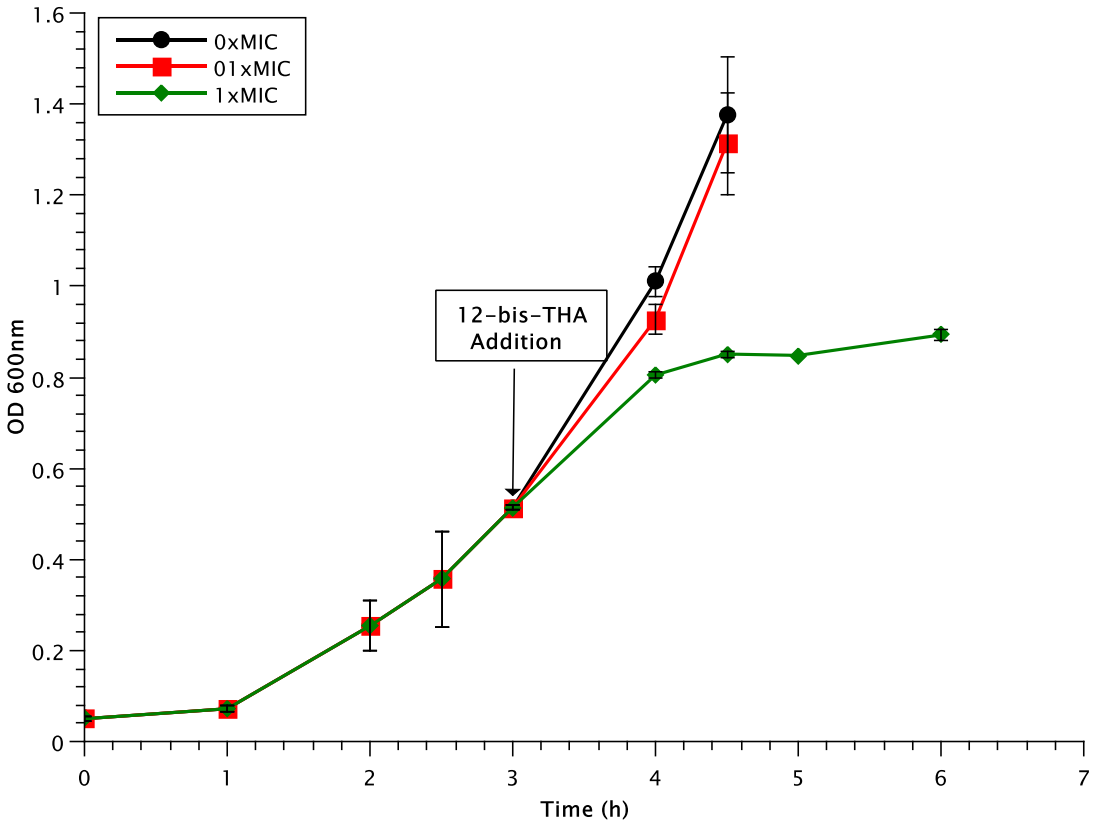

Figure 4.1 Growth Curves of P. aeruginosa PA14 treated with 12-bis-THA. Cultures were grown to OD_{600nm} 0.5 then split and 0, 0.1 and 1x MIC 12-bis-THA was added to the culture. Bacteria were grown at 37°C and 200 rpm. At OD_{600nm} 1.4 bacteria were harvested and readings stopped. For 1x MIC readings were halted at 6 h as no notable increase in OD_{600nm} had occurred. n=2

4.3.3 Proteomic Samples and Quality Control

Following the growth impact investigations above, the target OD_{600nm} was adjusted to 0.8 as OD_{600nm} 1.4 could not be reached. An OD_{600nm} of 0.8 was chosen as the harvesting point as this was the highest OD_{600nm} consistently reached at 1x MIC. Although not the late log phase/beginning of stationary phase of OD_{600nm} of 1.4, a target OD_{600nm} of 0.8 provided sufficient biological matter for proteomic analysis. Published studies investigating the proteome of bacteria in response to stress have successfully utilised a sampling strategy at mid log phase,

generating rich datasets which display significant proteomic changes in response to stress [75]. Therefore, it was determined that an OD_{600nm} of 0.8 target was justified.

The growth curves for all 3 biological replicates (Fig. 4.2) shows that the target OD_{600nm} of 0.8 was reached within an average of 3 h 30 ± 6 min for 0x MIC, 3 h 32 min ± 2 min for 0.1x MIC and 4 h 57 min ± 20 min for 1x MIC treatment condition. For 0 and 0.1 x MIC the target OD_{600nm} was reached at a similar time across the three replicates. However, at 1x MIC a delay of 1h 20 min in reaching the target OD_{600nm} was observed. The growth rates of the proteomic samples followed the same trend as *E. coli* with the target OD_{600nm} being reached at approximately the same time for 0 and 0.1x MIC and a delay seen at 1x MIC. Additionally, at 1x MIC the time to reach the target OD_{600nm} showed the greatest variability of all the treatment conditions. The time taken to reach the harvesting OD_{600nm} for *P. aeruginosa* was almost three times longer than that of *E. coli*. Although *P. aeruginosa* has a longer doubling time than *E. coli* (20 min *vs.* 30 min [132]) this does not fully explain the delay. It is more likely that this impact is due to the effect of 12-bis-THA on metabolism.

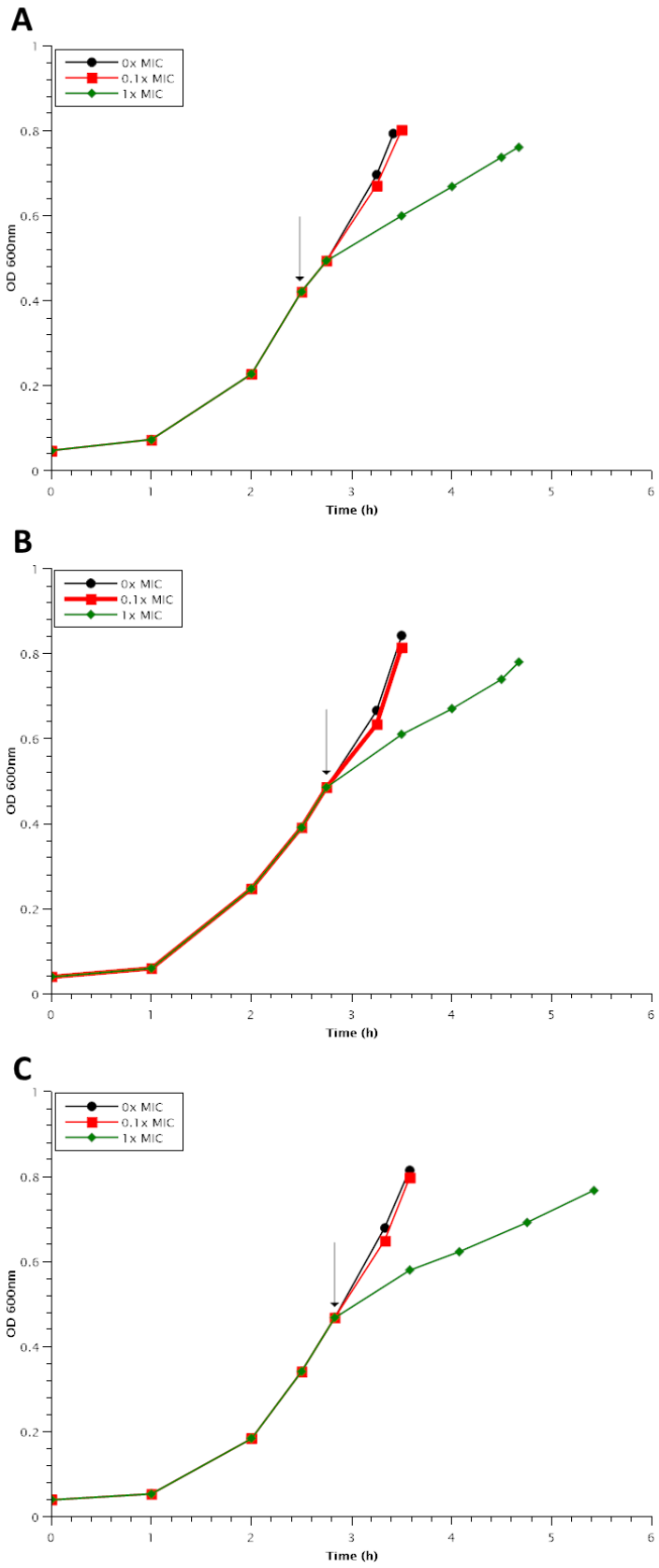

Figure 4.2 Growth Curves generated for P. aeruginosa PA14 Proteomic Samples. (A) Replicate 1, (B) Replicate 2 and (C) Replicate 3. Arrow indicates 12-bis-THA addition of 0, 0.1 and 1x MIC. Bacteria was grown at 37°C and 200 rpm until an OD600nm of 0.8 was reached.

Due to the high concentration of 12-bis-THA used at 1x MIC and the clear impact on the growth rate, the neutralising broth Dey Engley was added in a 1:10 ratio during harvesting prior to the PBS washes. This was an additional step to the protocol developed using the *E. coli* model. This prevented 12-bis-THA from impacting the proteome during the processing steps and potentially altering the results through continued activity during the wash steps.

In relative quantitative proteomics equal loading of samples is key for the accurate comparison of treatment conditions, therefore robust controls are required to verify this. The BCA assay is a highly precise quantification assay and therefore used as the main method for determining equal loading of samples for proteomic analysis. As a secondary control a Western blot to detect for RpoB in the top half of the SDS-PAGE gels was conducted.

Figure 4.3 shows the results of the RpoB Western blot of the top half gel region of samples prepared for proteomic analysis. At 1x MIC for all three samples bands were diffuse and larger in size compared to the bands obtained for the other two test conditions. In order to improve the quality of the blots a switch from nitrocellulose membranes to PVDF membranes was made. The technical difficulties of using small sections of gel for the Western blot had some impact on the quality of the bands obtained, however this did not explain the diffuse bands seen at 1x MIC only. The amount of protein loaded onto the gel was increase to 100 µg for 20 µg in the *P. aeruginosa* experiments as advised by the Bristol Proteomics Faculty, as a 20 µg protein fraction was desired for proteomic analysis. This increase may have impacted the quality of the blot but this does not fully explain the results as dense bands were obtained at 0 and 0.1x MIC for all three replicates. Another possible cause was the primary antibody used, which was targeted to RpoB in *E. coli*. The homology of RpoB in *P. aeruginosa* and *E. coli* is 66 % and this difference could explain some of the problems observed with the Western blot and does explain the increase in exposure time to 30 s from 1 s as the partial homology reduced the sensitivity,

however, once again this does not fully explain the results observed with the 1x MIC bands alone.

Once again Western blot bands were often uneven or fragmented due to the challenges associated with the transfer of small, low percentage gel fragments to the blotting apparatus. Due to technical difficulties of the protein transfer it was difficult to quantify the bands using imaging software. The results of the densitometric analysis can be seen in table 4.1. The average densiometric value across all nine bands was determined to be 210 ± 18 and coefficient of variation (CV) of 8.57 %. It was interesting to note that within each replicate the CV was less than ten, indicating that the precision was very good. However, when taking these values in the context of the Western Blot images generated confidence in their accuracy is greatly reduced. As larger areas had to be selected for the densiometric analysis of the 1x MIC bands, it is likely this brought in some inaccuracy that was not fully compensated for. The principal assay in determining equal sample loading for proteomic analysis was the BCA assay with the Western Blot acting as a secondary verification tool. Given that there were no noteworthy differences in the BCA and that protein concentrations were normalised using these values it was decided that the semiquantitative Western Blot data should be omitted from the quality control process.

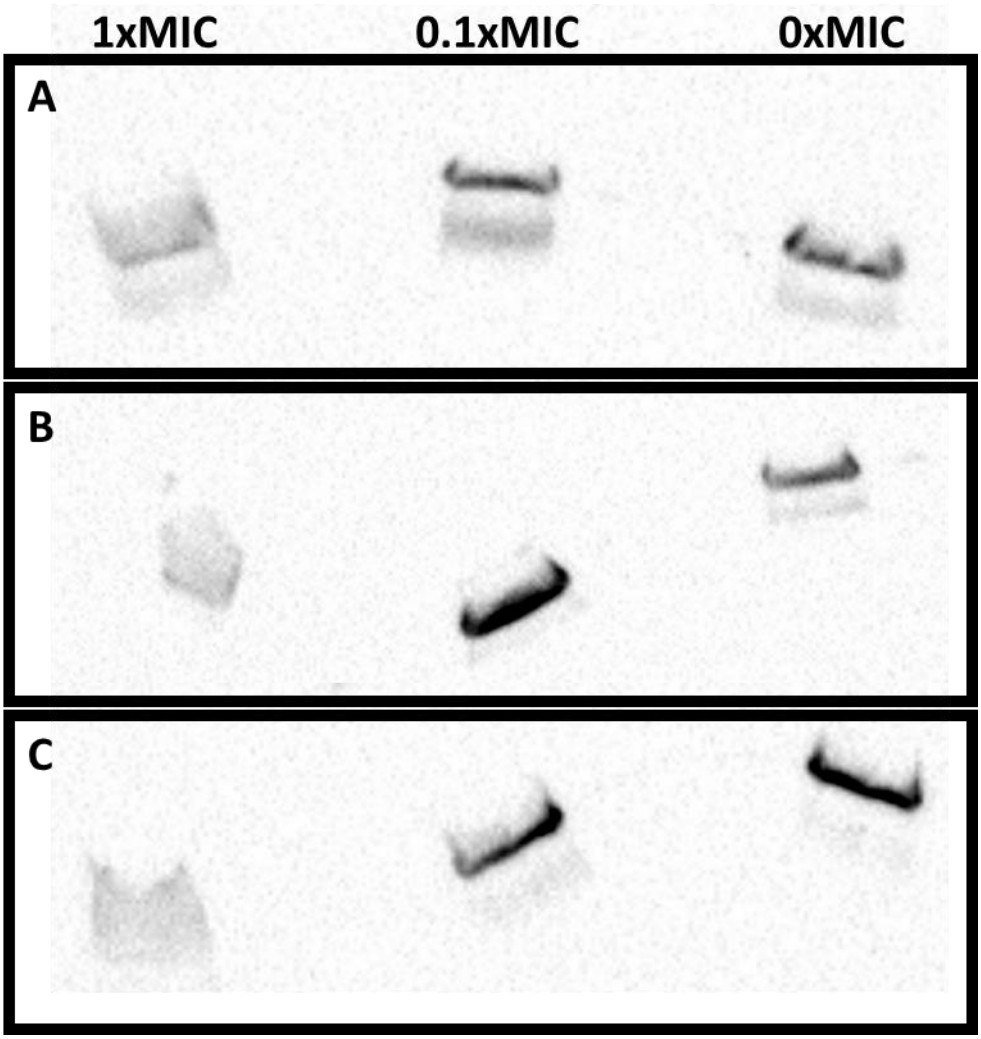

Figure 4.3 RpoB Western Blot of high molecular weight gel region of P. aeruginosa PA14 treated with 0, 0.1x and 1.0x MIC of 12-bis-THA. (A) Replicate 1, (B) Replicate 2 and (C) Replicate 3. Exposure 60 s.

Table 4.1 Densiometric Analysis of RpoB Western blot bands

	Replicate 1	Replicate 2	Replicate 3
0 x MIC	226	228	229
0.1 x MIC	214	172	217
1 x MIC	218	217	195
Standard Deviation	1.24	17.1	10.6
Coefficient of Variation (%)	0.565	8.31	4.96

4.3.4 Proteomic Data Analysis

Many proteomic software packages are available for the analysis of MS based proteomic data [133, 134]. Two of these are the free to use MaxQuant [97] produced by Mattias Mann's group and the proprietary Proteome Discoverer developed by ThermoFisher. Both of these software are closed source and utilise two different search engines, Andromeda for MaxQuant and SEQUEST for Proteome Discoverer. The mass spectra generated for the *P. aeruginosa* investigations were analysed in Proteome Discoverer by the Bristol Proteomics Faciality. As the proteomic analysis for *E. coli* was conducted using MaxQuant a quick comparison between the two software was conducted with the *P. aeruginosa* proteomic data. The .raw MS3 files provided by the Bristol Proteomics Facility and subjected to a MaxQuant analysis for use in this comparison.

Figure 4.4 shows the overlap of the two outputs. The majority of the proteins identified were found in both lists, with an overlap of 87.5 %. As the Proteome Discoverer output utilised a less robust FDR of 5 % compared to an FDR of 1 % used in the MaxQuant analysis a further investigation into the overlap was conducted using proteins identified at a confidence of FDR=1 % (Fig 4.4B). Once again, a high level of overlap was seen (88.3 %) however, it was observed at FDR= 1 % that an overall similar number of total proteins were identified by the two software.

The Proteome Discoverer data contained a total of 16 contaminants compared to MaxQuant which contained a total of 60 contaminants and reverse sequence proteins. The total number of proteins identified by Proteome Discoverer was found to be 3154 and 2917 for MaxQuant. This represented a total proteome coverage of 53.6 % and 49.6 %, respectively. Overall, the outputs of the two packages were 88.3 % similar at an FDR of 1 % indicating that the results were comparable.

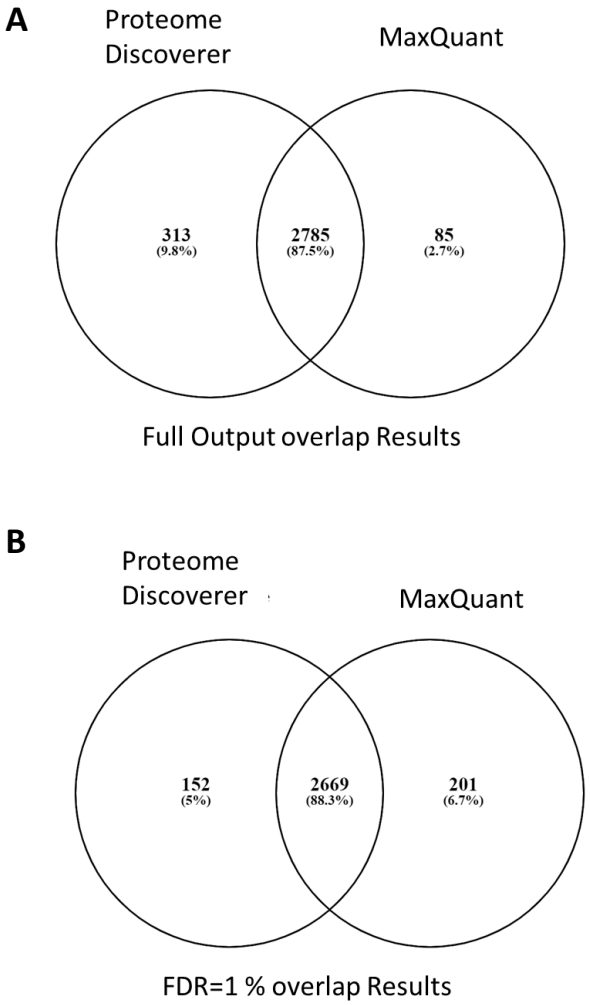

Figure 4.4 Venn diagrams showing overlap of proteins identified in P. aeruginosa PA14 using Proteome Discoverer and MaxQuant for (A) total proteins identified and (B) proteins identified at an FDR= 1 %

Figure 4.5 shows the *P. aeruginosa* PA14 proteome identified by each software compared to the reference proteome group by mass. Both MaxQuant and Proteome Discoverer showed a similar mass distribution of proteins identified. Increased coverage at 20-50 kDa is observed compared to the reference proteome.

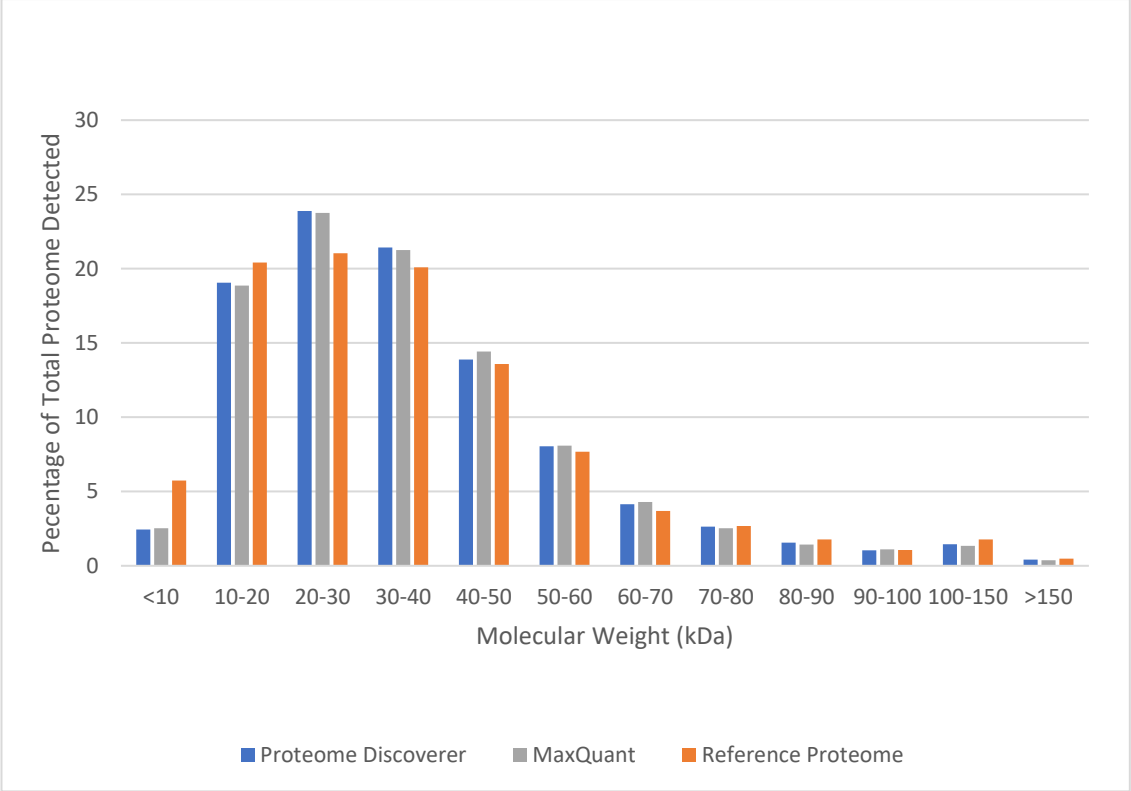

Figure 4.5 Percentage breakdown of total unique proteins detected by molecular weight range in each dataset compared to the reference proteome.

Parallel proteomic studies on *Burkholderia thailandensis* and *Acinetobacter baumannii* within the research group utilised Proteome Discoverer with excellent results in terms of TF detection. Given the overall similarity of the proteins identified by both software and the used of Proteome Discoverer by the parallel studies, Proteome Discoverer was chosen for the *P. aeruginosa* analysis.

The total Proteome Discoverer output was analysed using Perseus. Hierarchical clustering shows good reproducibility between the replicates for each condition (Fig 4.6). At 1x MIC one replicate showed higher intensities compared to the other two (column marked by an asterisk). At 0 and 0.1x MIC little differences in overall intensities were seen, whereas at 1x MIC an average drop in intensity for most of the identified proteins was observed. This is especially evident in the lower half of the clusters, where strong blues are seen at 1x MIC compared to light greens and yellows at 0 and 0.1x MIC.

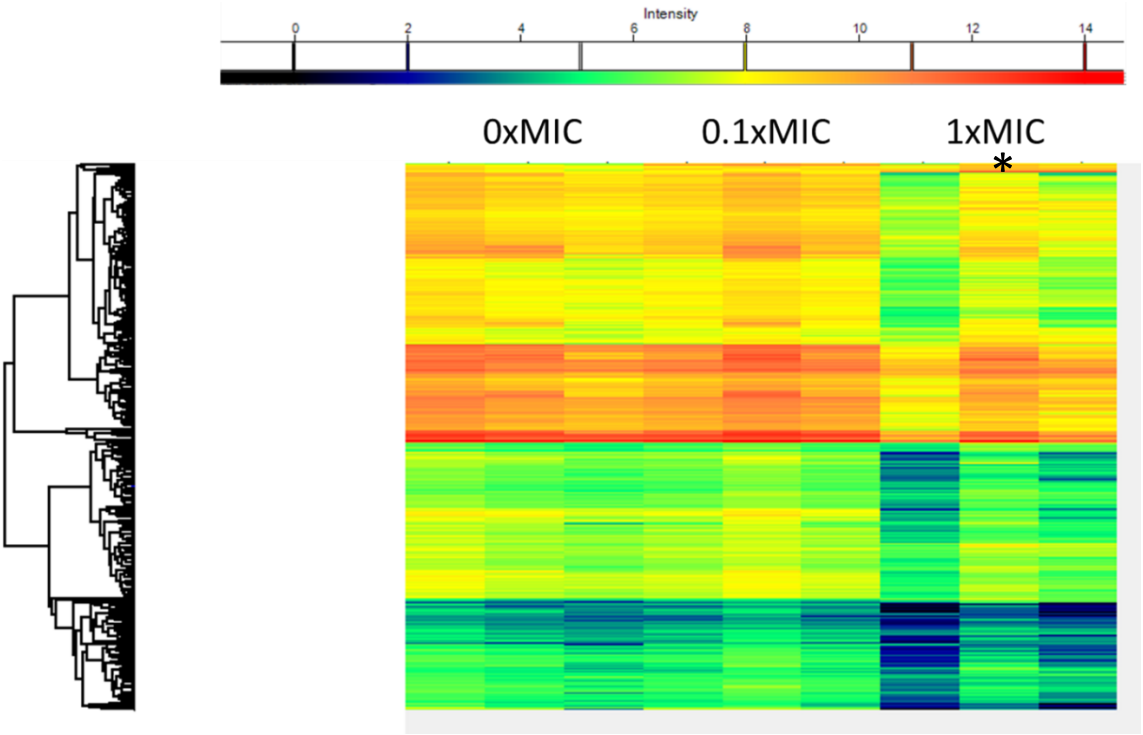

Figure 4.6 Heatmap Showing Sample Reproducibility of PA14 TMT Samples. Each row indicates a unique protein and each column indicates a sample. Samples are grouped by treatment condition. Cool colours represent a low abundance of detected protein and warmer colours indicate a high abundance of protein. Horizontal clustering is due to imputation order of protein in the file and not functionality. * indicates a column of interest

Figure 4.7 shows the volcano plots generated for the statistical analysis of the total Proteome Discoverer search results. At 0 *vs.* 0.1x MIC total of seven proteins were significantly upregulated and none were significantly downregulated. At 0 *vs.* 1x MIC 28 proteins were upregulated and 832 downregulated. For 0.1 *vs.* 1x MIC 25 proteins were significantly upregulated and 1544 significantly downregulated. Of the six proteins significantly upregulated at 0 *vs.* 0.1x MIC four were also upregulated at 0 *vs.* 1x MIC with the abundance ratio increasing in a dose dependent manner. Of the proteins found to be downregulated at 0 *vs.* 1x MIC, 827 were also found to be significantly downregulated at 0.1 *vs.* 1x MIC suggesting a dose dependent response for these proteins.

A GO annotation analysis of downregulated proteins at 0 *vs.* 1x MIC found of the 832 proteins identified 417 were involved in catalytic activity, 43 were linked to transporter activity and 277 to metabolic processes. When conducting the analysis for proteins downregulated at 1x MIC

compared to 0.1x MIC 825 were involved in catalytic activity, 66 linked to transporter activity and 560 to metabolic processes.

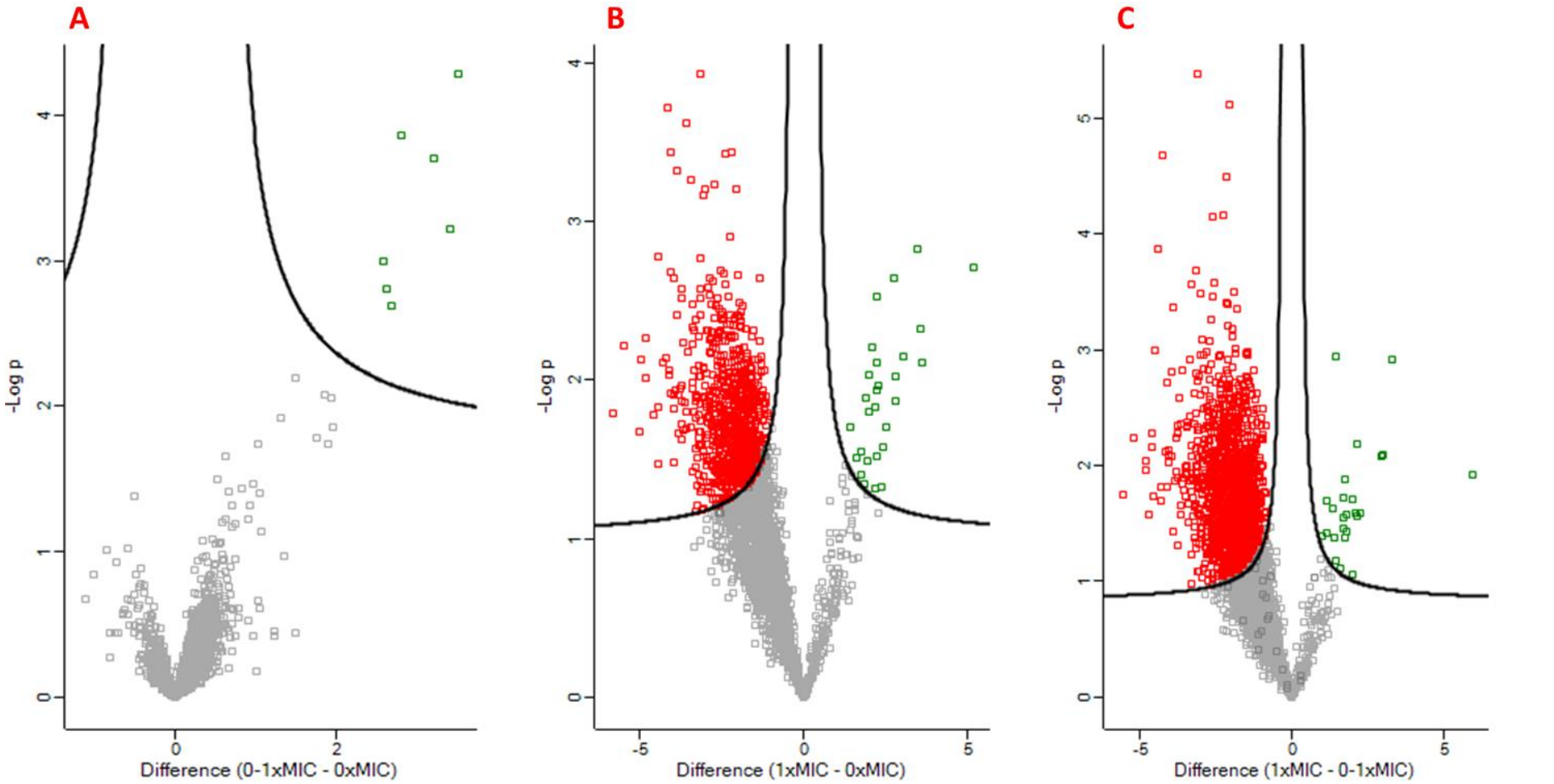

Figure 4.7 Volcano Plots of Protein Comparisons between (A) 0 vs. 0.1x MIC, (B) 0 vs. 1x MIC and (C) 0.1 vs. 1x MIC. FDR = 0.05 and the s0 =0.2 Proteins above the black lines show significance changes in abundance. Solid lines indicate the statistical boundaries of significance n=3. Significant increases are highlighted in green while significant decreases are highlighted in red

Tables 4.2-4.6 show the top ten up and downregulated proteins for each comparison in terms of fold change.

Table 4.2 Significantly upregulated proteins ordered by fold change at 0 *vs*. 0.1x MIC

Protein	Gene Name	Abundance Ratio: 0.1/0x MIC	t-test Difference
Multidrug efflux RND membrane fusion protein	*mexC*	10.09	3.52
Putative major facilitator superfamily (MFS) transporter	PA14_47640	9.37	3.40
Outer membrane protein OprJ	*oprJ*	8.48	3.21
Transcriptional regulatory protein NfxB	*nfxB*	6.05	2.80
Resistance-Nodulation-Cell Division (RND) multidrug efflux membrane fusion protein	PA14_38395	5.67	2.68
Riboflavin synthase alpha chain	*ribC*	5.21	2.57

Table 4.3 Top 10 significantly upregulated proteins ordered by fold change at 0 *vs*. 1x MIC

Protein	Gene Name	Abundance Ratio: 1/0x MIC	t-test Difference
Uncharacterized protein	PA14_40800	74.81	5.15
Putative transcriptional regulator	PA14_64500	25.53	3.57
DNA binding-protein	*amrZ*	24.99	3.58
RNA-binding protein Hfq	*hfq*	23.53	3.44
Putative small heat shock protein	*ibpA*	17.04	3.03
Riboflavin synthase alpha chain	*ribC*	14.95	2.80
Uncharacterized protein	PA14_43150	14.53	2.77
Multidrug efflux RND membrane fusion protein	*mexC*	13.74	2.72
Osmotically inducible lipoprotein OsmE	*osmE*	11.90	2.49
Putative sterol carrier protein	PA14_40860	11.30	2.36

Table 4.4 Top 10 significantly downregulated proteins ordered by fold change at 0 *vs*. 1xMIC

Protein	Gene Name	Abundance Ratio: 1/0x MIC	t-test Difference
Respiratory nitrate reductase delta chain	*narJ*	0.01	-3.04
Uncharacterized protein	PA14_53600	0.02	-3.09
Putative lipid carrier protein	PA14_13320	0.06	-4.11
Putative uroporphyrin-III c-methyltransferase	*nirE*	0.06	-5.50
Uncharacterized protein	PA14_68940	0.06	-5.79
Uncharacterized protein	PA14_61950	0.08	-4.80
Probable ClpA/B-type protease	PA14_33990	0.08	-4.80
Putative nitrite extrusion protein	*narK1*	0.09	-4.95
Putative sulfite or nitrite reductase	*cysI*	0.09	-5.01
Putative lipoprotein	PA14_00590	0.10	-4.55

Table 4.5 Top 10 significantly upregulated proteins ordered by fold change at 0.1 *vs*. 1xMIC

Protein	Gene Name	Abundance Ratio: 1/0.1x MIC	t-test Difference
Rho_N domain-containing protein	PA14_64490	100.00	1.80
Uncharacterized protein	PA14_40800	99.63	5.95
RNA-binding protein Hfq	*hfq*	23.65	3.29
Putative small heat shock protein	*ibpA*	19.32	3.01
DNA binding-protein	*amrZ*	18.84	2.96
Putative transcriptional regulator	PA14_64500	11.81	2.26
Uncharacterized protein	PA14_06010	10.68	2.17
Thioredoxin reductase	*trxB2*	10.61	2.14
Putative membrane protein	PA14_16370	10.26	1.99
Osmotically inducible lipoprotein OsmE	*osmE*	10.01	2.09

Table 4.6 Top 10 significantly downregulated proteins ordered by fold change at 0.1 *vs*. 1xMIC

Protein	Gene Name	Abundance Ratio: 1/0.1x MIC	t-test Difference
Respiratory nitrate reductase delta chain	*narJ*	0.01	-2.03
Uncharacterized protein	PA14_53600	0.04	-2.60
Uncharacterized protein	PA14_04700	0.07	-3.32
Putative uroporphyrin-III c-methyltransferase	*nirE*	0.08	-5.25
Uncharacterized protein	PA14_68940	0.08	-5.60
Putative lipid carrier protein	PA14_13320	0.09	-3.62
Uncharacterized protein	PA14_61950	0.09	-4.84
Putative lipoprotein	PA14_00590	0.09	-4.83
Sulfurtransferase	PA14_30370	0.10	-4.60
Probable ClpA/B-type protease	PA14_33990	0.10	-4.63

Of the top 10 significantly downregulated proteins it was found that the majority were theoretical proteins, however of the ones which had defined gene associations, NirE, NarJ, NarK1 and CysI, it was found that they all but NirE were associated with nitrate reductase.

When investigating the significantly upregulated proteins at 0.1x MIC compared to the non-treatment control (Table 4.2) it was found the all but RibC (aka RibE) were associated with membrane associated efflux systems. The transcriptional repressor NfxB was found to have no significant changes in expression at 1x MIC. Stress response proteins such as Hfq, IbpA and OsmE were found to be significantly upregulated at 1x MIC when compared to the sub-MIC treatment and control (Tables 4.3 and 4.5). Comparison of the top 10 significantly upregulated proteins found that MexC, AmrZ, OsmE and PA14_64500 showed increased expression in a dose dependent manner.

In order to investigate the known associations between the differentially expressed proteins detected a string analysis was conducted. Due to the large number of proteins this produced a large and complex network which cannot be feasibly shown in this thesis. Figure 4.8 shows the medium confidence String analyses of the significantly upregulated proteins for (A) 0 *vs.* 0.1x MIC, (B) 0 *vs.* 1x MIC and (C) 0.1 *vs.* 1x MIC. For both 0 *vs.* 1x MIC and 0.1 *vs.* 1x MIC the sigma

factor RpoH is the central node linking the protein network of the significantly upregulated proteins. For 0 *vs.* 0.1x MIC all but one (RibE aka RibC) of the significantly upregulated proteins are shown to have direct associations. These were Multidrug efflux RND membrane fusion protein MexC (shown as AcrA in Fig 4.8A), outer membrane protein OprJ and transcriptional regulatory protein NfxB.

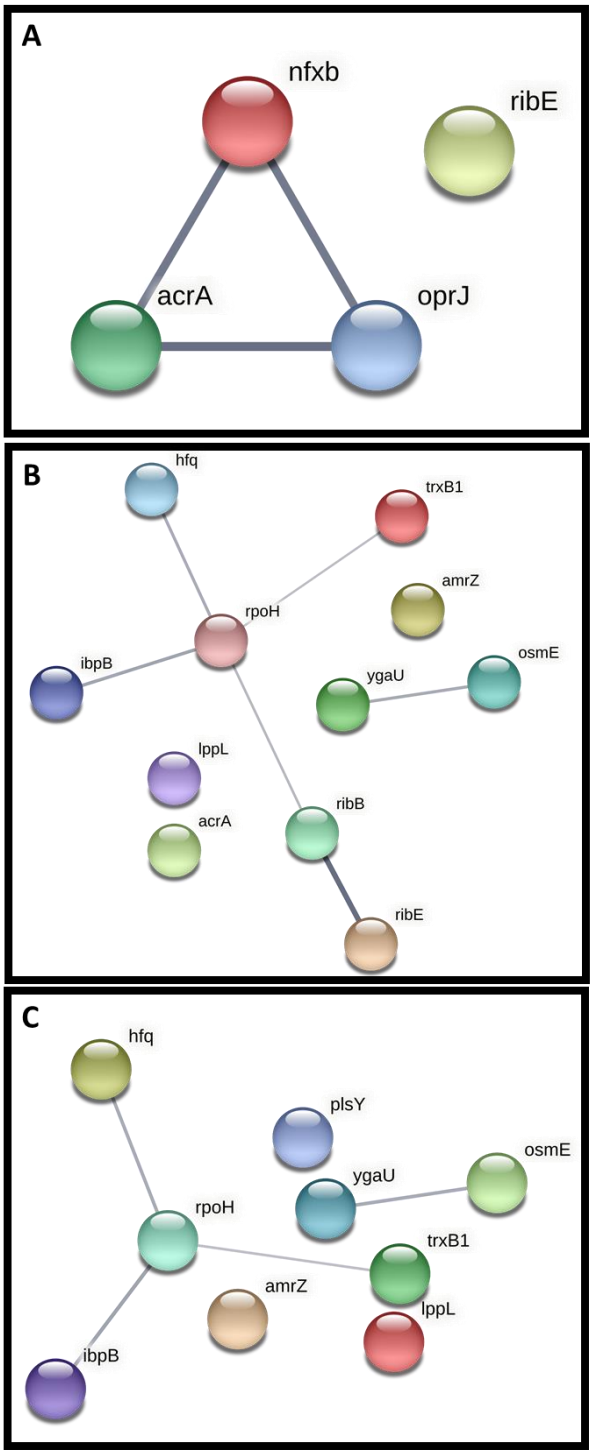

Figure 4.8 StringDB analysis of upregulated proteins at (A) 0 vs. 0.1x MIC, (B) 0 vs. 1x MIC and (C) 0.1 vs. 1x MIC. Confidence was set to medium (0.4). Lines indicate associations, thickness of lines indicate increased amounts of evidence

In response to sub-MIC treatment few significant proteomic changes were observed in the proteome of *P. aeruginosa*, but the significant changes are of great interest. There was no statistically significant downregulation of protein expression at the sub-MIC treatment when

compared to the untreated control. However, there was significant upregulation of efflux systems which have been reported in the response observed with DQC treatment including [100]. The clinically relevant multidrug efflux system MexCD-OprJ was found to be upregulated at both treatment conditions when compared to the untreated control. At 1x MIC MexC showed a 13-fold change, MexD a 5-fold change and OprJ a 7-fold change when compared to the non-treated control. At 0.1x MIC MexC showed a 10-fold change, MexD a 5-fold change and OprJ an 8-fold change when compared to the non-treated control. MexCD-OprJ has been shown to play a role in intrinsic, acquired and transient resistance with an upregulation of expression shown to induce resistance to quinolones, tetracyclines and chloramphenicol [135-138]. This upregulation of MexCD-OprJ expression is in line with that of the parental compound DQC, which has been reported to induce this efflux system via induction of envelope stress in *P. aeruginosa* [100, 136]. Interestingly, the TF repressor of this efflux system NfxB [139] was also observed to be significantly upregulated (6-fold) alongside the increased levels of MexC, MexD and OprJ. The proteomic methodology used in this study is a snapshot of the proteome at a given time it is not wholly unreasonable to assume the impact of NfxB on MexCD-OprJ had not yet taken effect. When taking into consideration the timescales involved in transcription and translation of mRNA to proteins which can take several minutes these findings are not wholly unreasonable. The formation of multimers required for the functional activity of NfxB [139] additionally contributes to the delay in repression. It is worthy of note that in published literature for DQC in *P. aeruginosa* PAO1 [136] increased levels of MexCD-OprJ were detected up to 120 min post DQC exposure. Hence, the upregulation observed of MexC, MexD and OprJ despite the increased levels of their repressor can be explained.

Of the remaining three proteins found to be significantly upregulated at sub-MIC treatment, two were found also found to be involved in efflux and transport, PA14_47640 and PA14_38395, with PA14_38395 determined to be an analogue of the PAO1 multidrug efflux protein MexX [140]. Therefore, it can be determined that following sub-MIC treatment of 12-bis-THA in *P.*

aeruginosa the bacterial stress response is to upregulate efflux systems which in turn would likely induce an increased resistance phenotype. Indeed a induced transient resistance phenotype has been reported for DQC in *P. aeruginosa* PAO1 [136].

At the 1x MIC three of the top 10 upregulated proteins, PA14_64500, AmrZ and OsmE were found to be TFs and will be discussed later. Two proteins in this top 10 were found to be of interest. The RNA-binding protein Hfq, which displayed at 23-fold increase at 1x MIC compared to the control, is important for growth in *P. aeruginosa* and is known to drive the regulation of hundreds of proteins [48]. It has been shown to regulate virulence and stress tolerance through global posttranscriptional regulation with the use of small regulatory RNAs and target RNAs [48, 141, 142]. The loss of Hfq has been shown to result in growth defects making this a potentially interesting target outside the scope of TFD development.

Another protein of interest significantly upregulated at 1x MIC was the putative heat shock protein, IbpA (17-fold increase). This protein has been reported in the literature to delay the aggregation of proteins during growth arrest [143] aiding in cell survival. Inhibition of IbpA often has little to no impact on survival due to redundancies in the network, however, in *Pseudomonas putida ibpA* deletion resulted in a severe growth defect and reduced survival in recovery under heat stress conditions [144].

At 1x MIC treatment hundreds of proteins were found to be significantly downregulated when compared to the other two conditions. An exploration of these proteins corroborates the theory that the antimicrobial mechanism of action of 12-bis-THA is similar to that of DQC. DQC has been shown to work via the disruption of bacterial membranes and loss of enzymatic activity by denaturation [100]. At high doses of DQC, protein denaturation and subsequent inhibition of metabolism occurs. The proteomic data obtained at 1x MIC of 12-bis-THA indicates that these processes have occurred. For example, the statistically significant downregulation of TFs involved ATP synthesis proteins such as ATP synthase subunit a, TFs involved in reduction such

as Respiratory nitrate reductase delta chain and loss of protein involved in anaerobic respiration such as DNR and Anr (0.3 and 0.7-fold respectively). Although many of the proteins reported are putative and have not been fully investigated many proteins involved in synthesis processes were significantly downregulated. Furthermore, ATP dependent proteins, ATP synthase proteins such as AtpB (0.8-fold) and NADH related proteins, such as Ndh (0.3-fold) were also found to be significantly downregulated. These observed downregulations likely explain the growth delay effect observed for the 1x MIC treatments during sample preparation.

4.3.5 Transcription Factor Reference List Generation

The R scripts written for use in this thesis utilised a transcription factor reference list in order to computationally extract TFs from the proteomic outputs for a TF focused analysis. Therefore, to extract this data from the Proteome Discoverer output a robust reference list needed to be generated. Due to the lack of a resource in *P. aeruginosa* like RegulonDB [95] for *E. coli* this list had to be manually curated. Below, three methods of curating a reference list are shown.

4.3.5.1 Pseudomonas.com generated Transcription Factor List

The term 'transcription' was used to extract all proteins with transcription present in their description. A list of 370 protein were returned, of these 72 had assigned gene names (i.e. not in the ordered locus PA14_##### format). A String [112] analysis was conducted on this protein list in order to investigate the interconnectivity of the network and establish a baseline of the information available on these proteins. A total of 63 proteins were successfully identified and mapped by String. The search used a medium confidence level of 0.4.

An advantage of the list generated from this search method was that it contained UniprotKB accession numbers. As the Proteome Discoverer database search used a Uniprot reference genome this introduced a common term between the Proteome Discoverer results and this TF list.

4.3.5.2 Pseudomonas.com GO annotation-based Transcription Factor List

An alternative TF reference list was generated from a search of GO (gene ontology) annotation terms on pseudomonas.com for the term, 'transcription'. This resulted in a list of 451 proteins. A String search of this list found and mapped 103 proteins and functional analysis using a UniprotKB search confirmed DNA-binding. Manual interrogation of this list prompted the removal of 36 sigma factors to produce a list of 415 transcription factors.

4.3.5.3 KEGG Ontology Transcription Factor List

The KEGG database [130] (updated 2018) was searched for the term 'transcription' . This produced a list of only 122 proteins.

4.3.5.4 Choice of Transcription Factor Reference List

Following comparison of the three TF reference lists generated the pseudomonas.com list generated in 4.3.6.1 was selected as the reference list due to the large number of TFs listed and lower number of false positives found. This list was then compared to the literature [131] alongside the Proteome Discoverer output. It was found that five TFs were present in the Proteome Discoverer output which were not extracted using the TF reference list. Therefore, a second search of pseudomonas.com was then conducted. An advanced text search was used in this case generating a list of 393 proteins, 21 more than the first reference list. This list was then subject to a UniprotKB ID search to generate a list with gene name/locus assigned to each protein. The resulting list indicated that 383 proteins had assigned gene or locus names and 10 did not.

Uniprot [89] analysis of the TF reference list developed determined that of the 383 identified TFs 24 has a molecular weight greater than 50 kDa and only 9 had a molecular weight greater than 60 kDa. Therefore, the molecular weight cut-off applied for fractionation remained at 50 kDa. Overall, the coverage of the ≤50 kDa proteome was 53.4 % using Proteome Discoverer, indicating a good detection rate for the desired protein mass fraction. The fractionation method

also resulted in increased percentage coverage between 20-40 kDa when compared to the reference proteome, verifying the findings for the methodology in chapter 3. With regards to TFs, 51 % of TFs present on the reference list were detected, indicating that good TF enrichment had occurred using the fractionation method.

4.3.6 Transcription Factor Focused Proteomic Data Analysis

Following analysis of the proteomic dataset, TF hits were extracted from this using R and the reference TF list. A total of 195 TFs were identified for statistical analysis. Perseus analysis was then conducted on the TF extract. A total of 178 TFs met the criteria for statistical analysis; 17 were excluded because of missing values and matrix reductions. Figure 4.9 shows the volcano plots generated (FRD 0.05 and s0 0.1).

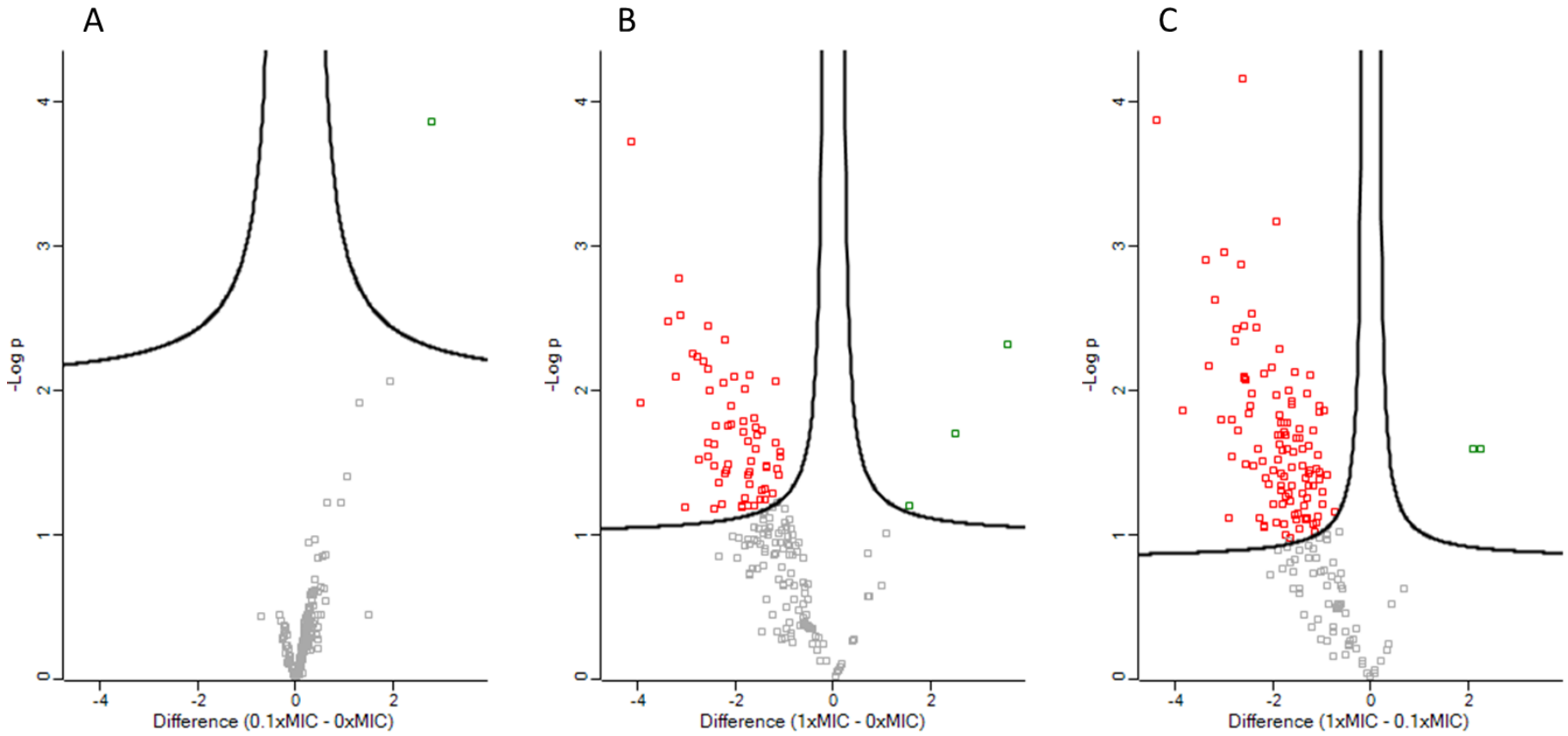

Figure 4.9 Volcano Plots of TF Comparisons between (A) 0 vs. 0.1x MIC, (B) 0 vs. 1x MIC and (C) 0.1 vs. 1x MIC. FDR = 0.05 and the s0 =0.1 Proteins above the black lines show significance changes in abundance. Solid lines indicate the statistical boundaries of significance. n=3. Significant increases are highlighted in green while significant decreased are highlighted in red

Only one TF, NfxB, was upregulated in in 0.1x MIC group and none were significantly downregulated. At 0 *vs.* 1x MIC 3 TFs were significantly upregulated (abundance ratio 25-12) and 52 were significantly downregulated (abundance ratio 0.14-1.01). At 0.1 *vs.* 1x MIC 3 TFs were significantly upregulated (abundance ratio 19-10) and 114 significantly downregulated (abundance ratio 0.13-1.4). Tables 4.7-11 show the top up and top 10 downregulated TFs by fold change for each comparison. The distribution of proteins in the volcano plots was similar to the distribution seen in figure 4.7.

Table 4.*7* Significantly upregulated TFs at 0 *vs*. 0.1x MIC

Protein	Gene Name	Abundance Ratio: 0.1/0x MIC	t-test Difference
Transcriptional regulatory protein NfxB	*nfxB*	6.05	2.80

Table 4.8 Significantly upregulated TFs at 0 *vs*. 1x MIC ordered by fold change

Protein	Gene Name	Abundance Ratio: 1/0x MIC	t-test Difference
Putative transcriptional regulator	PA14_64500	25.53	3.57
DNA binding-protein	*amrZ*	24.99	3.58
Osmotically inducible lipoprotein OsmE	*osmE*	11.90	2.49

Table 4.9 Top 10 Significantly downregulated TFs at 0 *vs*. 1x MIC ordered by fold change

Protein	Gene Name	Abundance Ratio: 1/0x MIC	t-test Difference
Transcriptional regulator AguR	*aguR*	0.14	-3.96
Putative transcriptional regulator	PA14_40150	0.14	-4.13
Heme d1 biosynthesis protein NirG	*nirG*	0.20	-3.39
Transcriptional regulator MvfR	*mvfR*	0.22	-3.22
Putative transcriptional regulator	PA14_10320	0.23	-3.15
Putative transcriptional regulator	PA14_47910	0.24	-3.15
Putative transcriptional regulator	PA14_19380	0.27	-2.88
Acylhomoserine lactone dependent transcriptional regulator	*rhlR*	0.30	-2.78
Transcriptional regulator PhhR	*phhR*	0.31	-2.75
HTH-type transcriptional regulator BetI	*betI*	0.32	-2.67

Table 4.10 Significantly upregulated TFs at 0.1 *vs*. 1x MIC ordered by fold change

Protein	Gene Name	Abundance Ratio: 1/0.1x MIC	t-test Difference
DNA binding-protein	*amrZ*	18.84	2.96
Putative transcriptional regulator	PA14_64500	11.81	2.26
Osmotically inducible lipoprotein OsmE	*osmE*	10.01	2.09

Table 4.11 Top 10 significantly downregulated TFs at 0.1 *vs*. 1xMIC ordered by fold change

Protein	Gene Name	Abundance Ratio: 1/0.1x MIC	t-test Difference
Putative transcriptional regulator OS	PA14_40150	0.13	-4.404
Transcriptional regulator AguR OS	*aguR*	0.17	-3.86
Putative transcriptional regulator OS	PA14_10320	0.23	-3.37
Transcriptional regulator MvfR OS	*mvfR*	0.23	-3.33
Heme d1 biosynthesis protein NirG OS	*nirG*	0.25	-3.21
Transcriptional regulator PhhR OS	*phhR*	0.29	-3.05
Putative transcriptional regulator OS	PA14_47910	0.29	-3.02
Putative transcriptional regulator OS	PA14_48830	0.43	-2.9
Putative transcriptional regulator, AraC family OS	PA14_30620	0.34	-2.86
Putative transcriptional regulator, LysR family OS	PA14_17380	0.35	-2.85

Of the three TFs found to be significantly upregulated at 1x MIC when compared to the sub-MIC treatment and non-treatment control, changes in abundance were found to be does dependent (tables 4.8-4.10). Interestingly, the one TF found to be upregulated at 0.1x MIC *vs.* 0x MIC, NfxB, was found to be significantly downregulated at 0.1 *vs.* 1x MIC.

All TFs found to be significantly downregulated at 1x MIC *vs.* non-treatment were also found to be significantly downregulated at 1x MIC *vs.* 0.1x MIC, indicating a dose dependent response to 12-bis-THA treatment. When investigating the functionality of the downregulated TFs it was found that TFs involved in anaerobic respiration, (DNR, Anr, NarL), quorum sensing, (LasR and MvfR), biosynthesis control (GntR and HexR) and heavy metal resistance (ArsR and CueR) were present. When comparing these finding to the total proteomic output, the large number of

significantly downregulated proteins is explained, with many of these proteins being involved in biosynthesis, heavy metal resistance and ATP driven processes.

Osmotically inducible lipoprotein OsmE

Also referred to as DNA-binding transcriptional activator OsmE, little information of note is available for this TF. Investigations in the literature have determined that OsmE is induced as a result of osmotic shock [145]. Additionally, *osmE* activation is dependent on the sigma factor AlgU, a key sigma factor in alginate biosynthesis, with the promotor region found upstream of *osmE* [146]. Blast analysis of the *osmE* sequence found no orthologs outside the *Pseudomonas* species with an identity greater than 50 %, determining that investigations into OsmE orthologs was unsuitable in this situation. Due to the lack of information available for this TF and its downstream network, it was dismissed as a TFD target.

Transcriptional regulatory protein NfxB

As previously mentioned NfxB is the direct inhibitor of the RND efflux system MexCD-OprJ [139, 147]. Loss of NfxB functionality is associated with overexpression of MexCD-OprJ leading to increased fluroquinolone resistance [135, 139, 148] (Fig. 4.10). One study found the MIC of ciprofloxacin of *P. aeruginosa* PA14 Δ*nfxB* to be 4x higher than that of the parental strain [135]. It is worth noting that the *P. aeruginosa* PA14 used in this thesis is clinically suspectable to levofloxacin [149], with an MIC of 1 µg/mL (MIC method used as described in 2.1.3). Interestingly, loss of NfxB functionality was also linked to increased ß-lactam resistance in biofilms. The AmpC ß-lactamase can be permeated from the cell via MexCD-OprJ. The subsequent overexpression of MexCD-OprJ via NfxB loss results in lowered periplasmic AmpC but higher AmpC level within the biofilm matrix [150]. Therefore, in biofilm conditions loss of NfxB functionality can potentially lead to MDR. However, in the planktonic setting NfxB loss can potentially lead to increased ß-lactam susceptibility. If one considers the clinical application of TFDs targeting *P. aeruginosa* such as CF patients who often have *P. aeruginosa* biofilm present

within their lungs it becomes clear that targeting NfxB is a poor choice as knocking down this TF would only result in resistance to traditional antibiotics.

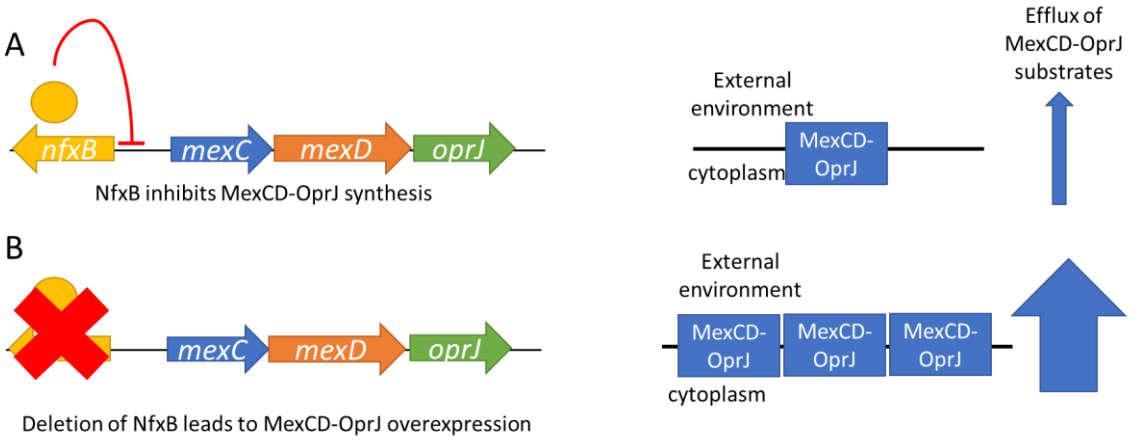

Figure 4.10 Schematic of NfxB function. (A) NfxB inhibits the expression of RND efflux pump MexCD-OprJ, reducing the efflux of its substrates. (B) Deletion of *nfxB* results in overexpression of MexCD-OprJ leading to increased efflux of its substates such as fluroquinolones and AmpC as indicated by larger arrow.

DNA binding-protein AmrZ

Originally described as AlgZ, this was renamed AmrZ and is also known as the alginate and motility regulator Z. A global transcriptional regulator, AmrZ acts as both a repressor and activator and is under the control of the sigma factor AlgU (aka AlgT) [151]. Although AlgU was detected within the proteomic output, it was not found to have significantly changed its expression at either the high or lower 12-bis-THA concentration tested. AmrZ forms a tetramer in solution and binds to DNA as a dimer of dimers [152]. The repressor of AmrZ is AmrZ itself and binds to two sites on the *amrZ* promoter (*amrZ1* and *amrZ2*) [151].

AmrZ has been shown to play a role in biofilm activation and architecture, where it aids in driving the mucoidal phenotype [153]. AmrZ has been shown to be required for AlgD transcriptional activation [151, 152], which is important for alginate biosynthesis. Additionally, alongside this AmrZ had also been shown to be a repressor of a non-mucoidal biofilm exopolysaccharide (ESP), psl [153, 154]. Therefore, AmrZ plays a role in the switch from psl to algD expression and a non-

mucoidal to a mucoidal biofilm phenotype [153]. Alongside its role in biofilm architecture and composition, AmrZ also controls the motility of *P. aeruginosa* via regulation of type IV pili biogenesis and twitching motility [154], [155].

Additionally of note, AmrZ has been found to be a surface-specific repressor of CRISPER-Cas activity [156]. Considering this alongside the global regulatory nature of AmrZ, this TF is indeed a great candidate for TFD development.

Putative transcriptional regulator PA14_64500 (BrlR)

Although only known by its locus tag of PA14_64500 in *P. aeruginosa* PA14, this TF has been defined as the biofilm resistance locus regulator BrlR in *P. aeruginosa* PAO1, with 100 % homology of the gene found between the two strains [129]. A MerR like transcriptional regulator, BrlR contains a helix-turn-helix domain and a GyrI-like binding domain [157] and has shown to form dimers and dimer of dimers in solution [157-159]. BrlR has been shown to confer antibiotic tolerance in biofilms via activation of two RND multidrug efflux systems, MexAB-OprM and MexER-OprN. A direct transcription activator BrlR binds to the promoter regions of the *mexAB-oprM* and *mexEF-oprN* operons [160]. Within the proteomic output only MexE was found to have significant changes in expression, with an increase observed at 1x MIC compared to the control. It has also been shown to be an activator of ABC Transporters, binding to a promotor of PA1874-77 in *P. aeruginosa* PAO1 [161]. Interestingly, BrlR, when initially described, was found to be absent in the planktonic proteome [162] and its activity appears to be dependent on the culture conditions of the biofilm [158, 163]. One study found a 3.5 log reduction in tobramycin tolerance in *ΔbrlR P. aeruginosa* PAO1 flow cell biofilms but no change in microtiter biofilms [158], additionally another study utilising drip-flow biofilms found no change in tolerance in *brlR* mutants, though they hypothesised that this was due to the use of lower concentrations of tobramycin used [163]. Indeed, the study by Liao and Sauer [158] found that changes in tobramycin tolerance occurred at the higher concentrations of tobramycin.

Interestingly one study managed to activate BrlR driven tobramycin tolerance in planktonic *P. aeruginosa* PAO1 [159]. By inducing BrlR with pyocyanin a lower reduction in cfu/mL was observed for the WT compared to a *ΔbrlR* post treatment with a high dose of tobramycin.

Interestingly despite an increased biofilm tolerance to many antibiotics such as tobramycin, trimethoprim, norfolaxacin and kanamycin driven by BrlR activity, a reduction in colistin tolerance has also been observed. This has been shown to be related to the repression of *phoPQ* by BrlR binding to *oprH-phoPQ* promotor [164]. Therefore, indicating that biofilm tolerance to antibiotics via BrlR is agent specific.

Activation of BrlR is thought to be autoregulated and driven by c-di-GMP binding [157]. Two c-di-GMP binding sites have be identified and shown to be involved in *brlR* expression [159] and biding of one c-di-GMP molecule to BrlR has been shown to enhance BrlR-DNA binding [157, 159]. It is thought that the high levels of c-di-GMP found in biofilms is partially responsible for the activation of BrlR expression observed within biofilms [157].

When considering the role of BrlR in antibiotic tolerance in biofilms and the clinical relevance of biofilms in CF patients, BrlR is a good target for TFD development as there is potential for application alongside traditional antibiotics such as tobramycin in a multidrug therapy.

4.4 General Discussion

The aim of this chapter was to identify significant changes in TF expression in response to stresses induced by 12-bis-THA treatment in order to identify potential TFD targets in *P. aeruginosa*. Following the successful development of a proteomic sample preparation method that enriched for TFs in chapter 3 using the model organism *E. coli*, this methodology was applied to *P. aeruginosa* PA14.

Improvement of coverage and reproducibility with TMT

A different MS quantification approach was utilised for *P. aeruginosa* studies following the lack of statistically significant results in chapter 3. The use of TMT eliminated many of the factors which affected the *E. coli* analysis, including run-to-run variations. Additionally, the use of a TMT approach improved the depth of the proteomic coverage, 3154 proteins detected, when compared to the LFQ approach in *E. coli* where the largest dataset returned 1529 proteins, a result which has been reflected in the literature [80, 128]. The results of the hierarchical clustering showed good reproducibility between the three biological replicates. However, it should be noted that the second replicate for 1x MIC displayed higher overall intensities for the detected proteins compared to the other two replicates. The most likely explication for this disparity is likely to be that this sample contained a larger amount of loaded protein, however this cannot be verified as the Western blot was unsuitable. Given the process step taken in Perseus, where normalisation and imputation were undertaken, the impact of this sample on the data was minimised.

Impact of 12-bis-THA and Stress Response

The TFD delivery molecule 12-bis-THA delivers TFDs through the disruption of the outer and cytoplasmic membranes [53, 57] and is thought to interact with LPS and cardiolipin present at the poles and dividing septum of the cell. With this delivery ability 12-bis-THA also displays an

antimicrobial effect at varying organism dependent concentrations. The antimicrobial mechanism of action of 12-bis-THA has not yet been fully determined but it is thought to be similar to that of DQC which is dual faceted. DQC exacts action via disturbances of the cell membrane and loss of enzymatic function via protein denaturation and nucleic acid precipitation[100]. The analysis of the proteomic result of 12-bis-THA treatment in *P. aeruginosa* appear to corroborate this theory that the antimicrobial mechanism of 12-bis-THA is like that of DQC.

Impact of 12-bis-THA on Transcription Factor Expression

Unfortunately, the majority of TFs were found to be downregulated at 1x MIC in comparison to the control and 0.1x MIC. Due to the mechanism of TFD efficacy these were not suitable targets for potential TFD development. Of the top 10 downregulated TFs little of note has been reported in the literature.

Only four TFs in total were found to be significantly upregulated in treatment conditions when compared to the control. These were AmrZ, PA14_64500 (BrlR), NfxB and OsmE.

Conclusion

This chapter investigated and established potential TFs targets for the development of TFDs following treatment with 12-bis-THA using a proteomic approach. The proteomic protocol established in chapter 3 was utilised and improved upon by a switch from LFD to TMT based proteomics. Analysis of the resulting proteomic dataset allowed for investigation of the stress response brough about by 12-bis-THA treatment in *P. aeruginosa* PA14 and corroboration of the potential antimicrobial mechanism of action of 12-bis-THA. Four TFs were identified as potential TFD targets in *P. aeruginosa* PA14 and two, AmrZ and BrlR were determined to be suitable targets for TFD development. These TFDs were developed and investigated in chapter 5.

Chapter 5: Design, Delivery and Activity of *Pseudomonas aeruginosa* Targeted Transcription Factor Decoys

5.1 Introduction

The bolaamphiphilic dequalinium analogue 12-bis-THA forms nanoparticles in solution which are capable of encapsulating and condensing oligonucleotides [53, 57]. Previous studies have shown that upon interaction with bacterial membranes these nanoparticles release the encapsulated DNA into the bacterial cell [53, 57], therefore making this molecule suitable for transcription factor decoy (TFD) delivery.

Following proteomic analysis of *P. aeruginosa* PA14 four transcription factors (TFs) were found to be significantly upregulated in response to 12-bis-THA induced stress. These four TFs were the alginate and motility regulator AmrZ, PA14_64500 which is an orthologue of the PAO1 TF biofilm resistance locus regulator BrlR, transcriptional regulator NfxB and osmotically inducible lipoprotein E OsmE. Investigations into the literature determined that AmrZ and BrlR were suitable targets for TFD development and that knockout strains were available for AmrZ in *P. aeruginosa* PA14 and BrlR in *P. aeruginosa* PAO1.

This chapter aimed to design and test TFDs against TFs found to be upregulated by 12-bis-THA induced stress. Initial experiments investigated the delivery of rhodamine green tagged TFDs into *P. aeruginosa* PA14 planktonic cells alone and with the aid of TFD-laden nanoparticles (LNPs) containing 12-bis-THA. Further experiments investigated the impact of LNP based TFD delivery on growth rates and a phenotypic study investigated the impact of a BrlR targeted TFD on pyocyanin induced tobramycin resistance.

5.2 Materials and Methods

Materials

Luria broth agar, Luria broth Miller, Muller-Hinton cation adjusted broth (MHB2), pyocyanin, tobramycin, resazurin, Ethylenediaminetetraacetic acid (EDTA), SYBR safe DNA gel stain, Phosphate buffered saline, Tetramethylethylenediamine (TEMED), PCR primers and Fluoromount were obtained from Sigma Aldrich (Gillingham). Kartell cuvettes, folded capillary cells 40 % acrylamide, ammonium persulfate (APS), tris base, boric acid, agarose, wheat germ agglutinin AlexFluor 647 (WGA647), Superfrost slides, O'Range 5 bp ladder and petri dishes were obtained from Fisher Scientific (Loughborough). Gel loading de purple (6x), Low molecular weight DNA ladder, deoxynucleotide (dNTP) mix, Q5 high fidelity DNA polymerase and Q5 high fidelity reaction buffer were obtained from New England Biolabs (Hitchin). 96 well polystyrene plates were obtained from Greiner BioOne (Stonehouse). TFDs were obtained from Integrated DNA Technologies (Belgium). Parental wildtype and Δ*brlR*PAO1 *P. aeruginosa* strains were kindly provided by Lichuan Gu (Shandong University, China).

TFD Design and Annealing

Transcription factor decoys are short synthetic double stranded DNA molecules that contain the binding site for a specific transcription factor. They contain a central loop region so that on annealing they spontaneously form hairpin structures, or long stem-loops with the binding site contained within the stem. The 3' and 5' ends are modified with phosphorothioate nucleotides to give protection from exonuclease degradation. In certain TFDs the 3' end can also be modified by a fluorescent label, typically rhodamine green. This can allow detection of bacterial internalisation by confocal laser scanning microscopy and there may be a property of such cationic lipidic dyes in transfecting bacteria itself.

The transcription binding sites were designed using sequences published in the literature. For AmrZ the active TFD sequence was based on the wildtype *amrZ1* binding site described by Pryor

et al 2012 [151] and the scrambled TFD sequence based off the TTC/GC *amrZ1* mutant from the same reference source. For BrlR active TFD was based off the prom19bp sequence described by Chambers et al 2014 [157] with the addition of three nucleotides to either end of the sequence based off the full genomic sequence of BrlR. For the scrambled version of the BrlR TFD random substitutions were made to the binding site sequence. All TFD sequences had the addition of GAA to allow for a hairpin turn [165] (table 5.2).

To form TFDs into hairpins lyophilised powders were suspended to a concentration of 1 mg/mL in ultrapure water then heated to 95 °C for 2 minutes. TFDs were then left to cool at room temperature for 20 minutes. Confirmations of annealing was confirmed using Native PAGE. TFDs and an LMW DNA ladder were subjected to electrophoresis on a 20 % polyacrylamide gel at 110 V for 100 min. The gel was subsequently stained with SYBR safe for 30 mins and imaged (Syngene G:Box Chemi XRS).

Formation of Nanoparticles

To form loaded nanoparticles (LNPs) 1 mg/mL TFD and 200 µg/mL 12-bis-THA were mixed to obtain 1:10 ratio TFD:12-bis-THA and vortexed for 30 s. To form empty nanoparticles (ENPs) 12-bis-THA was vortex alone for 30 s. Nanoparticles were created in aqueous solution and used with seven days of formation.

Dynamic Light Scattering

Particle size characterization of empty (ENPs) and loaded (LNPs) nanoparticles was performed with dynamic light scattering (DLS) analysis using a Malvern Zetasizer Nano (Malvern Instruments). Samples were equilibrated for 20 s at 25 °C and the analysed using backscattering mode. For each sample a total of 3 independent measurements of 11 runs each were taken, with each run lasting 10 s. For stability studies samples were stored at room temperature and analysed by DLS every 24 h for 7 days. All samples were formed in aqueous solution.

Zeta Potential

Z-potential measurements were recorded with Malvern Zetasizer Nano using laser Doppler velocimetry and phase analysis light scattering technique. Experiments were conducted at 25°C and all samples were in aqueous solution.

Primer Design

Primers were designed using sequences obtained from UniProt *P. aeruginosa* UCBPP-PA14 [89] and Primer-BLAST [166].

Colony PCR

For each bacterial strain one colony was taken from fresh streak plates grown on LB agar and resuspended in 100 µL of PBS. 2.5 µL of this was then added to reaction tubes containing 5 µL Q5 reaction buffer, 0.5 µL dNTPs, 0.125 µL Q5 high fidelity DNA polymerase and 0.5 µL of forward primer and 0.5 µL of reverse primer. Primers used are listed in table 5.1. Reaction volumes were made up to a final volume of 25 µL using nuclease free water. The cycle parameters were set to initial denaturation at 95 °C for 1 min followed by 35 cycles of denaturing at 95 °C for 30 s, primer annealing at 68 °C for 45 s and extension at 72 °C for 45 s. A final extension of 7 minutes followed at 72 °C.

Table 5.1 PCR Primers

Target Gene	Forward Primer	Reverse Primer
brlR	CACTGGAGGATCCGCAACAT	AGTATTCCATGCCCACCACG
rpoD	CTTCGGCTTGCTCTTCAGGA	CACGAGACCGACGAGAAGTG

PCR fragments were visualised on SYBR safe pre-stained 1.8 % TAE agarose gels which were electrophoresed at 80 V for 180 min (Syngene G:Box Chemi XRS).

P. aeruginosa PA14 Growth Curves

96 well microtiter plates were seeded as described in 2.1.5. Plates were incubated for 18 h in microbiology plate readers (Biotek Eon or Biotek Powerwave) at 37 °C, with continuous shaking at 200 rpm. Readings were taken every hour at OD_{600nm}. Cell viability at the end point was confirmed via a visual resazurin assay [167]. Briefly, to each well 20 µL of 0.015 % resazurin solution was added. Plates were then incubated statically at 37 °C for 1 h. Metabolism of blue resazurin solution to pink confirmed viability, whereas a lack of colour changed indicated cell death.

Confocal Laser Scanning Microscopy of TFD Delivery

Overnight cultures of *P. aeruginosa* PA14 were diluted 2 % into MHB2 and grown at 37 °C and shaking at 150 rpm until an OD_{600nm} of 0.3 was reached. To 500 µL of culture 500 µL of ENP or LNP (1:10 TFD:12-bis-THA) loaded with either rhodamine green (RhGn) tagged BrlR TFD (RhGN-BrlR) or RhGn-AmrZ TFD was added, resulting in a final 12-bis-THA concentration of 50 µg/mL. For the control 500 µL of sterile water was added to 500 µL of culture. For TFD alone 10 µL of rhodamine tagged TFD was added to 500 µL of culture. Samples were then vortexed for 10 s and incubated at 37 °C and 150 rpm shaking for 1 h. Following this 10 µL of 1 mg/mL WGA647 was added to each sample and samples were further incubated for 30 minutes at 37 °C and 150 rpm shaking. Samples were then centrifuged (Eppendorf) at 4000 *xg* for 10 min and the supernatant removed. Pellets were resuspended in 50 µL of PBS. The suspension was then transferred onto a Superfrost slide and left to incubate for 30 min in the dark. Slides were then washed once with PBS and dried. Slides were visualised using a Zeiss LSM800 microscope (Zeiss) and ZEN software. A X63 water objective was used with emission filters set to Hoechst H3258 for 12-bis-THA detection, AlexFlour647 for bacterial membranes (stained with WGA647) and Rhodamine Green for RhGn tagged TFDs.

Tobramycin Tolerance Experiments

In order to investigate the phenotypic impact of the BrlR targeted TFD, tobramycin tolerance studies were conducted. Colonies of *P. aeruginosa* PAO1 wild type and Δ*brlR*PAO1 were taken from fresh streak plates and suspended to a McFarland standard of 0.5. Bacteria were grown in the presence or absence of 0.2mM pyocyanin in MHB and varying concentrations of 12-bis-THA nanoparticles containing either active BrlR TFD (HP), scrambled BrlR TFD control (SCR) or empty (ENP). Bacteria were grown at 37 °C with shaking at 200 rpm for 8 h in a 96 well microtiter plate. Cultures were then treated with a final concentration of 50 µg/mL tobramycin for 1 h at 37 °C with shaking at 200 rpm. Cultures were then spot plated (10 µL) on LB agar and incubated overnight at 37 °C. Colonies were counted and cfu/mL calculated as per 2.1.3.

5.3 Results and Discussion

5.3.1 TFD Targets and Design

Of the four TFs found to be significantly upregulated in response to 12-bis-THA treatment two, AmrZ and BrlR, were taken forward for TFD investigations. Both TFs selected have published investigations into the binding site sequences [150, 156]. TFD of 50 bp were designed using these binding domain sequences. Investigations into the binding site sequences for both TFs were conducted in the P. aeruginosa PAO1 reference strain. Both AmrZ and PA14_64500 were shown to have 100 % sequence match with their PAO1 orthologs, therefore PAO1 binding site sequences were used [90]. Active (HP) and scrambled (SCR) TFDs were designed to target AmrZ and BrlR. Rhodamine Green fluorescent tags were added to the 5' end of HP TFD sequence to produce fluorescent TFDs for use in confocal microscopy. Table 5.2 shows the sequences of TFDs.

Table 5.2 TFD sequences used in this study

Name	Type	Target TF	Sequence
AmrZ HP	Hairpin	AmrZ	5-GTA CTG GCA AAA CGC CGG CAC GGA ACG TGC CGG CGT TTT GCC AGT AC-3
AmrZ SCR	Scr version	n/a	5-GTA CTT TCC GCG CGA AGG CAC GGA ACG TGC CTT CGC GCG GAA AGT AC-3
RhGn-AmrZ	Conjugate	AmrZ	5-RhoGn- GTA CTG GCA AAA CGC CGG CAC GGA ACG TGC CGG CGT TTT GCC AGT AC-3
BrlR HP	Hairpin	BrlR	5-ACC TTG CCC CAG GGG CAA TCC GTA GGA ACT ACG GAT TGC CCC TGG GGC AAG GT-3
BrlR SCR	Scr version	n/a	5-ACC ACA TTG AAC TTT GTC TCC GTA GGA ACT ACG GAG ACA AAG TTC AAT GTG GT-3
RhGn-BrlR	Conjugate	BrlR	5-RhoGN- ACC TTG CCC CAG GGG CAA TCC GTA GGA ACT ACG GAT TGC CCC TGG GGC AAG GT-3

Red nucleotides indicate the hairpin turn sequence

TFDs are designed to be delivered in a hairpin conformation, therefore the oligonucleotides were annealed. Confirmation of TFD annealing was conducted on 20 % Native PAGE gels. Figure 5.1 shows strong banding at 25 bp indicating the majority of the TFD population had annealed into a secondary hairpin conformation. A much smaller population at 50 bp can be seen indicating that some TFD remained in a linear form.

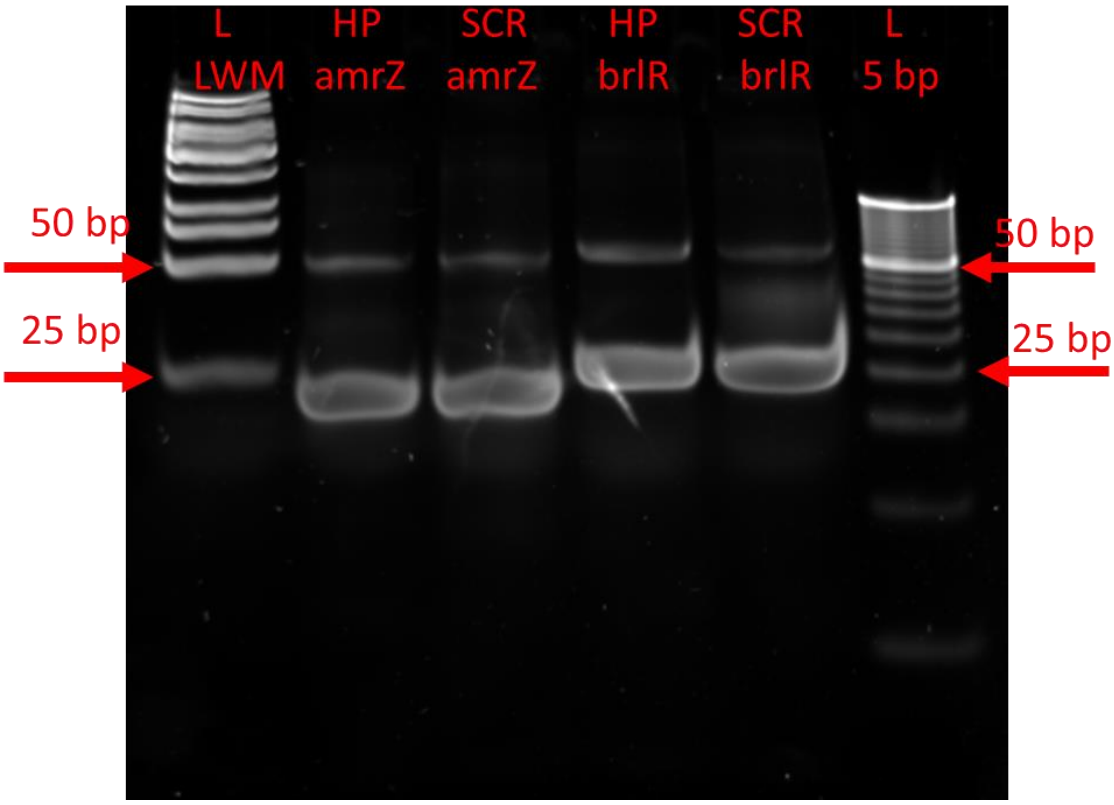

Figure 5.1 Native PAGE of annealed TFDs. 20 % polyacrylamide gel was post stained with SYBR safe for 30 minutes. L LMW=LMW ladder, L 5 bp=5 bp ladder, HP=targeted, SCR=scrambled. 1 µL of each ladder and 0.5 µL of each 1 mg/mL TFD was loaded.

5.3.2 Nanoparticle Stability Investigations in Water

The major component of the proposed TFD based antimicrobial system is the delivery of TFDs via 12-bis-THA based nanoparticles. In order for this system to work TFDs are required to be encapsulated by 12-bis-THA molecules to form stable LNPs. To confirm the formation of LNPs the techniques of DLS and zeta potential were utilised.

The physical properties of the various species to be tested was examined by DLS. Table 5.3 shows the result of DLS and Zeta potential analysis of AmrZ HP, AmrZ SCR, BrlR HP and BrlR SCR LNPs and ENPs. Cumulant analysis of the measured correlation curve allows for the estimation of mean size average (Z average) of monodisperse or narrow distribution populations. Cumulant analysis can also generate a Polydispersity index (PDI) which describes the width of size distribution of the particles in the sample and is calculated by $(width/mean)^2$. The suitability of the use of cumulant analysis to calculate these values can be determined via the interpretation of the correlograms. Figure 5.2 show the correlograms of each tested nanoparticle. The steep decline indicates the monodisperse nature of the samples. The overlapping of curve for each replicate measurement indicated the absence of sedimentation.

Table 5.3 DLS and Zeta Potential of LNPs and ENPs n=3

Nanoparticle	Z Avg of Diameter (nm)	Z Avg ST Dev	PDI	PDI ST Dev	ZP (mV)	ZP ST Dev	DCR (kcps)	DCR ST Dev
LNP amrZ HP	145	0.974	0.182	0.010	23.2	0.754	1387	407
LNP amrZ SCR	138	2.36	0.132	0.001	25.1	0.450	1497	113
LNP brlR HP	136	2.70	0.133	0.011	24.3	0.634	2638	1129
LNP brlR SCR	159	1.55	0.213	0.003	26.3	0.990	1836	206
ENP	202	3.28	0.158	0.020	43.7	0.411	580	274

Z Avg= Size diameter average, PDI=Polydispersity Index, ZP=Zeta Potential, DCR=derived count Rate, ST Dev=Standard Deviation, kcps=kilo counts per a second

As previously discussed, the ZP is a measure of the surface charge of a nanoparticle and an important factor in determining nanoparticle stability and adsorption to cell membranes [63, 64]. The zeta potential of all LNPs was found to be mildly cationic and lower than that of the ENP control. These findings are in keeping with previously published data [53, 57, 168]. The drop in ZP is indicative of TFD encapsulation as this is indicative of the electrostatic interactions between the polar headgroups of 12-bis-THA and polyanionic TFDs that have previously been described [53]. The overall positive charge is desirable as it aids in the adsorption of LNPs to the primarily anionic lipid membranes of bacterial cells [168].

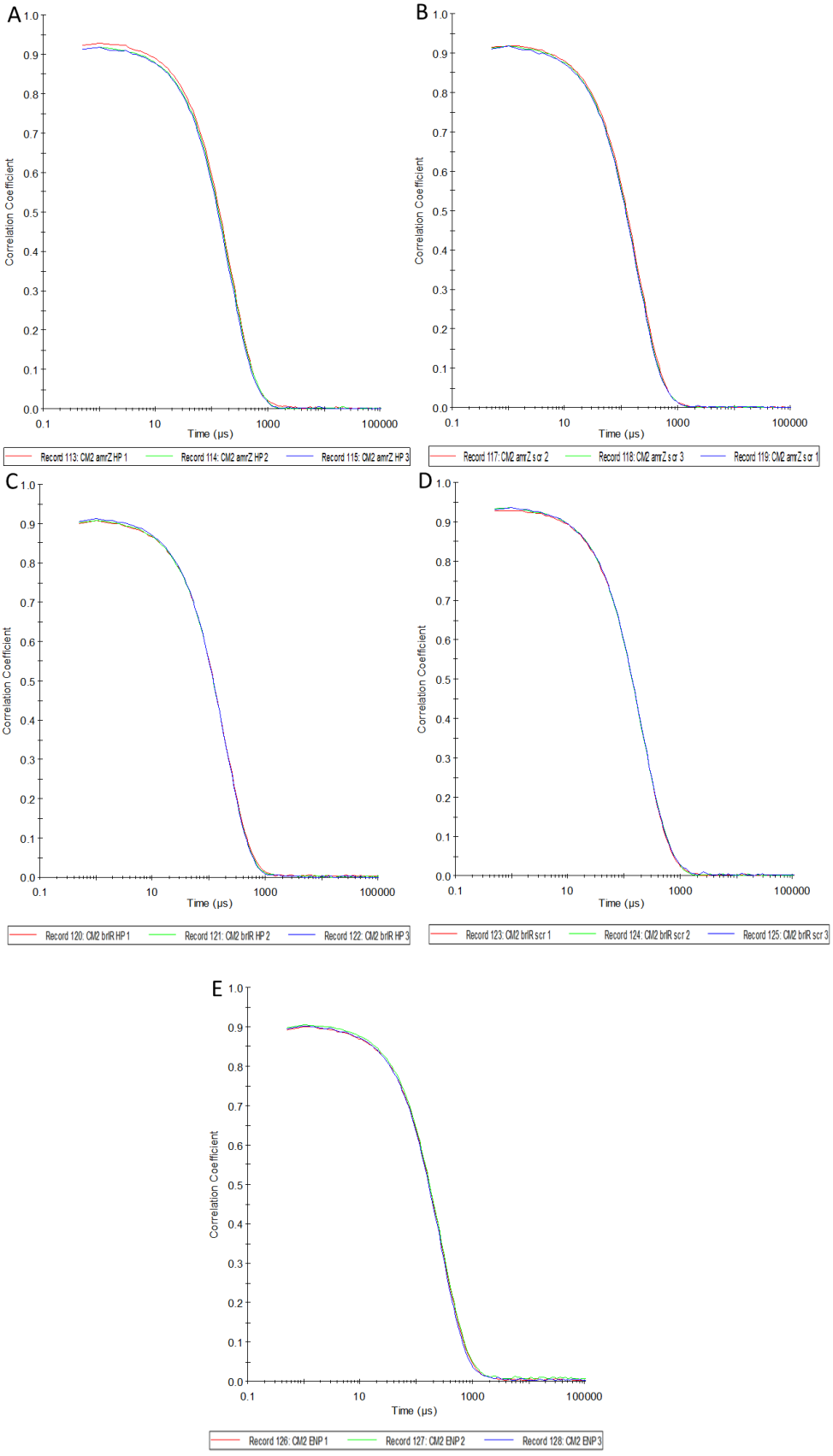

Figure 5.2 Correlograms of (A) AmrZ HP LNP,(B) AmrZ SCR LNP, (C) BrlR HP LNP, (D) BrlR SCR LNP and (E) ENP. Samples were in aqueous solution and analysed at 25 °C. n=3

DLS utilises the principles of Brownian motion and light scattering in order to determine the size of nanoparticles and homogeneity of nanoparticle suspensions [62].

Analysis of DLS data indicated that consistently sized small nanoparticles were formed with deviations from the average less than 2 % for all tested nanoparticles. LNPs were consistently shown to form smaller nanoparticles than 12-bis-THA alone (ENP). The observed drop in diameter is likely caused by ionic interactions between the anionic TFD and cationic 12-bis-THA driving formation of more closely formed nanoparticles. Low PDI indicated that all nanoparticle formulations resulted in homogenous populations aiding in the determination of the stability of the nanoparticles. The PDI indicated little deviation in population size for all analysed nanoparticles indicating consistency within the nanoparticle populations and the absence of large aggregates. When comparing the derived count rate (DCR) of LNPs to ENPs it was observed that the LNPs displayed a three-fold increase in DCR. Although not a direct measure of particle count, the derived count rate (DCR), a normalised measure of detected events, can be used as an indicator for the concentration and/or particle size. Larger DCR indicate the higher concentration, larger particles, or higher concentration and larger particles. The increase in DCR when taken into consideration with the lower Z-average for LNPs highlighted a larger population of nanoparticles were formed when TFD was loaded compared to 12-bis-THA alone. These findings are in line with previously investigated LNPs [53, 168, 169]

Stability Study of 12-bis-THA Nanoparticles in Water

Following confirmation of TFD-12-bis-THA LNPs the stability of these nanoparticles was investigated. DLS measurements were used to assess the stability of LNPs and ENPs. Figure 5.3 shows the change in Z average diameter overtime was minimal within each nanoparticle tested. Little deviation within the three technical reads was observed. ENPs were shown to be consistently larger than all LNPs tested. The seven-day average Z value for each nanoparticle

can be seen in Table 5.4. ENPs showed the greatest deviation in Z average of 4.77 nm and BrlR HP-LNP showed the least deviation of 1.66 nm.

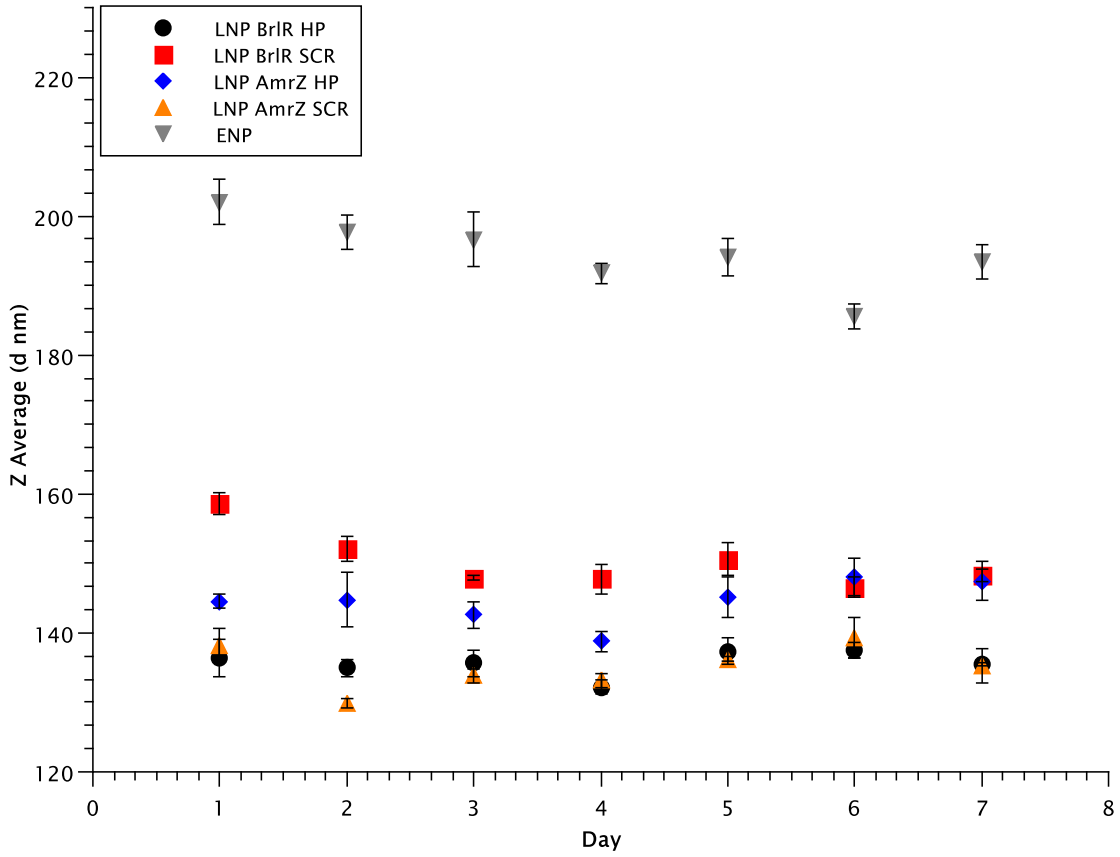

Figure 5.3 Stability of nanoparticles as a function of size-DLS measurements n=3±SD

Table 5.4 Seven-day size average of nanoparticle analysed by DLS n=3

Nanoparticle	Z Avg of Diameter (nm)	Z Avg Standard Deviation
LNP AmrZ HP	144	2.88
LNP AmrZ SCR	135	2.97
LNP BrlR HP	136	1.66
LNP BrlR SCR	150	3.81
ENP	194	4.77

The lack of any observed increase in size of time indicated that nanoparticles did not dissociate and form aggerates when left in solution. These findings combined with low standard deviations

and PDIs recorded over seven days concluded that all formed nanoparticles were stable at room temperature in water.

5.3.3 Confocal Microscopy of TFD Delivery

Following conformation of the formation of stable LNPs for TFD delivery the decomplexation and release of TFD into bacterial cells upon LNP-membrane interaction needed to be investigated. CSLM was used to visualise delivery of RhGn conjugated TFDs using LNPs and alone. ENPs were investigated as a control positive control and an untreated sample imaged as a negative control. Figures 5.4-9 illustrate the results. The presence of a green signal indicated that TFD was present. Blue related to 12-bis-THA and the red membrane stain related to the presence of a bacterial cell. Overlap of signals indicated the co-localization of two or more TFD, 12-bis-THA and *P. aeruginosa* PA14 cells in respect to the colour observed. The presence of a diffuse green signal within the bacterial cells indicated the successful delivery of TFDs by LNPs.

Figure 5.4 shows the confocal images of untreated *P. aeruginosa* PA14. Only the red signal of the membrane stain, WGA 647 is detected, indicating that any fluorescence detected in the green and blue channels for the nanoparticle treated samples was not due to the bacterial cells themselves.

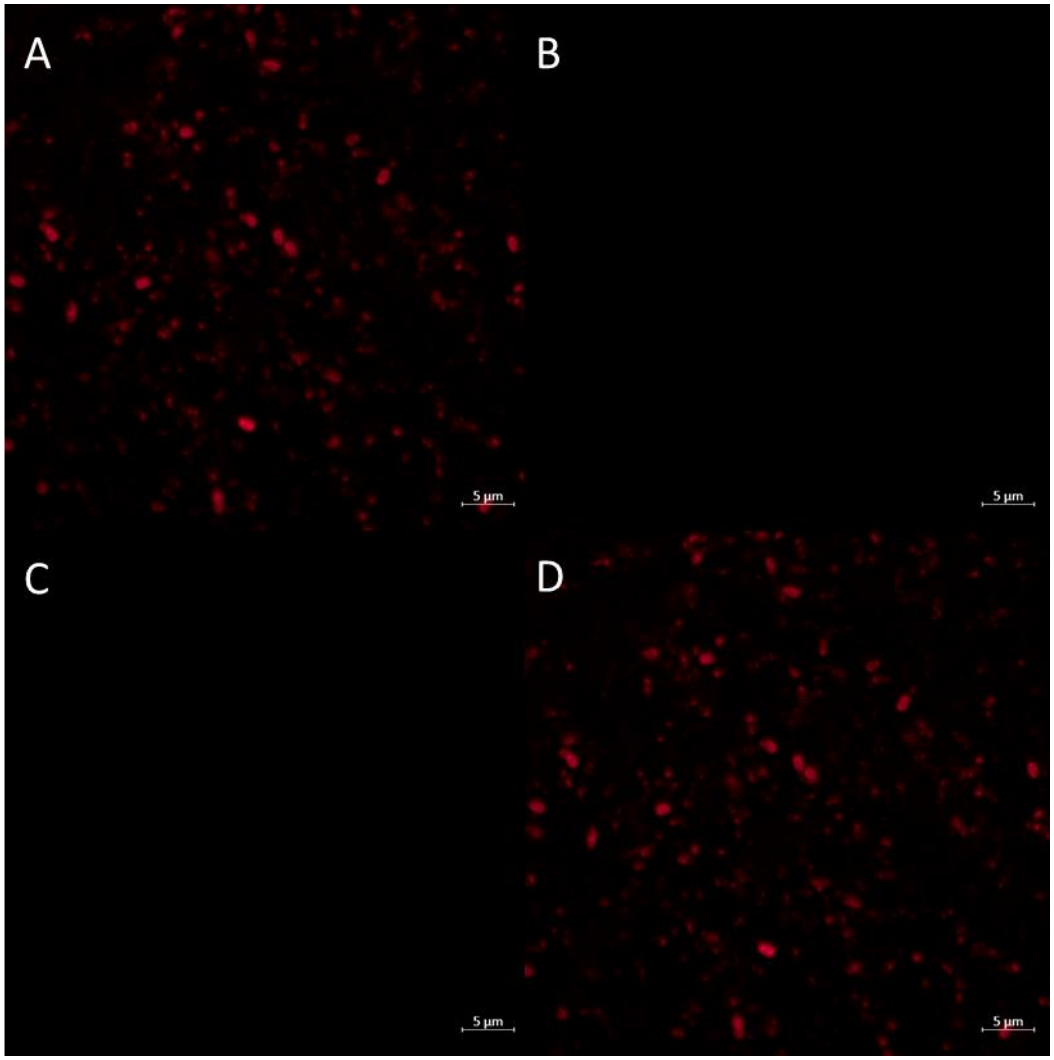

Figure 5.4 Confocal Images of untreated P. aeruginosa PA14 control. (A) depicts the red channel, (B) depicts the green channel, (C) depicts the blue channel, (D) depicts the three merged channels. Emission filters were set as Red: AlexFlour647, Green: Rhodamine Green and Blue: Hoechst H3258.

For ENP treatment (Fig 5.5) the colocalization of 12-bis-THA within the bacterial cell is observed. The combined channels (Fig 5.5D) confirmed that 12-bis-THA was evenly distributed throughout the cell and internalised, with all imaged cells appearing to contain the compound. Additionally, it was noted that there appeared to be little evidence of cell lysis, with all cells observed to be whole.

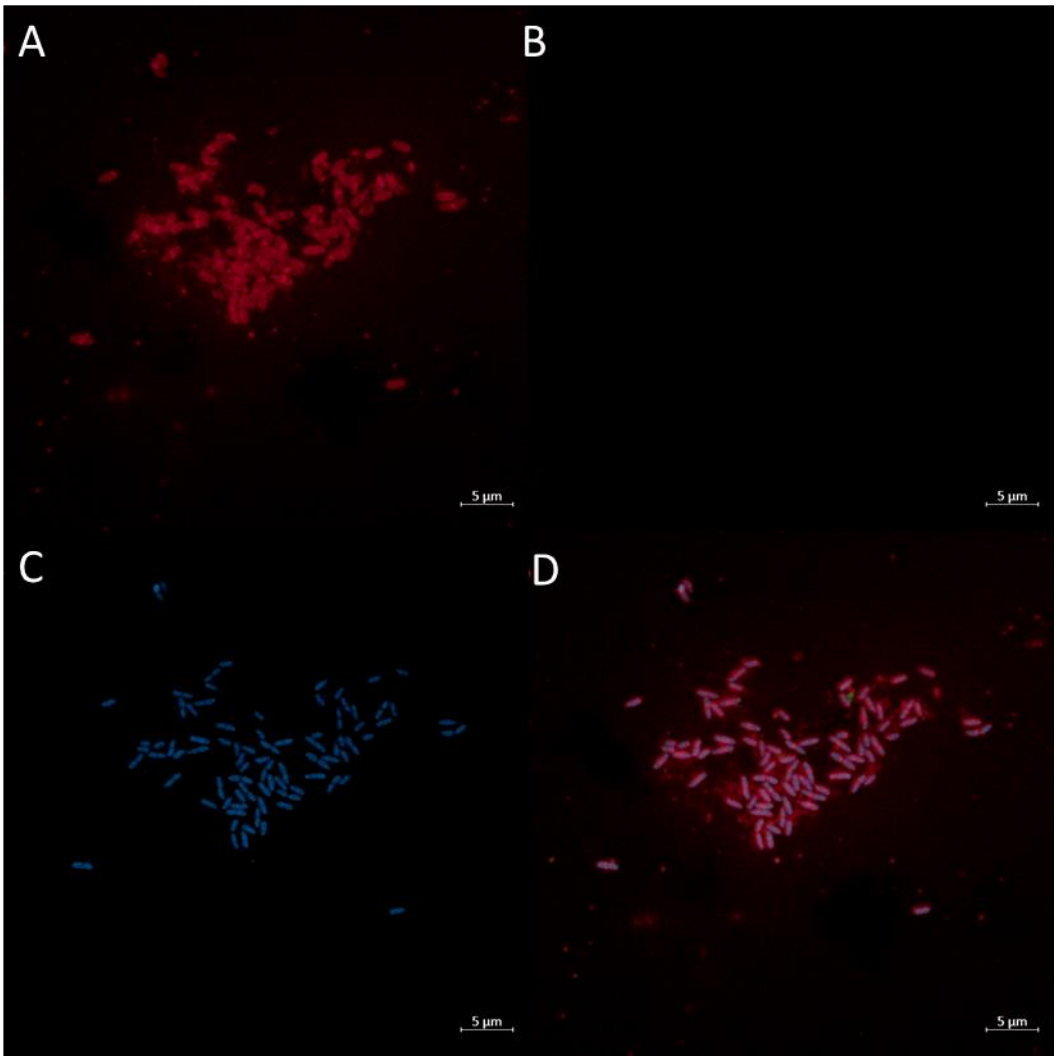

Figure 5.5 Confocal Images of P. aeruginosa PA14 treated with ENP. (A) depicts the red channel, (B) depicts the green channel, (C) depicts the blue channel, (D) depicts the three merged channels. Emission filters were set as Red: AlexFlour647, Green: Rhodamine Green and Blue: Hoechst H3258.

Figures 5.6 and 5.7 illustrate the delivery of RhGn-AmrZ and RhGn-BrlR TFDs using LNPs respectively. Once again internalisation of 12-bis-THA was observed. Isolation of the green channel (Fig 5.6B and 5.7B) indicate internalisation of RhGn-TFD. Analysis of the green channel also displays the presence of RhGn-TFD on the surface of bacterial cells with a propensity to be found on the poles of the cells. This is more greatly observed with RhGn-AmrZ TFD (Fig 5.6B). These findings are in keeping with previous conclusions that 12-bis-THA based LNPs preferentially bind to cardiolipin rich sites [53]. Merged images (Fig 5.6D and 5.7D) show that internalised 12-bis-THA and RhGn-TFD were colocalised. The presence of the WGA 647 marks the external boundary of the cell wall, providing contrast aiding in the determination of

internalised 12-bis-THA and RhGn-TFD observed in Fig 5.6D and 5.7D. Analysis of the blue signal generated by 12-bis-THA compared to the red membrane signal driven by WGA 647 in the LNP and ENP images show that 12-bis-THA was internalised and does not disassociate from the bacterial cell once TFD delivery has occurred, which is in keeping with previous investigations [61].

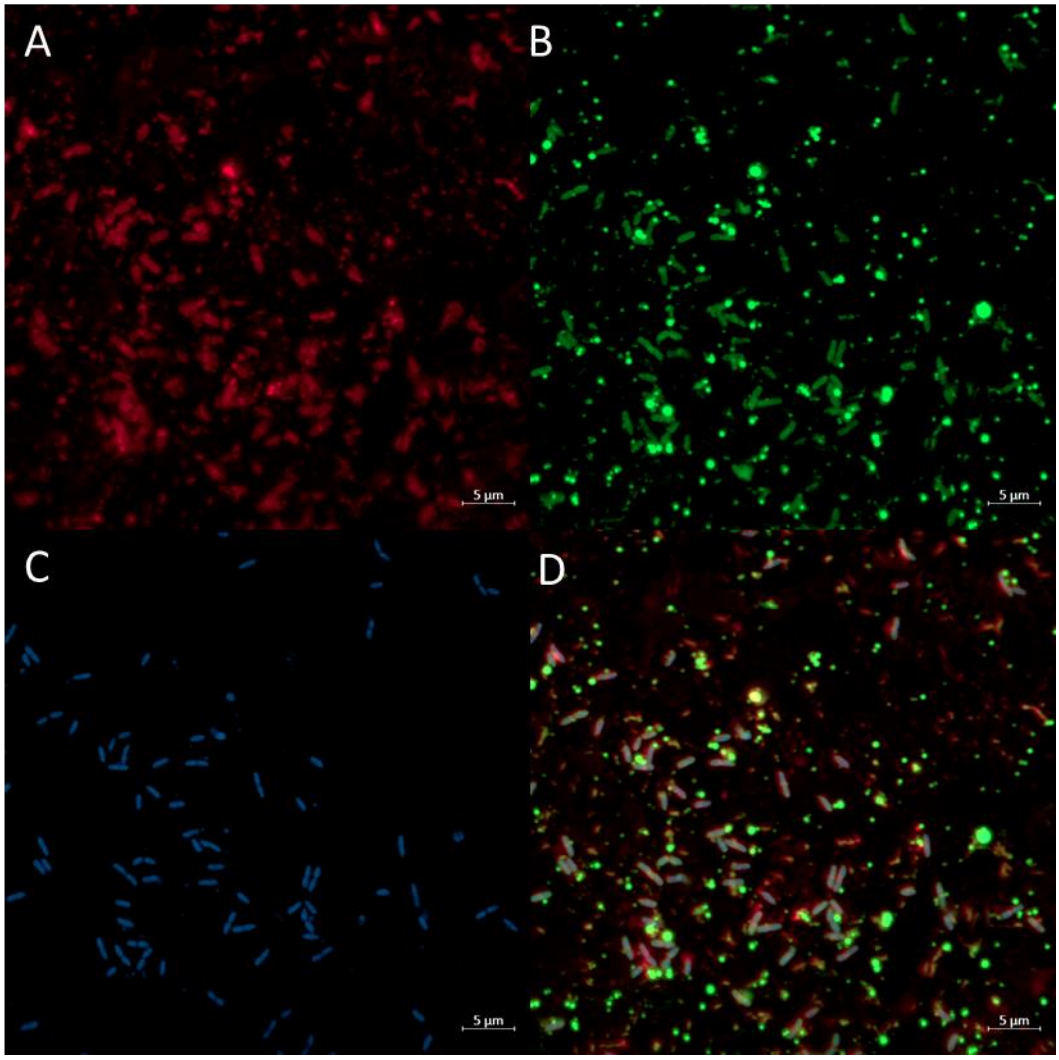

Figure 5.6 Confocal Images of P. aeruginosa PA14 treated with RhGn-AmrZ LNP. (A) depicts the red channel, (B) depicts the green channel, (C) depicts the blue channel, (D) depicts the three merged channels. Emission filters were set as Red: AlexFlour647, Green: Rhodamine Green and Blue: Hoechst H3258.

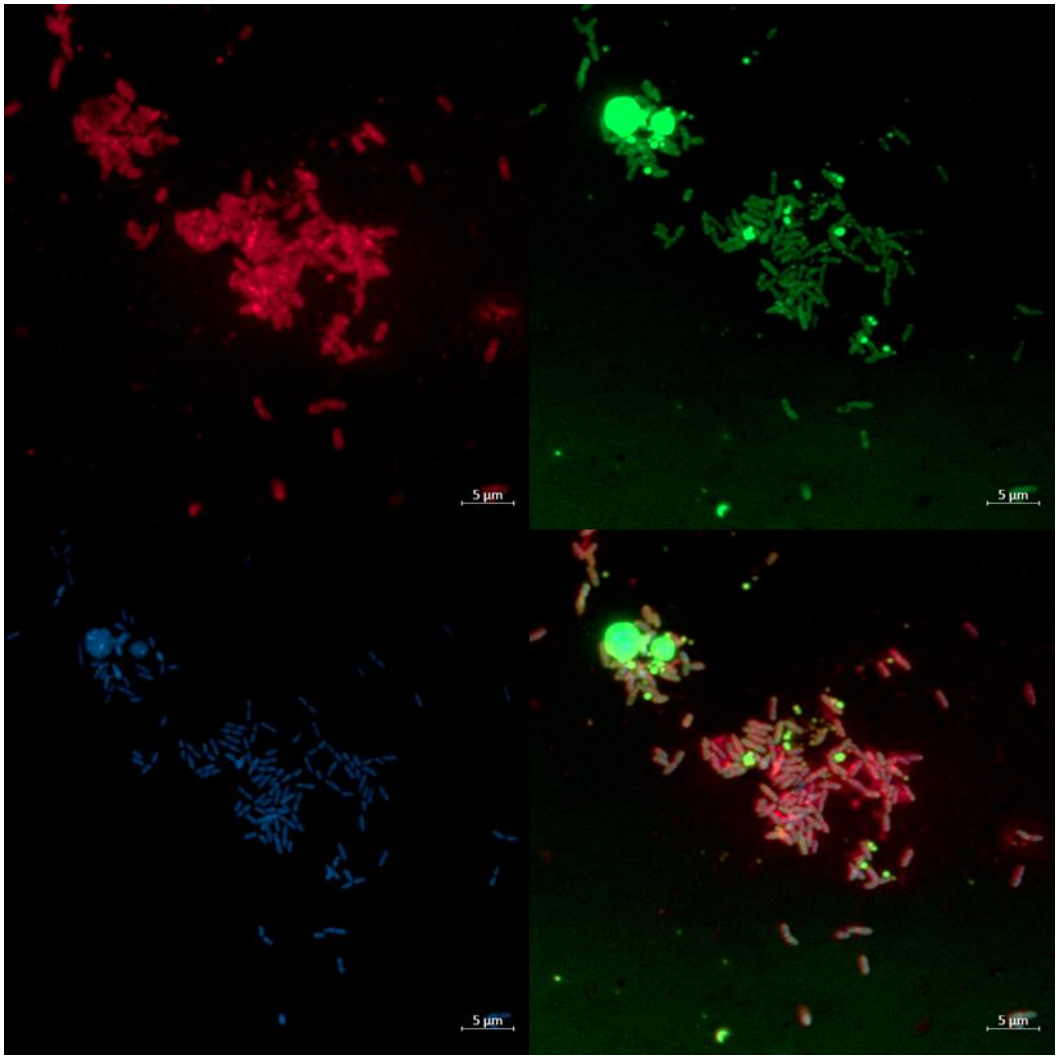

Figure 5.7 Confocal Images of P. aeruginosa PA14 treated with RhGn-BrlR LNP. (A) depicts the red channel, (B) depicts the green channel, (C) depicts the blue channel, (D) depicts the three merged channels. Emission filters were set as Red: AlexFlour647, Green: Rhodamine Green and Blue: Hoechst H3258.

As rhodamine has been shown to self-deliver conjugated molecules [170] the delivery of RhGn-TFDs alone was investigated.

Analysis of confocal images of PA14 treated with RhGn-TFD alone (Fig 5.8, 5.9) showed a reduced rate of internalisation of TFD in comparison to LNP based delivery (Fig 5.6, 5.7). The disparity in delivery is most evident when comparing RhGn-AmrZ delivery (Fig 5.6, 5.7). Although TFD delivery is reduced, successfully delivery of TFD is observed.

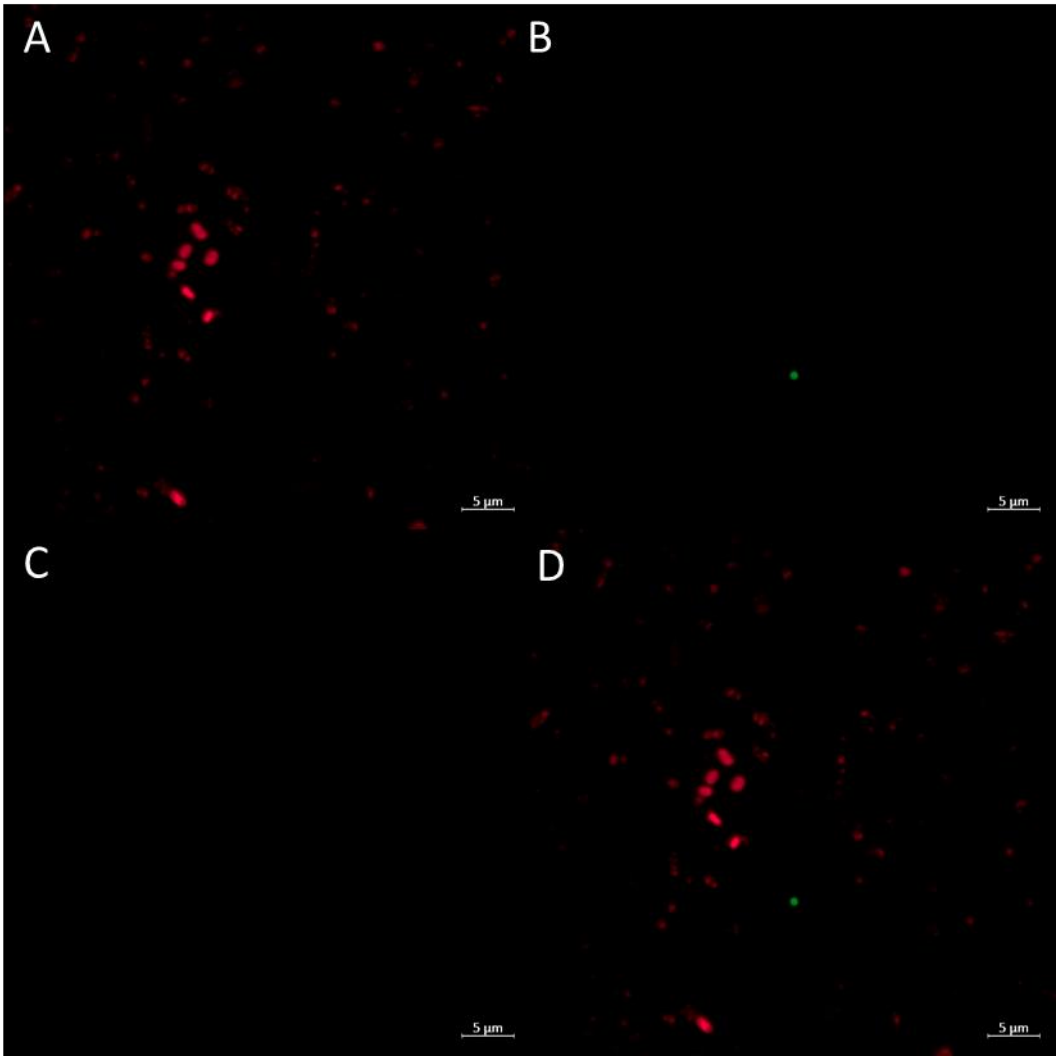

Figure 5.8 Confocal Images of P. aeruginosa PA14 treated with RhGn-AmrZ alone. (A) depicts the red channel, (B) depicts the green channel, (C) depicts the blue channel, (D) depicts the three merged channels. Emission filters were set as Red: AlexFlour647, Green: Rhodamine Green and Blue: Hoechst H3258.

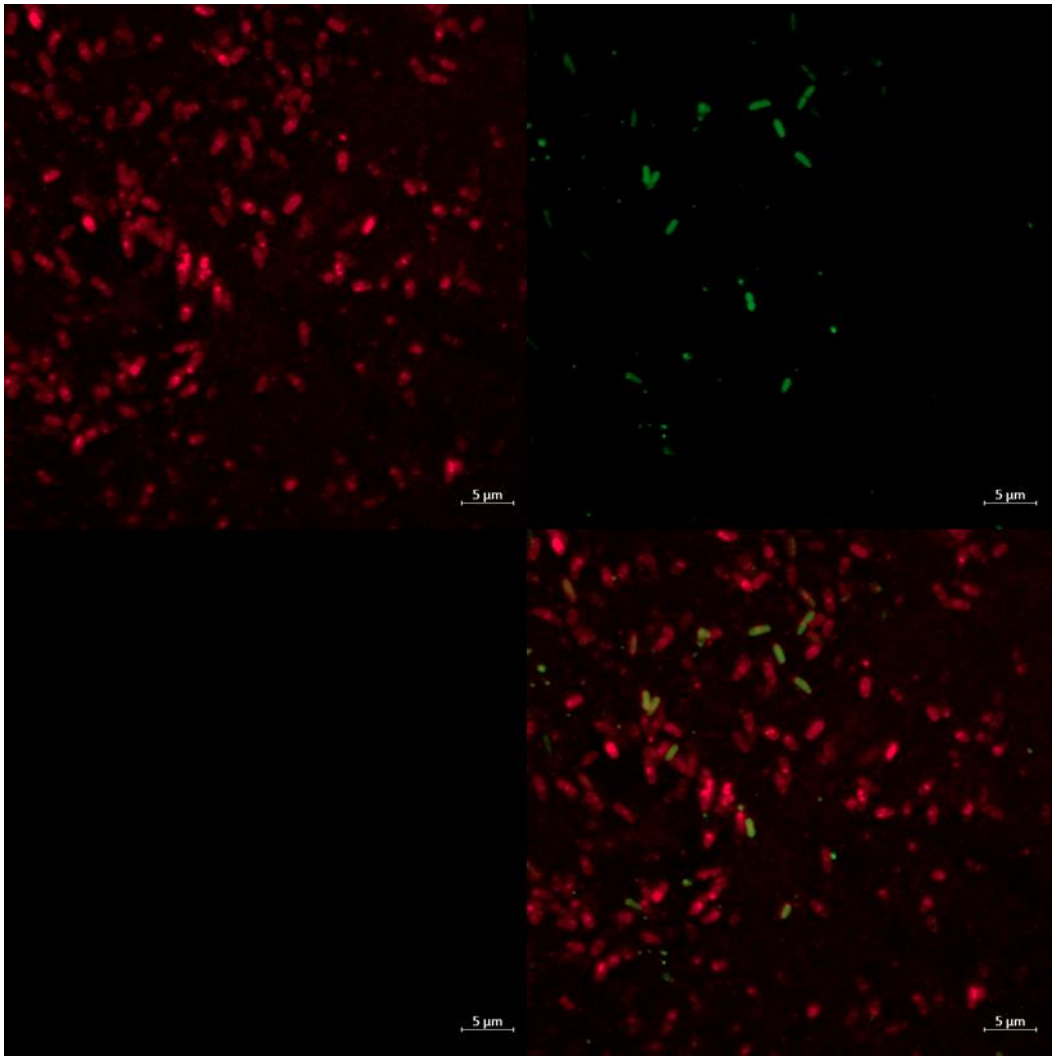

*Figure 5.9 Confocal Images of P. aeruginosa PA14 treated with RhGn-BrlR alone. (*A) depicts the red channel, (B) depicts the green channel, (C) depicts the blue channel, (D) depicts the three merged channels. Emission filters were set as Red: AlexFlour647, Green: Rhodamine Green and Blue: Hoechst H3258.

As the methodology of sample preparation involved a centrifugation and resuspension step to increase the concentration of bacterial cells for imaging, the lack of green signal in RhGn-AmrZ can be explained. As this resuspension step results in any non-cell associated TFD or nanoparticle being lost to the effluent. Although some green signal was found to be internalised in RhGn-BrlR, it was much less intense and wide spread compared to the results found RhGn-BrlR LNP. Regarding why of the TFD only CLSM images only RhGn-BrlR displayed some green signal a possible explanation could be that this signal is due to the uptake of degraded RhGn-BrlR, where only a small oligonucleotide fragment remains attached to the rhodamine green

marker. This fragment is then internalised by the bacterial cell resulting in the observed green signal. In order to corroborate this theory further studies into the stability of the conjugated TFD in these conditions need to be conducted.

Overall, the findings of these experiments confirmed that the observed TFD delivery by LNPs was primarily due to 12-bis-THA membrane associations and not driven by rhodamine conjugation.

5.3.4 Effect of TFD & Nanoparticle Treatment on Growth Rates

Initial investigations explored the impact of TFD delivery on growth rate of *P. aeruginosa* PA14. Figure 5.10 shows the resultant growth curves of bacteria challenged with BrlR HP and SCR LNPs and ENP. Little overall difference between the three treatments was observed across all tested concentrations of nanoparticles. At 100 µg/mL, a concentration 2 doubling dilutions higher than the MIC determined in chapter 4, for all three nanoparticles cell death occurred within 5 h of incubation, confirmed by the resazurin assay. For the lowest four concentrations of nanoparticles tested little difference in OD_{600nm} end point was observed.

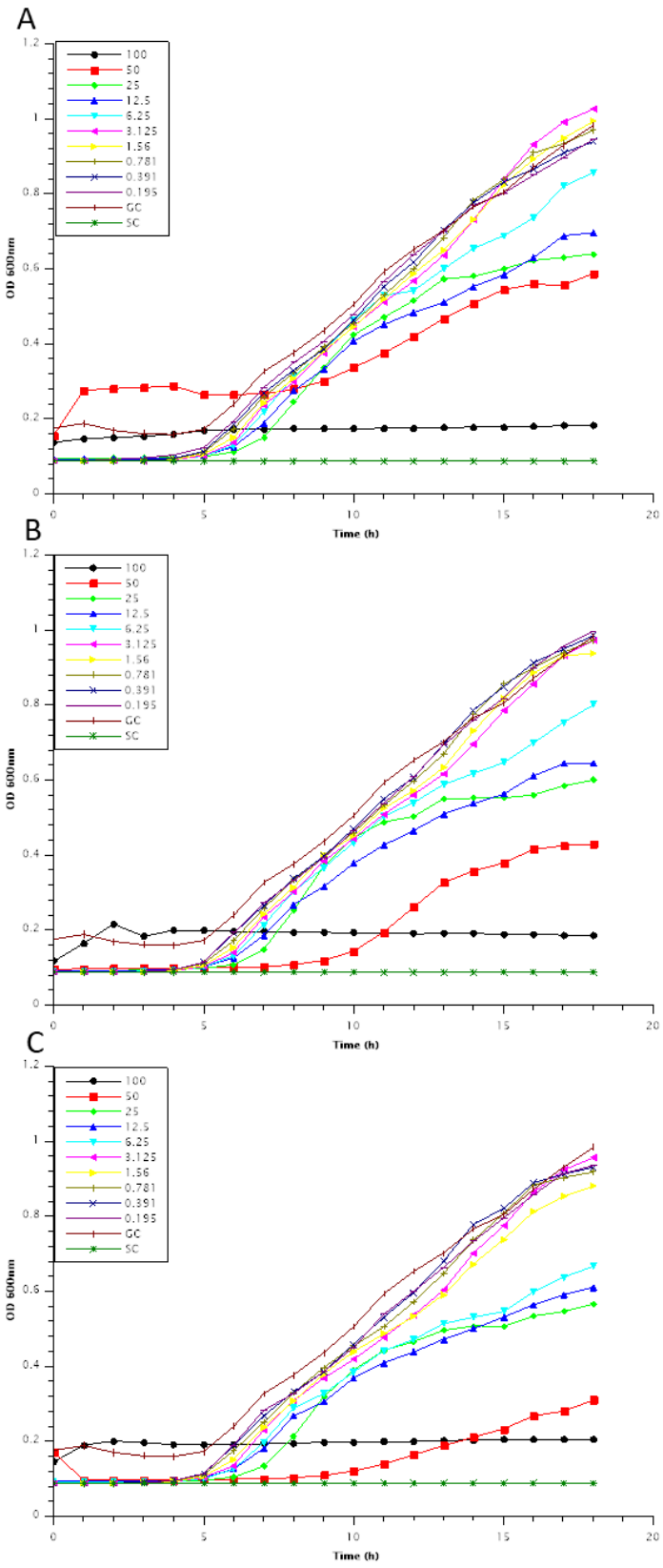

Figure 5.10 Growth of P. aeruginosa PA14 treated with varying concentrations of (A) BrlR HP LNP, (B) BrlR SCR LNP and (C) ENP. Concentrations of LNP and ENP are displayed by the 12-bis-THA component. All Concentrations are in µg/mL. GC=growth control, SC= sterility control. Bacteria were grown at 37°C and 200 rpm. n=3. Readings taken on Biotek Eon

Figure 5.11 displays the resultant growth curves of bacteria challenged with AmrZ HP and AmrZ SCR LNPs and ENP. The results were similar to BrlR HP and BrlR SCR nanoparticle investigations with the addition of complete cell death occurring at 50 µg/mL for all three tested conditions, confirmed by the resazurin assay. Little changes in growth rate were observed between the three types of nanoparticles tested at all concentrations. This result was expected as published investigations had shown no reduction in growth rate for Δ*amrZ*PA14 [154].

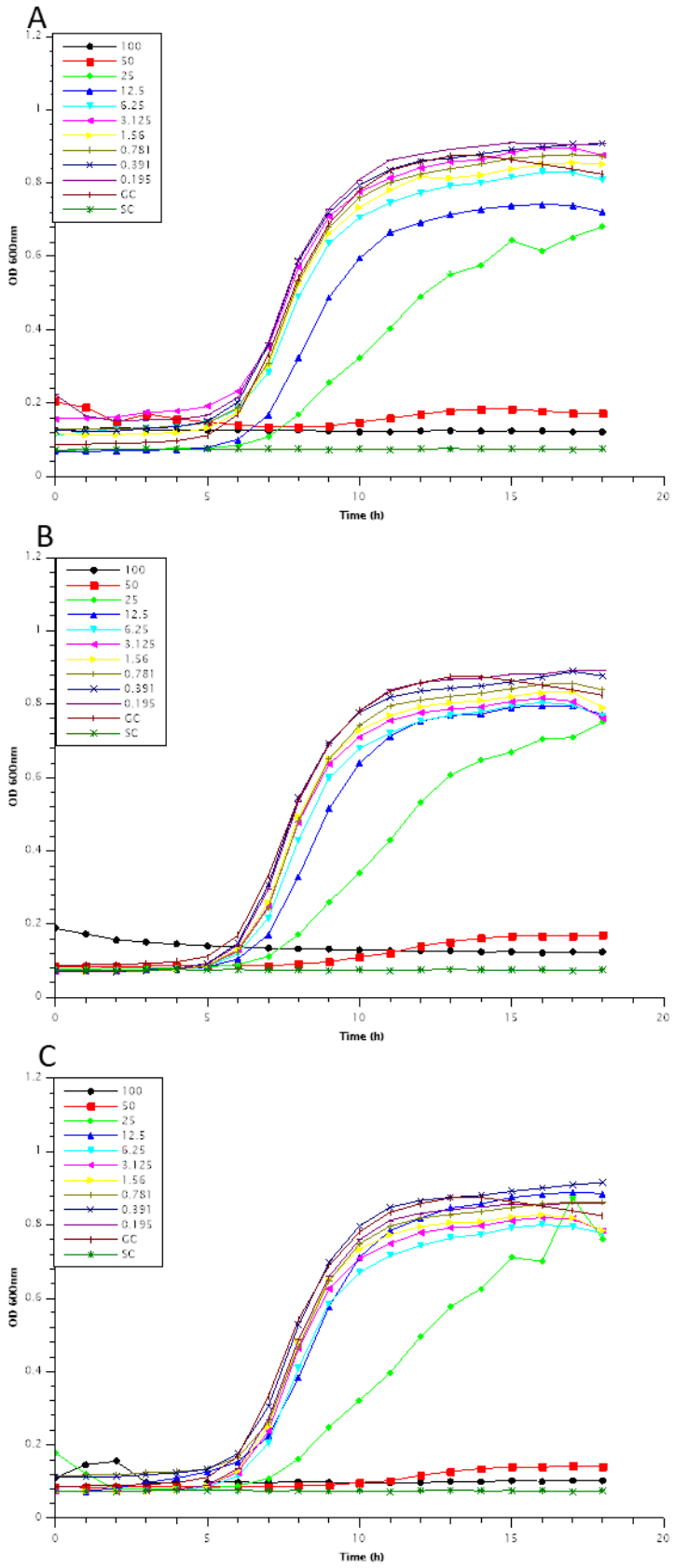

Figure 5.11 *Growth of P. aeruginosa PA14 treated with varying concentrations of (A) AmrZ HP LNP, (B) AmrZ SCR LNP and (C) ENP*. Concentrations of LNP and ENP are displayed by the 12-bis-THA component. All Concentrations are in µg/mL. GC=growth control, SC= sterility control. Bacteria were grown at 37°C and 200 rpm. n=3. Reading taken on Biotek Powerwave.

5.3.5 Confirmation of Δ*brlR*PAO1 Knockout

In order to confirm the genetic knockout of *brlR* in the Δ*brlR*PAO1 strain gifted by Lichuan Gu colony PCR of Δ*brlR*PAO1 and the parental strain (WTPAO1) was conducted. The sigma factor RpoD was used as a control. Bands for *brlR* were expected at 73 bp and 51 bp for *rpoD.* Figure 5.12 shows the results of the agarose gel electrophoresis confirming knockout of *brlR* in the mutant and presence of *brlR* in the parental strain.

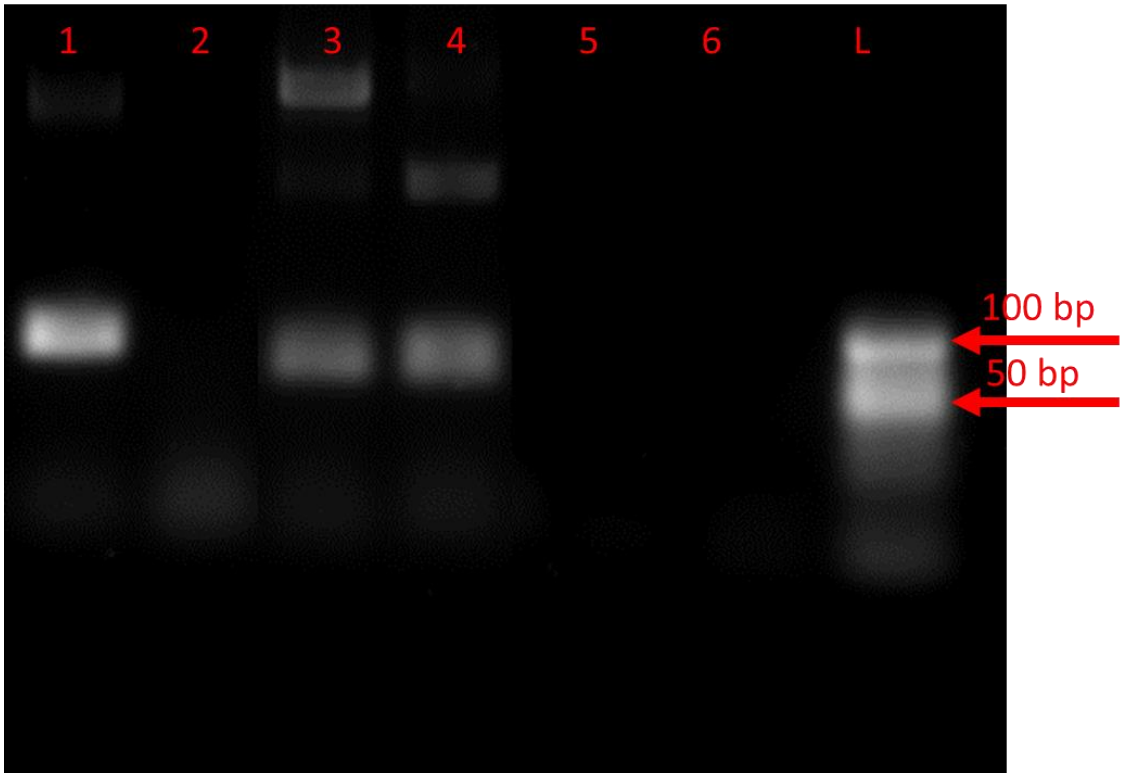

Figure 5.12 Agarose gel image confirming knockout of brlR. L=ladder. 1: Presence of blrR PCR product in WTPAO1, 2 brlR PCR product in ΔbrlRPAO1, 3 rpoD in WTPAO1, 4 rpoD in ΔbrlRPAO1, 5 no template control of brlR primers, 6 no template control of rpoD primers. PCR products between 100-50 bp.

5.3.6 Change in Tobramycin Tolerance in Response to TFD Treatment

As no impact on growth was associated with TFD delivery was observed investigations focused on determining whether any phenotypic changes could be detected upon TFD treatment. Published investigations into BrlR activity have determined that in Δ*brlR*PAO1 flow cell biofilms a decrease in tobramycin tolerance is observed when compared to the wildtype. Interestingly,

this is not observed in microtiter plate formed biofilms and subsequent investigations concluded that BrlR is not active in these conditions [158]. Additionally, this group also concluded that *ΔbrlR* strains did not display any significant changes in antibiotic resistance in planktonic conditions in relation to the wildtype. These findings made determining a phenotypic change in response to BrlR HP TFD delivery difficult. Further studies by Wang et al. [159] established a methodology for detecting BrlR induced antimicrobial tolerances in planktonic conditions. They concluded that BrlR can be induced by pyocyanin binding in planktonic conditions. In the presence of 0.2 mM pyocyanin an approximate 2 log increase in cell survival post tobramycin treatment was observed for wildtype PAO1. This increased tolerance was absent in the knockout strain. Therefore, this methodology was adapted to determine the phenotypic effect of the BrlR HP TFD using the *ΔbrlR*PAO1 and WT PAO1 kindly provided by this group.

To determine whether a BrlR targeted TFD was successful in blocking its activity upon delivery, the phenotypic change in tobramycin tolerance was investigated. Figure 5.13 shows the cfu/mL determined post tobramycin treatment for PAO1. When treated with BrlR HP LNPs at 6.25 μg/mL a 4-5 $\log_{10}$ increase in cfu/mL was observed when PAO1 was grown in the presence of pyocyanin compared to a control (Fig 5.13A). At 50 μg/mL little difference in cfu/mL in either condition was noted. For BrlR SCR LNPs (Fig 5.13B) consistently there was more cfu/mL in the presence of pyocyanin compared to the absence. No discernible trend is seen with ENP treatment (Fig 5.13C). Statistical analysis using a one tailed Students t-test found no statistical significance, $p \leq 0.05$, between cfu/mL determined in the presence or absence of pyocyanin. However, at 0 μg/mL and BrlR HP at 6.25 μg/mL significance was seen at $p \leq 0.1$. The p value of BrlR SCR at 6.25 μg/mL was found to be 0.15.

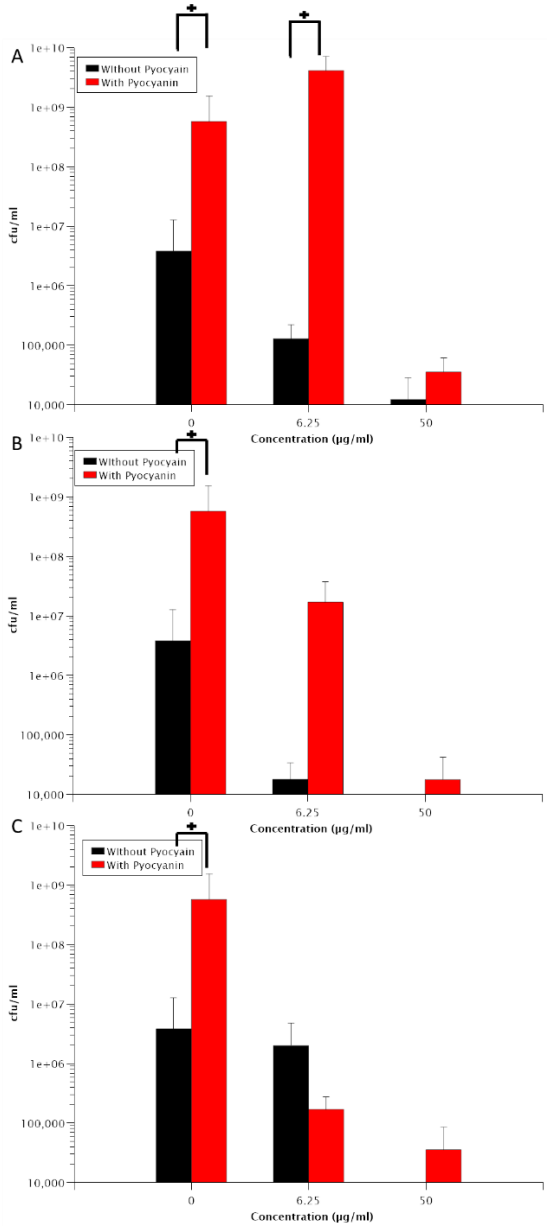

Figure 5.13 Comparison of PAO1 cfu/mL post tobramycin treatment in the presence or absence of 0.2 mM pyocyanin when co-treated with (A) HP LNPs, (B) SCR LNPs and (C) ENPs. Concentrations are expressed in relation to the 12-bis-THA component of the nanoparticles. No bars indicate of cfu/mL of 0. At p≤0.05 there is no statical significance. However statistical significance was observed at p≤0.1 indicated by +

Figure 5.14 shows the comparison of cfu/mL for the PAO1 parental strain and *ΔbrlR*PAO1 post tobramycin treatment when bacteria were grown in the presence of BrlR HP LNPs. For *ΔbrlR*PAO1 (Fig5.14B) there is little difference seen between cfu/mL when grown in the presence or absence of pyocyanin. For the two lowest LNP concentrations there is a greater log increase in cfu/mL in the presence of pyocyanin for the wild type compared to the knockout.

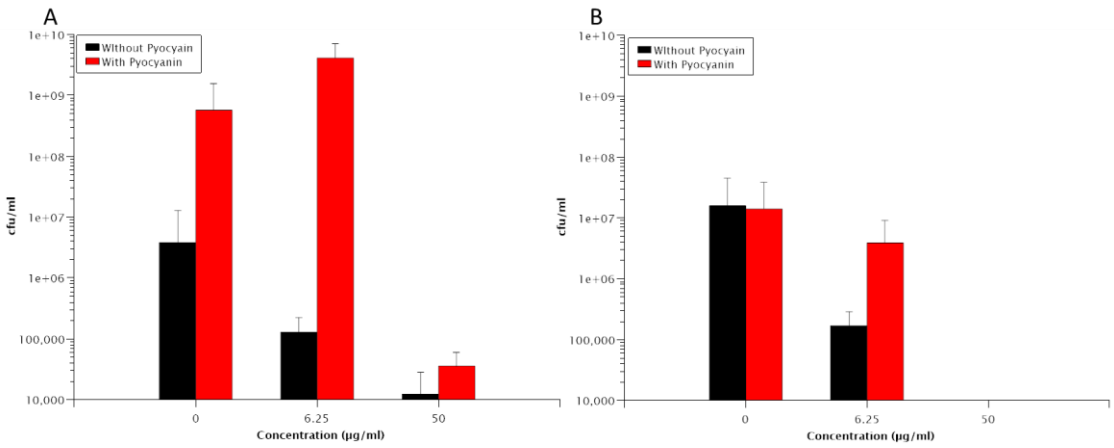

Figure 5.14 Comparison of cfu/mL post tobramycin treatment in the presence and absence of 0.2 mM pyocyanin when treated with HP LNPs for (A) PAO1 and (B) ΔbrlRPAO1. Concentrations are expressed in relation to the 12-bis-THA component of the nanoparticles. No bars indicate cfu/mL of 0.

Initial investigations in PAO1 established at approximate 3 log increase in cfu/mL in the presence of pyocyanin versus absence of pyocyanin, mimicking the findings of Wang et al. For both targeted TFD (BrlR HP) and the non-targeted (BrlR SCR) TFD control, at the lower concentration of 6.25 µg/mL there was no observed loss of tobramycin tolerance in the presence of pyocyanin indicating that neither TFD had imparted a phenotypic effect at the doses tested. At the higher LNP concentrations tested there was no statistically significant difference in cfu/mL between bacteria grown in the presence or absence of pyocyanin. When comparing these results to the ENP control it is likely that these similar cfu/mL results were due to 12-bis-THA activity rather than TFD activity. An interesting point of note is that the structure of pyocyanin is similar to that of the head group of 12-bis-THA (Fig 5.15), occupying a similar planar space. Therefore, there is the possibility that 12-bis-THA may compete with the binding site of pyocyanin on BrlR. This may somewhat explain the increase cfu/mL in the non-pyocyanin condition compared to the pyocyanin condition observed for ENPs at 6.25 µg/mL. However, further investigations are required to fully confirm this theory.

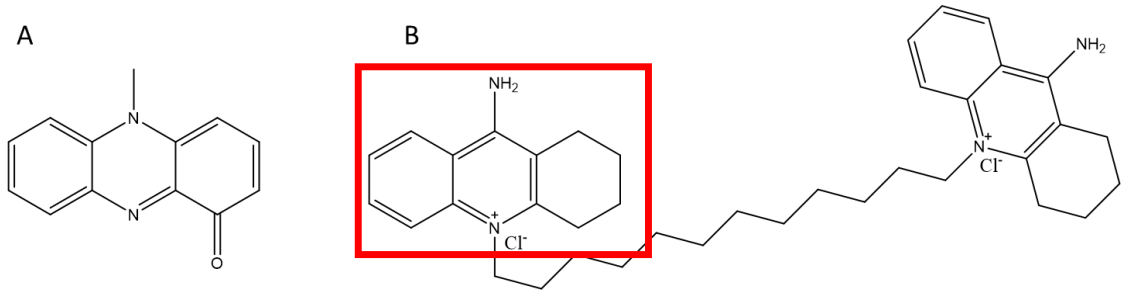

Figure 5.15 Chemical Structure of (A) Pyocyanin and (B) 12-bis-THA. The headgroup of 12-bis-THA highlighted is by red frame.

Comparison of BrlR HP LNP treated PAO1 and Δ*brlR*PAO1 determined that no knockdown of the pyocyanin induced phenotype occurred. At the higher concentration of LNP cfu/mL of PAO1 was found to be similar to that of Δ*brlR*PAO1, however once again it is most likely that the cause of this similarity is due to 12-bis-THA activity rather than TFD induced knockdown. One point of note of these studies is that only final cfu/mL values post tobramycin treatment were compared. Within the Wang et al. study increased tobramycin tolerance was recorded by log reduction of cfu/mL post tobramycin treatment as a function of pre tobramycin cfu/mL. Therefore, further studies need to be conducted for BrlR HP activity where pre tobramycin treatment cfu/mLs are available. With the current available data, the activity of BrlR HP TFD cannot be established.

5.4 General Discussion

The aims of this chapter were to design and test TFDs against TF targets identified from *P. aeruginosa* proteomic investigations. Unforutanaly due to time constrains caused by the COVID-19 pandemic investigations into AmrZ HP TFD activity were not completed.

Unsuccessful Efficacy of Targeted TFDs Despite Successful Delivery

Despite CLSM experiments proving successful delivery of the two TFDs designed in this chapter, no efficacy was established in regards to phenotypic response. When taking into account both phenotypic experiments conducted it is worth of note that nanoparticles addition occurred at 0 h. Although stability in aqueous solution has been proven for all nanoparticles tested in this chapter, the stability in media and physiological temperatures is unknown. Therefore, taking these two factors into account, it may be possible that lack to targeted TFD efficacy may be in part due to nanoparticle instability in these conditions. Further investigations are required to determine the stability of the tested nanoparticles in these conditions as changes in the ionic composition of the solvent may have accelerated particle degradation and aggregation. Indeed, the ZP of the nanoparticles may have been altered as this measure is dependent not only on the surface of the nanoparticle but also the nature of the solvent [64].

Conclusion

This chapter established TFDs targeted towards AmrZ and BrlR as well as non-targeted controls. DLS and zeta potential measurements confirmed the formation of stable nanoparticles in water. Confocal microscopy established that these LNPs successfully delivered the encapsulated TFDs into planktonic *P. aeruginosa.* Unfortunately, initial phenotypic studies were unable to establish a phenotypic activity of the BrlR targeted TFD. Further investigations into AmrZ HP and BrlR HP TFDs need to be conducted in order to determine efficacy.

Chapter 6: General Discussion, Conclusions and Future Work

The overall aims of this thesis were to establish a proteomic workflow that could successfully identify valid targets for the novel TFD/12-bis-THA antimicrobial system in *P. aeruginosa*. The work in this thesis established a sample preparation protocol utilising the model organism *E. coli*, for which there was a readily available TF reference source. Shortcomings of the statistical analysis of the *E. coli* proteomic datasets informed the proteomic workflow design for investigations in *P. aeruginosa* where a swich from LFQ to TMT based quantification overcame these. The results of the proteomic analysis of *P. aeruginosa* PA14 treated with 12-bis-THA informed the selection of TFs for TFD development. These TFDs were then developed and tested *in vitro* to determine uptake and efficacy. The rich proteomic dataset generated in chapter 4 allowed for the identification and selection of TF targets. The targets were subsequently targeted with TFDs developed in chapter 5. Unforutanaly the efficacy of these TFDs was unable to be established. However, the proteomics-based approach has enabled a targeted TFD development pipeline to be established with a protocol that can be applied to other organisms for future investigations.

6.1 Challenges in the Proteomic Approach

6.1.1 Sample Preparation

A vital and often overlooked step of proteomics is the sample preparation. Within LC-MS/MS based proteomics the 'crud in, crud out' principle applies as the resultant spectra are highly influenced by the composition of the sample being analysed [102, 107]. The impact of common contaminants such as keratin from the environment can waste processing time and potentially mask protein/peptide signals [171]. Additionally, as previously discussed, when applying proteomics for TF detection, fractionation is often key in preventing TF peptide signal masking [76]. With the importance of these two principles in mind, reducing contamination and purifying samples for TFs, a sample preparation protocol was developed. Using the model organism *E. coli,* for which there is readily available TF resource [95] a successful in-gel fractionation method

was developed and applied to the bacterium of interest, *P. aeruginosa*. Although the true impact of fractionation on TF identification was not fully established in this thesis due to problems in the LC-MS/MS process for the TPL sample, this sample preparation methodology did yield good TF coverage, reaching 51 % in the improved proteomic workflow applied to *P. aeruginosa*.

6.1.2 Quantification Approach

Following the lack of statistically significant results using LFQ LC-MS/MS in *E. coli* a change in the proteomic approach was made for *P. aeruginosa* analysis. The addition of the isobaric tags known as tandem mass tags allowed for all nine proteomic samples to be mixed and analysed on the mass spectrometers simultaneously. This reduced the impact of run-to-run variations which had greatly affected the results of chapter 3 and reduced the amount of missing data present in the *P. aeruginosa* output compared to the *E. coli* datasets. It has been shown in the literature [128] that TMT SPS-MS3 results in less missing data compared to LFQ based proteomics as the impact of low intensity peaks is less prevalent in this methodology. LFQ proteomics is dependent on spectral peaks crossing a threshold to be quantified, therefore it is inherently more likely to fail to detect low intensity proteins such as TFs. This is not the case in a TMT based approach at the reporter ion peaks are used in quantification. Additionally, the use of a TMT approach improved the depth of the proteomic coverage, 3154 proteins detected, when compared to the LFQ approach in *E. coli* where the largest dataset returned 1529 proteins, a result which has been reflected in the literature [80, 128]. The improvement in the depth of coverage is additionally improved by the use of high pH, reverse phase chromatography. This allowed for greater separation of the peptide mixture as it was fractioned into four, resulting in four separate mass spectral outputs. This separation aided in improving the accuracy of the proteomic analysis as it allowed for the detection of a greater number of peaks.

6.2 TFD Delivery and Efficacy

From the findings of chapter 4, two TFs of interest, AmrZ and BrlR, were identified and taken forward for TFD development and testing. Both TFs had information about binding site sequences available in the literature, allowing for the design of TFDs. Additionally, the availability of knockout strains aided in investigations into phenotypic changes brought about by LNP treatment.

6.2.1 LNPs

DLS and zeta potential experiments established that both targeted and scrambled TFDs for AmrZ and BrlR formed stable LNPs with 12-bis-THA in aqueous solution. Thus, establishing that LNPs were of suitable quality when used in phenotypic experiments.

CLSM using rhodamine tagged TFD based LNPs indicated that the 12-bis-THA based delivery system did indeed successfully deliver the TFDs of interest into planktonic bacterial cells as expected when compared to previously published studies [53].

6.2.2 Does Successful TFD Delivery Induce a Measurable Phenotypic Response?

Following the establishment of successful TFD delivery using 12-bis-THA based nanoparticles, investigations into phenotypic response were conducted. After initial growth rate experiments found no phenotypic change targeted investigations into changes in tobramycin susceptibility in response to BrlR targeted TFD treatment were investigated. Design of a phenotypic assay for the BrlR targeted TFD was difficult as previously published studies had found BrlR to only be active in flow cell conditions [158]. The adaptation of the protocol by Wang et al. [159] allowed for the investigation into phenotypic response to BrlR HP LNP treatment. The findings of the phenotypic response studies indicated that the BrlR targeted TFD likely had no measurable impact on tobramycin tolerance. However, the experimental design was limited to two treatment conditions. Further investigations are needed to determine the efficacy of TFD

activity and its impact. Additional experiments including an additional cfu sampling point prior to tobramycin treatment would give further insight into the change in cell viability post treatment. This additional sample would allow for the calculation of log reduction of cfu/mL in response to tobramycin treatment and provide a more in-depth analysis of BrlR phenotypic activity. This use of log reduction for BrlR phenotypic analysis would also result in an experiment closer in design to the original described by Wang et al. which utilised log cfu/mL reductions in their analysis.

6.3 Future Research

6.3.1 Further LNP Stability Studies

Initial LNP stability investigations focused on aqueous suspensions at room temperature to establish the stability of LNP stocks used in experiments. Further investigations need to be conducted into LNP stability in culture media and at experimental temperatures. This will inform whether the LNPs are active throughout fitness cost studies. Additionally, time kill investigations will also inform the efficacy of LNPs over time in culture conditions.

6.3.2 Investigations into TF Activity Following 12-bis-THA Treatment

Initial proteomic investigations utilised at bottom-up shotgun approach to generate a large dataset in a cost-effective manner. However, by design, the bottom-up technique results in the loss of protein structural information as proteins are enzymatically digested prior to MS analysis. Therefore, although the presence of TFs can be established via this method, the information regarding whether the TF was in the active or inactive conformation at the point of harvest is lost as only the primary protein structure is returned via this method. Further analysis into TF conformation may be possible via either a top-down targeted proteomic approach or investigations utilising ChIP. As top-down proteomics involves ionisation of the intact protein the resultant data will return structural information, however this approach may be cost limited

and would require the development of an additional sample preparation protocol. The alternative of ChIP has been previously utilised in TF studies in *E. coli* [66, 67] and would not only return information about activity but also information regarding binding sites.

6.3.3 Further TFD Activity Investigations

Investigations into TFD activity in this thesis were limited to initial phenotypic investigations. Studies into AmrZ HP TFD activity were not completed due to the COVID-19 pandemic. As this is a global TF it is investigations into this target should be pursued. As initial BrlR targeted phenotypic studies indicated a lack of TFD activity upon delivery a rethink of the phenotypic experimental design is required.

Phenotypic response assays are difficult to establish for BrlR in planktonic conditions due to the reported inactivity of BrlR in these conditions [158]. Therefore, the use of qPCR should be considered. The use of qPCR to investigate the regulons of BrlR and AmrZ would aid in establishing TFD efficacy. These assays would establish whether a knockdown of BrlR or AmrZ expression had been achieved via a reduction in reported fluorescent signal compared to the controls.

6.3.4 Testing of Alternative 12-bis-THA Doses

The proteomic experiments conducted in *P. aeruginosa* involved investigating only two treatment conditions. As the majority of TFs detected were found to be downregulated at 1x MIC when compared to both the control and 0.1x MIC investigations into intermediate doses may be of interest. Testing of doses between 0.1 and 1x MIC would greatly inform the TF response to 12-bis-THA treatment and may highlight additional TF targets.

6.4 Conclusion

TFD based therapy has the potential to be a good alternative to traditional small molecule-based antimicrobials. Alongside its 12-bis-THA delivery compound a bacterium specific system can be

established allowing for targeted therapies against TFs upregulated by 12-bis-THA mediated stress.

In this thesis a proteomic workflow was established for the investigation into changes in TFs in response to 12-bis-THA treatment. This has allowed for the identification of TFD targets which were taken forward for development. Although initial investigations were unable to establish a TFD-specific effect, further investigations are required to establish whether this is conclusive.

The proteomic workflow established show great potential and can be applied to other organisms of interest and alternative delivery molecules, allowing for the identification of further TFD targets.

References

1. Trust, C.F. Frequently asked questions about cystic fibrosis. 2021 [cited 2021 12/05/2021]; Available from: https://www.cysticfibrosis.org.uk/what-is-cystic-fibrosis/faqs#.
2. Cutting, G.R. Cystic fibrosis genetics: from molecular understanding to clinical application. *Nat Rev Genet*, 2015. 16(1):45-56.
3. Chmiel, J.F. and Davis, P.B. State of the Art: Why do the lungs of patients with cystic fibrosis become infected and why can't they clear the infection? *Respiratory Research*, 2003. 4(8).
4. Scheid, P., Kempster, L., Griesenbach, U., Davies, J.C., Dewar, A., Weber, P.P., Colledge, W.H., Evans, M.J., Geddes, D.M., and Alton, E.W.F.W. Inflammation in cystic fibrosis airways: relationship to increased bacterial adherence. *Eur Respir J,* 2001. 17(1): 27-35.
5. Turcios, N.L., Cystic Fibrosis Lung Disease: An Overview. *Respir Care*, 2020. 65(2):233-251.
6. Bhagirath A.Y., Li Y., Somayajula D., Dadashi M., Badr S. and Duan K. Cystic fibrosis lung environment and *Pseudomonas aeruginosa* infection. *BMC Pulm Med*. 2016;16(1):174.
7. Folkesson A, Jelsbak L, Yang L, Johansen HK, Ciofu O, Høiby N, Molin S. Adaptation of *Pseudomonas aeruginosa* to the cystic fibrosis airway: an evolutionary perspective. *Nat Rev Microbiol.* 2012. 10(12):841-51.
8. Gilligan, P.H., Microbiology of airway disease in patients with cystic fibrosis. *Clin Microbiol Rev*, 1991. 4(1):35-51.
9. Williams, H. D., Behrends, V., Bundy, J. G., Ryall, B., and Zlosnik, J. E. Hypertonic Saline Therapy in Cystic Fibrosis: Do Population Shifts Caused by the Osmotic Sensitivity of Infecting Bacteria Explain the Effectiveness of this Treatment?. *Frontiers in microbiology*. 2010. 1.
10. Kreda, S.M., Davis, C.W. and Rose, M.C. CFTR, mucins, and mucus obstruction in cystic fibrosis. *Cold Spring Harb Perspect Med*. 2012. 2(9)
11. Coburn, B., Wang, P.W., Diaz Caballero, J., Clark, S.T., Brahma, V., Donaldson, S., Zhang, Y., Surendra, A., Gong, Y., Elizabeth Tullis, D., Yau, Y.C., Waters, V.J., Hwang, D.M. and Guttman, D.S. Lung microbiota across age and disease stage in cystic fibrosis. *Sci Rep*. 2015. 5
12. Crull, M.R., Somayaji, R., Ramos, K.J., Caldwell, E., Mayer-Hamblett, N., Aitken, M.L., Nichols, D.P., Rowhani-Rahbar, A. and Goss, C.H. Changing Rates of Chronic *Pseudomonas aeruginosa* Infections in Cystic Fibrosis: A Population-Based Cohort Study. *Clin Infect Dis.* 2018 14;67(7):1089-1095
13. Elrod, R.P. and Braun, A.C. *Pseudomonas aeruginosa*: Its Role as a Plant Pathogen. *J Bacteriol,* 1942. 44(6):633-45.
14. Moradali, M.F., Ghods, S. and Rehm, B.H. *Pseudomonas aeruginosa* Lifestyle: A Paradigm for Adaptation, Survival, and Persistence. *Front Cell Infect Microbiol*, 2017. 7:39.
15. Wright, E.A., Fothergill, J.L., Paterson, S., Brockhurst, M.A. and Winstanley, C. Sub-inhibitory concentrations of some antibiotics can drive diversification of *Pseudomonas aeruginosa* populations in artificial sputum medium. *BMC Microbiol* 2013. 13:170
16. Lambert, P.A. Mechanisms of antibiotic resistance in *Pseudomonas aeruginosa*. *J R Soc Med.* 2002. 95 Suppl 41(Suppl 41):22-26..
17. Organisation, W.H. WHO publishes list of bacteria for which new antibiotics are urgently needed. 2017 [cited 2017 10/08/2017]; Available from: http://www.who.int/mediacentre/news/releases/2017/bacteria-antibiotics-needed/en/.
18. Santajit, S. and Indrawattana, N. Mechanisms of Antimicrobial Resistance in ESKAPE Pathogens. *Biomed Res Int*, 2016. 2061:2475067.

19. Jimenez, .PN., Koch, G., Thompson, J.A., Xavier, K.B., Cool, R.H. and Quax, W.J. The multiple signaling systems regulating virulence in *Pseudomonas aeruginosa*. *Microbiol Mol Biol Rev.* 201. 76(1):46-65.
20. Delcour, A.H. Outer membrane permeability and antibiotic resistance. *Biochim Biophys Acta.* 2009. 1794(5):808-816.
21. Nikaido, H. and Vaara, M. Molecular basis of bacterial outer membrane permeability. *Microbiol Rev.* 1985. 49(1):1-32.
22. Nikaido, H. Molecular basis of bacterial outer membrane permeability revisited. *Microbiol Mol Biol Rev*. 2003. 67(4):593-656.
23. Maldonado, R.F., Sa-Correia, I. and Valvano, M.A. Lipopolysaccharide modification in Gram-negative bacteria during chronic infection. *FEMS Microbiol Rev,* 2016. 40(4):480-93.
24. Bell, A., Bains, M. and Hancock, R.E. *Pseudomonas aeruginosa* outer membrane protein OprH: expression from the cloned gene and function in EDTA and gentamicin resistance. *J. Bacteriol*, 1991. 173(21): 6657-6664.
25. Lam, J.S., Taylor, V.L., Islam, S.T., Hao, Y. and Kocíncová, D. Genetic and Functional Diversity of *Pseudomonas aeruginosa* Lipopolysaccharide. *Front Microbiol*. 2011. 2:118.
26. Stefani, S., Campana, S., Cariani, L., Carnovale, V., Colombo, C., Lleo, M.M., Iula, V.D., Minicucci, L., Morelli, P., Pizzamiglio, G. and Taccetti, G. Relevance of multidrug-resistant *Pseudomonas aeruginosa* infections in cystic fibrosis. *Int J Med Microbiol*. 2017. 307(6):353-362.
27. Sugawara, E., Nestorovich, E.M., Bezrukov, S.M. and Nikaido, H. *Pseudomonas aeruginosa* porin OprF exists in two different conformations. *J Biol Chem*. 2006. 281(24):16220-9.
28. Hancock, R.E. and Speert, D.P. Antibiotic resistance in *Pseudomonas aeruginosa*: mechanisms and impact on treatment. *Drug Resist Updat*. 2000. 3(4):247-255.
29. El Solh, A.A. and Alhajhusain, A. Update on the treatment of *Pseudomonas aeruginosa* pneumonia. *J Antimicrob Chemother*. 2009. 64(2):229-38.
30. Wagner, S., Sommer, R., Hinsberger, S., Lu, C., Hartmann, R.W., Empting, M. and Titz, A. Novel Strategies for the Treatment of *Pseudomonas aeruginosa* Infections. *J Med Chem*. 2016. 59(13):5929-69.
31. National Institute for Health and Care Excellence. Cystic fibrosis: diagnosis and management [NICE Guideline NG78]. 2017. [cited 2017 10/08/2017]; Available from https://www.nice.org.uk/guidance/ng78
32. Kohanski, M.A., Dwyer, D.J. and Collins, J.J. How antibiotics kill bacteria: from targets to networks. *Nat Rev Microbiol*. 2010. 8(6):423-35.
33. Krause, K.M., Serio, A.W., Kane, T.R. and Connolly, L.E. Aminoglycosides: An Overview. *Cold Spring Harb Perspect Med*. 2016. 6(6):a027029
34. Vaara, M., Agents that increase the permeability of the outer membrane. *Microbiol Rev*, 1992. 56(3):395-411.
35. Poirel, L., Jayol, A. and Nordmann, P. Polymyxins: Antibacterial Activity, Susceptibility Testing, and Resistance Mechanisms Encoded by Plasmids or Chromosomes. *Clin Microbiol Rev.* 2017. 30(2):557-596.
36. Pang, Z., Raudonis, R., Glick, B.R., Lin ,T.J. and Cheng, Z. Antibiotic resistance in *Pseudomonas aeruginosa*: mechanisms and alternative therapeutic strategies. *Biotechnol Adv*. 2019. 37(1):177-192
37. Schweizer, H.P. Efflux as a mechanism of resistance to antimicrobials in *Pseudomonas aeruginosa* and related bacteria: unanswered questions. *Genet Mol Res.* 2003. 2(1): 48-62.
38. Czaplewski, L., Bax, R., Clokie, M., Dawson, M., Fairhead, H., Fischetti, V.A., Foster, S., Gilmore, B.F., Hancock, R.E., Harper, D., Henderson, I.R., Hilpert, K., Jones, B.V.,

Kadioglu, A., Knowles, D., Ólafsdóttir, S., Payne, D., Projan, S., Shaunak, S., Silverman, J., Thomas, C.M., Trust, T.J., Warn, P. and Rex, J.H. Alternatives to antibiotics-a pipeline portfolio review. *Lancet Infect Dis*. 2016. 16(2):239-51.

39. Hurley, M.N., Cámara, M. and Smyth, A.R. Novel approaches to the treatment of *Pseudomonas aeruginosa* infections in cystic fibrosis. *Eur Respir J.* 2012. 40(4):1014-23.
40. Taylor, P.K., Yeung, A.T. and Hancock, R.E. Antibiotic resistance in *Pseudomonas aeruginosa* biofilms: towards the development of novel anti-biofilm therapies. *J Biotechnol.* 2014. 191:121-30.
41. Furiga, A., Lajoie, B., El Hage, S., Baziard, G. and Roques, C. Impairment of *Pseudomonas aeruginosa* Biofilm Resistance to Antibiotics by Combining the Drugs with a New Quorum-Sensing Inhibitor*. Antimicrob Agents Chemother*. 2015. 60(3):1676-86.
42. Hraiech, S., Brégeon, F. and Rolain, J.M. Bacteriophage-based therapy in cystic fibrosis-associated *Pseudomonas aeruginosa* infections: rationale and current status. *Drug Des Devel Ther*. 2015. 9:3653-63.
43. Guo, M., Feng, C., Ren, J., Zhuang, X., Zhang, Y., Zhu, Y., Dong, K., He, P., Guo, X. and Qin, J. A Novel Antimicrobial Endolysin, LysPA26, against *Pseudomonas aeruginosa*. *Front Microbiol.* 2017. 8:293.
44. Johansen, H.K. and Gøtzsche, P.C. Vaccines for preventing infection with *Pseudomonas aeruginosa* in cystic fibrosis. *Cochrane Database Syst Rev*. 2015. 2015(8):CD001399
45. Priebe, G.P. and Goldberg, J.B. Vaccines for *Pseudomonas aeruginosa*: a long and winding road. *Expert Rev Vaccines*. 2014. 13(4):507-19.
46. Sharma, A., Krause, A. and Worgall, S. Recent developments for *Pseudomonas* vaccines. *Hum Vaccin*. 2011. 7(10):999-1011.
47. Woodford, N., Wareham and D.W.; UK Antibacterial Antisense Study Group. Tackling antibiotic resistance: a dose of common antisense? *J Antimicrob Chemother*. 2009. 63(2):225-9..
48. Dersch, P., Khan, M.A., Mühlen, S. and Görke, B. Roles of Regulatory RNAs for Antibiotic Resistance in Bacteria and Their Potential Value as Novel Drug Targets. *Front Microbiol*. 2017. 8:803.
49. Sully, E.K. and Geller, B.L. Antisense antimicrobial therapeutics. *Curr Opin Microbiol*. 2016. 33:47-55.
50. Good, L. and Nielsen, P.E. Antisense inhibition of gene expression in bacteria by PNA targeted to mRNA. *Nat Biotechnol*. 1998. 16(4):355-8.
51. Grainger, D.C. and Busby, S.J. Methods for studying global patterns of DNA binding by bacterial transcription factors and RNA polymerase. *Biochem Soc Trans*. 2008. 36(Pt 4):754-7
52. Mann, M.J. and Dzau, V.J. Therapeutic applications of transcription factor decoy oligonucleotides. *J Clin Invest*. 2000. 106(9):1071-5.
53. Marín-Menéndez, A., Montis, C., Díaz-Calvo, T., Carta, D., Hatzixanthis, K., Morris, C.J., McArthur, M. and Berti, D. Antimicrobial Nanoplexes meet Model Bacterial Membranes: the key role of Cardiolipin. *Sci Rep*. 2017. 7:41242.
54. McArthur, M. and Bibb, M.J. Manipulating and understanding antibiotic production in Streptomyces coelicolor A3(2) with decoy oligonucleotides. *Proc Natl Acad Sci U S A*. 2008. 105(3):1020-5.
55. Fraley, A.W., Pons, B., Dalkara, D., Nullans, G., Behr, J.P. and Zuber, G. Cationic oligonucleotide-peptide conjugates with aggregating properties enter efficiently into cells while maintaining hybridization properties and enzymatic recognition. *J Am Chem Soc.* 2006. 128(33):10763-71
56. Johnson, L., Mulcahy, H., Kanevets, U., Shi, Y. and Lewenza, S. Surface-localized spermidine protects the *Pseudomonas aeruginosa* outer membrane from antibiotic treatment and oxidative stress. *J Bacteriol.* 2012. 194(4):813-26.

57. Mamusa, M., Barbero, F., Montis, C., Cutillo, L., Gonzalez-Paredes, A. and Berti, D. Inclusion of oligonucleotide antimicrobials in biocompatible cationic liposomes: A structural study. *J Colloid Interface Sci*. 2017. 508:476-487.
58. Epand, R.M. and Epand, R.F. Lipid domains in bacterial membranes and the action of antimicrobial agents. *Biochim Biophys Acta*. 2009. 1788(1):289-94.
59. Montis, C., Joseph, P., Magnani, C., Marín-Menéndez, A.,, Barbero F., Estrada, A.R., Nepravishta, R., Angulo, J., Checcucci, A., Mengoni, A., Morris, C.J. and Berti, D. Multifunctional nanoassemblies target bacterial lipopolysaccharides for enhanced antimicrobial DNA delivery. *Colloids Surf B Biointerfaces*. 2020. 195:111266..
60. Di Blasio, S. Cationic Bolalipid Antimicrobrials: Mechanism of Action and SAR, in Institute of Pharmaceutical Science. 2018. PhD Thesis, King's Collage London.
61. Mamusa, M., Sitia, L., Barbero, F., Ruyra, A., Calvo, T.D., Montis, C., Gonzalez-Paredes, A., Wheeler, G.N., Morris, C.J., McArthur, M. and Berti, D. Cationic liposomal vectors incorporating a bolaamphiphile for oligonucleotide antimicrobials. *Biochim Biophys Acta Biomembr.* 2017. 1859(10):1767-1777
62. *Dynamic Light Scattering : An Introduction in 30 Minutes*. 2014. [cited 18/05/2021] Available from: https://www.research.colostate.edu/wp-content/uploads/2018/11/dls-30min-explanation.pdf
63. Clogston, J.D. and Patri, A.K. *Zeta Potential Measurement*, in *Characterization of Nanoparticles Intended for Drug Delivery*, S.E. McNeil, Editor. 2011, Humana Press: Totowa, NJ. p. 63-70.
64. *Zeta potential-An introduction in 30 minutes*. 2015 [cited 18/05/2021] Available from: https://www.research.colostate.edu/wp-content/uploads/2018/11/ZetaPotential-Introduction-in-30min-Malvern.pdf
65. Lowe, R., Shirley, N., Bleackley, M., Dolan, S. and Shafee, T. Transcriptomics technologies. *PLoS Comput Biol*. 2017. 13(5):e1005457.
66. Constantinidou, C., Hobman, J.L., Griffiths, L., Patel, M.D., Penn, C.W., Cole, J.A. and Overton, T.W. A reassessment of the FNR regulon and transcriptomic analysis of the effects of nitrate, nitrite, NarXL, and NarQP as *Escherichia coli* K12 adapts from aerobic to anaerobic growth*. J Biol Chem*. 2006. 281(8):4802-15.
67. Grainger, D.C., Aiba, H., Hurd, D., Browning, D.F. and Busby, S.J. Transcription factor distribution in *Escherichia coli*: studies with FNR protein. *Nucleic Acids Res*. 2007. 35(1):269-78.
68. Kuo, M.H. and Allis, C.D. In vivo cross-linking and immunoprecipitation for studying dynamic Protein:DNA associations in a chromatin environment. *Methods.* 1999. 19(3):425-33.
69. Orlando, V. Mapping chromosomal proteins in vivo by formaldehyde-crosslinked-chromatin immunoprecipitation. *Trends Biochem Sci.* 2000. 25(3):99-104.
70. Aslam, B., Basit, M., Nisar, M.A., Khurshid, M. and, Rasool, M.H. Proteomics: Technologies and Their Applications. *J Chromatogr Sci*. 2017. 55(2):182-196.
71. Graves, P.R. and Haystead, T.A. Molecular biologist's guide to proteomics. *Microbiol Mol Biol Rev.* 2002. 66(1):39-63;
72. Park, A.J., Krieger, J.R. and Khursigara C.M. Survival proteomes: the emerging proteotype of antimicrobial resistance. *FEMS Microbiol Rev*. 2016. 40(3):323-42.
73. Wu, X., Held, K., Zheng, C., Staudinger, B.J., Chavez, J.D., Weisbrod, C.R., Eng, J.K., Singh, P.K., Manoil, C. and Bruce, J.E. Dynamic Proteome Response of *Pseudomonas aeruginosa* to Tobramycin Antibiotic Treatment. *Mol Cell Proteomics*. 2015. 14(8):2126-37.
74. Hessling, B., Bonn, F., Otto, A., Herbst, F.A., Rappen, G.M., Bernhardt, J., Hecker, M. and Becher, D. Global proteome analysis of vancomycin stress in *Staphylococcus aureus*. *Int J Med Microbiol.* 2013. 303(8):624-34.

75. Pattrick, C.A., Webb, J.P., Green,. J, Chaudhuri, R.R., Collins, M.O. and Kelly, D.J. Proteomic Profiling, Transcription Factor Modeling, and Genomics of Evolved Tolerant Strains Elucidate Mechanisms of Vanillin Toxicity in *Escherichia coli*. *mSystems*. 2019. 4(4):e00163-19.
76. Simicevic, J. and Deplancke, B. Transcription factor proteomics-Tools, applications, and challenges. *Proteomics*. 2017. 17(3-4).
77. Han, X., Aslanian. A. and Yates, J.R. 3rd. Mass spectrometry for proteomics. *Curr Opin Chem Biol*. 2008. 12(5):483-90..
78. Zhu, W., Smith, J.W. and Huang, C.M. Mass spectrometry-based label-free quantitative proteomics. *J Biomed Biotechnol*. 2010. 2010:840518.
79. Schilling, B., Rardin, M.J., MacLean, B.X., Zawadzka,. AM.,, Frewen B.E., Cusack, M.P., Sorensen, D.J., Bereman, M.S., Jing, E., Wu, C.C., Verdin, E., Kahn, C.R., Maccoss, M.J. and Gibson, B.W. Platform-independent and label-free quantitation of proteomic data using MS1 extracted ion chromatograms in skyline: application to protein acetylation and phosphorylation. *Mol Cell Proteomics*. 2012. 11(5):202-14.
80. Hogrebe, A., von Stechow, L., Bekker-Jensen, D.B., Weinert, B.T., Kelstrup, C.D., Olsen, J.V. Benchmarking common quantification strategies for large-scale phosphoproteomics. *Nat Commun*. 2018. 9(1):1045.
81. Zhang, X., Yin, X., Yu, H., Liu, X., Yang, F., Yao, J., Jin, H. and Yang, P. Quantitative proteomic analysis of serum proteins in patients with Parkinson's disease using an isobaric tag for relative and absolute quantification labeling, two-dimensional liquid chromatography, and tandem mass spectrometry. *Analyst*. 2012. 137(2):490-5..
82. Rauniyar, N and Yates, J.R. 3rd. Isobaric labeling-based relative quantification in shotgun proteomics. *J Proteome Res*. 2014. 13(12):5293-309..
83. McAlister, G.C., Nusinow, D.P., Jedrychowski, M.P., Wühr, M., Huttlin, E.L., Erickson, B.K., Rad, R., Haas, W. and Gygi, S.P. MultiNotch MS3 enables accurate, sensitive, and multiplexed detection of differential expression across cancer cell line proteomes. *Anal Chem.* 2014. 86(14):7150-8.
84. Hare, N.J., Solis, N., Harmer, C., Marzook, N.B., Rose, B., Harbour, C., Crossett, B., Manos, J. and Cordwell, S.J. Proteomic profiling of *Pseudomonas aeruginosa* AES-1R, PAO1 and PA14 reveals potential virulence determinants associated with a transmissible cystic fibrosis-associated strain. *BMC Microbiol.* 2012 . 12:16.
85. Kukavica-Ibrulj, I., Bragonzi, A., Paroni, M., Winstanley, C., Sanschagrin, F., O'Toole, G.A. and Levesque, R.C. In vivo growth of *Pseudomonas aeruginosa* strains PAO1 and PA14 and the hypervirulent strain LESB58 in a rat model of chronic lung infection. *J Bacteriol.* 2008. 190(8):2804-13.
86. Wiegand, I., Hilpert, K. and Hancock, R.E. Agar and broth dilution methods to determine the minimal inhibitory concentration (MIC) of antimicrobial substances. *Nat Protoc*. 2008. 3(2):163-75.
87. Khan, I., K. Saeed, and I. Khan, Nanoparticles: Properties, applications and toxicities. *Arab. J. Chem.* 2019. 12(7): 908-931.
88. Srinivas, P.R., *Introduction to Protein Electrophoresis*, in *Protein Electrophoresis: Methods and Protocols*, B.T. Kurien and R.H. Scofield, Editors. 2012, Humana Press: Totowa, NJ. p. 23-28.
89. Consortium, U. UniProt: a worldwide hub of protein knowledge. *Nucleic Acids Res*, 2019. 47(D1):D506-D515.
90. Tusher, V.G., Tibshirani, R. and Chu, G. Significance analysis of microarrays applied to the ionizing radiation response. *Proc Natl Acad Sci U S A*. 2001. 98(9):5116-21.
91. Giai Gianetto, Q., Couté, Y., Bruley, C. and Burger, T. Uses and misuses of the fudge factor in quantitative discovery proteomics. *Proteomics.* 2016. 16(14):1955-60.

92. Team, R.C. *R: A language and environment for statistical computing. R Foundation for Statistical Computing, Vienna, Austria.* 2021.
93. Garza de Leon, F., Sellars, L., Stracy, M., Busby, S.J.W. and Kapanidis, A.N. Tracking Low-Copy Transcription Factors in Living Bacteria: The Case of the lac Repressor. *Biophys J*. 2017. 112(7):1316-1327.
94. Schmidt, A., Kochanowski, K., Vedelaar, S., Ahrné, E., Volkmer, B., Callipo, L., Knoops, K, Bauer, M., Aebersold, R, and Heinemann, M. The quantitative and condition-dependent *Escherichia coli* proteome. *Nat Biotechnol*. 2016. 34(1):104-10.
95. Santos-Zavaleta, A., Salgado, H., Gama-Castro, S., Sánchez-Pérez, M., Gómez-Romero, L., Ledezma-Tejeida, D, García-Sotelo, J.S., Alquicira-Hernández, K., Muñiz-Rascado, L.J., Peña-Loredo, P., Ishida-Gutiérrez, C, Velázquez-Ramírez, D.A., Del Moral-Chávez, V., -Martínez, C.D., Méndez-Cruz, C.F.,Galagan, J. and Collado-Vides, J. RegulonDB v 10.5: tackling challenges to unify classic and high throughput knowledge of gene regulation in *E. coli* K-12. *Nucleic Acids Res*. 2019. 47(D1):D212-D220.
96. Fic, E., Kedracka-Krok, S., Jankowska, U., Pirog, A. and Dziedzicka-Wasylewska, M. Comparison of protein precipitation methods for various rat brain structures prior to proteomic analysis. *Electrophoresis*. 2010. 31(21):3573-9.
97. Cox, J., Hein, M.Y., Luber, C.A., Paron, I., Nagaraj, N. and Mann, M. Accurate proteome-wide label-free quantification by delayed normalization and maximal peptide ratio extraction, termed MaxLFQ. *Mol Cell Proteomics*. 2014. 13(9):2513-26.
98. Tyanova, S., Temu, T. and Cox J. The MaxQuant computational platform for mass spectrometry-based shotgun proteomics. *Nat Protoc*. 2016. 11(12):2301-2319..
99. Tyanova, S., Temu, T., Sinitcyn, P., Carlson, A., Hein, M.Y., Geiger,. T, Mann, M. and Cox, J. The Perseus computational platform for comprehensive analysis of (prote)omics data. *Nat Methods*. 2016. 13(9):731-40.
100. Mendling, W., Weissenbacher, E.R., Gerber, S., Prasauskas, V. and Grob, P. Use of locally delivered dequalinium chloride in the treatment of vaginal infections: a review. *Arch Gynecol Obstet.* 2016. 293(3):469-84.
101. Bock, L.J., Hind, C.K., Sutton, J.M. and Wand, M.E. Growth media and assay plate material can impact on the effectiveness of cationic biocides and antibiotics against different bacterial species. *Lett Appl Microbiol*. 2018. 66(5):368-377.
102. Feist, P. and Hummon, A.B. Proteomic challenges: sample preparation techniques for microgram-quantity protein analysis from biological samples. *Int J Mol Sci*. 2015. 16(2):3537-63.
103. Karp, P.D., Billington, R., Caspi, R.,, Fulcher C.A., Latendresse, M., Kothari, A., Keseler, I.M., Krummenacker, M., Midford, P.E., Ong, Q., Ong, W.K., Paley, S.M. and Subhraveti, P. The BioCyc collection of microbial genomes and metabolic pathways. *Brief Bioinform*. 2019. 20(4):1085-1093.
104. Mahler, H.C., Huber, F., Kishore, R.S., Reindl, J., Rückert, P. and Müller, R. Adsorption behavior of a surfactant and a monoclonal antibody to sterilizing-grade filters. *J Pharm Sci.* 2010. 99(6):2620-7.
105. Van den Oetelaar, P.J.M., Mentink, I.M. and Brinks, G.J. Loss of Peptides and Proteins Upon Sterile Filtration Due to Adsorption to Membrane Filters. *Drug Dev Ind Pharm.* 1989. 15(1):97-106.
106. Lichtenberg, J.Y., Ling, Y. and Kim, S. Non-Specific Adsorption Reduction Methods in Biosensing. *Sensors (Basel*), 2019. 19(11):2488.
107. Rardin, M.J. Rapid Assessment of Contaminants and Interferences in Mass Spectrometry Data Using Skyline. *J Am Soc Mass Spectrom*. 2018. 29(6):1327-1330.
108. Mendes, M.A., Chies, J.M., de Oliveira Dias, A.C., Filho, S.A. and Palma, M.S. The shielding effect of glycerol against protein ionization in electrospray mass spectrometry. *Rapid Commun Mass Spectrom*. 2003. 17(7):672-7.

109. Balderas-Martínez, Y.I., Savageau, M., Salgado, H., Pérez-Rueda, E., Morett, E. and Collado-Vides, J. Transcription factors in *Escherichia coli* prefer the holo conformation. *PLoS One*. 2013. 12;8(6):e65723
110. Betancourt, L.H., Sanchez, A., Pla, I., Kuras, M., Zhou, Q., Andersson, R. and Marko-Varga, G. Quantitative Assessment of Urea In-Solution Lys-C/Trypsin Digestions Reveals Superior Performance at Room Temperature over Traditional Proteolysis at 37 °C. *J Proteome Res.* 2018. 17(7):2556-2561.
111. Johnson, M. Protein Quantitation. *Mater Methods.* 2012. 2:115.
112. Szklarczyk, D., Gable, A.L., Lyon, D., Junge, A., Wyde,r S., Huerta-Cepas, J., Simonovic, M., Doncheva, N.T., Morris, J.H., Bork, P., Jensen, L.J. and von Mering, C. STRING v11: protein-protein association networks with increased coverage, supporting functional discovery in genome-wide experimental datasets*. Nucleic Acids Res*, 2019. 47(D1): p. D607-D613.
113. Bittner, L.M., Arends, J. and Narberhaus, F. When, how and why? Regulated proteolysis by the essential FtsH protease in *Escherichia coli*. *Biol Chem*. 2017. 398(5-6):625-635.
114. Katz, C. and Ron, E.Z. Dual role of FtsH in regulating lipopolysaccharide biosynthesis in Escherichia coli. *J Bacteriol.* 2008. 190(21):7117-22.
115. Poole, K. Stress responses as determinants of antimicrobial resistance in Gram-negative bacteria. *Trends Microbiol*, 2012. 20(5):227-34.
116. Shimohata, N., Chiba, S., Saikawa, N., Ito, K. and Akiyama, Y. The Cpx stress response system of *Escherichia coli* senses plasma membrane proteins and controls HtpX, a membrane protease with a cytosolic active site. *Genes Cells*. 2002. 7(7):653-62.
117. Akiyama, Y. Proton-motive force stimulates the proteolytic activity of FtsH, a membrane-bound ATP-dependent protease in *Escherichia coli*. *Proc Natl Acad Sci U S A*. 2002. 99(12):8066-71.
118. Brown, D.R., Barton, G., Pan, Z., Buck, M. and Wigneshweraraj, S. Nitrogen stress response and stringent response are coupled in *Escherichia coli*. *Nat Commun.* 2014. 5:4115.
119. Brown, D.R. Nitrogen Starvation Induces Persister Cell Formation in *Escherichia coli. J Bacteriol*. 2019. 201(3).
120. Stewart, V. Biochemical Society Special Lecture. Nitrate- and nitrite-responsive sensors NarX and NarQ of proteobacteria*. Biochem Soc Trans*, 2003. 31(Pt 1):1-10.
121. Darwin, A.J., Ziegelhoffer, E.C., Kiley, P.J. and Stewart, V. Fnr, NarP, and NarL regulation of *Escherichia coli* K-12 napF (periplasmic nitrate reductase) operon transcription in vitro. *J Bacteriol*. 1998. 180(16):4192-8.
122. Rappsilber, J., Mann, M. and Ishihama, Y. Protocol for micro-purification, enrichment, pre-fractionation and storage of peptides for proteomics using StageTips. *Nat Protoc*. 2007. 2(8):1896-906.
123. Bizzotto, J., Vickers, S.L., Paez, A., Scorticati, C., Cotignola, J., Valacco, P., Mazza, O., Vazquesz, E. and Gueron, G., Mass spectrometry-based proteomics study makes apolipoprotein E a potential risk factor for prostate cancer*. Cancer Res*. 2018. 78(16):58-59.
124. Matallana-Surget, S., Leroy, B., Wattiez, R. Shotgun proteomics: concept, key points and data mining. *Expert Rev Proteomics*. 2010. 7(1):5-7.
125. Zhang, Y., Fonslow, B.R., Shan, B., Baek, M.C. and Yates, J.R. 3rd. Protein analysis by shotgun/bottom-up proteomics. *Chem Rev*. 2013. 113(4):2343-94.
126. de la Franch, C., Di Blasio, S., Lawrence, L., Mason, J. Morris, C. and McArthur, M. 2017 *Rational identification and validation of a novel Escherichia coli antimicrobial target*. [Unpublished Manuscript]. Procarta Biosystems Ltd, University of East Anglia
127. Schaffer, L.V., Millikin, R.J., Miller, R.M., Anderson, L.C., Fellers, R.T., Ge, Y., Kelleher, N.L., LeDuc, R.D., Liu, X., Payne, S.H., Sun, L., Thomas, P.M., Tucholski, T., Wang, Z., Wu,

S., Wu, Z., Yu, D., Shortreed, M.R. and Smith, L.M. Identification and Quantification of Proteoforms by Mass Spectrometry. *Proteomics*. 2019. 19(10):e1800361.
128. O'Connell, J.D., Paulo, J.A., O'Brien, J.J. and Gygi, S.P. Proteome-Wide Evaluation of Two Common Protein Quantification Methods. *J Proteome Res*. 2018. 17(5):1934-1942.
129. Winsor, G.L., Griffiths, E.J., Lo, R., Dhillon, B.K., Shay, J.A. and Brinkman, F.S. Enhanced annotations and features for comparing thousands of Pseudomonas genomes in the *Pseudomonas* genome database. *Nucleic Acids Res*. 2016. 44(D1):D646-53.
130. Kanehisa, M., Goto, S., Furumichi, M., Tanabe, M. and Hirakawa, M. KEGG for representation and analysis of molecular networks involving diseases and drugs. *Nucleic Acids Res.* 2010. 38(Database issue):D355-60.
131. Medeiros Filho, F., do Nascimento A.P.B., Dos Santos, M.T., Carvalho-Assef, A.P.D. and da Silva, F.A.B. Gene regulatory network inference and analysis of multidrug-resistant *Pseudomonas aeruginosa*. *Mem Inst Oswaldo Cruz.* 2019. 114:e190105..
132. Gibson, B.,, Wilson D.J., Feil, E. and Eyre-Walker, A. The distribution of bacterial doubling times in the wild. *Proc Biol Sci*. 2018. 285(1880):20180789.
133. Gonzalez-Galarza, F.F., Lawless, C., Hubbard, S.J., Fan, J., Bessant, C., Hermjakob, H. and Jones, A.R. A critical appraisal of techniques, software packages, and standards for quantitative proteomic analysis. *OMICS*. 2012. 16(9):431-42.
134. Välikangas, T., Suomi, T. and Elo, L.L. A comprehensive evaluation of popular proteomics software workflows for label-free proteome quantification and imputation. *Brief Bioinform*. 2018. 19(6):1344-1355.
135. Bruchmann, S., Dötsch, A., Nouri, B., Chaberny, I.F. and Häussler, S. Quantitative contributions of target alteration and decreased drug accumulation to *Pseudomonas aeruginosa* fluoroquinolone resistance. *Antimicrob Agents Chemother*. 2013. 57(3):1361-8.
136. Laborda, P., Alcalde-Rico, M., Blanco, P., Martínez, J.L., Hernando-Amado, S.. Novel Inducers of the Expression of Multidrug Efflux Pumps That Trigger *Pseudomonas aeruginosa* Transient Antibiotic Resistance. *Antimicrob Agents Chemother*. 2019. 63(11):e01095-19.
137. Laborda, P., Alcalde-Rico, M., Chini, A., Martínez, J.L. and Hernando-Amado, S. Discovery of inhibitors of *Pseudomonas aeruginosa* virulence through the search for natural-like compounds with a dual role as inducers and substrates of efflux pumps. *Environ Microbiol.* 2021. 23(12):7396-7411.
138. Masuda, N., Sakagawa, E., Ohya, S., Gotoh, N., Tsujimoto, H. and Nishino, T. Substrate specificities of MexAB-OprM, MexCD-OprJ, and MexXY-oprM efflux pumps in *Pseudomonas aeruginosa. Antimicrob Agents Chemother*. 2000. 44(12):3322-7
139. Purssell, A. and Poole, K. Functional characterization of the NfxB repressor of the mexCD-oprJ multidrug efflux operon of *Pseudomonas aeruginosa. Microbiology*. 2013. 159(Pt 10):2058-73.
140. Masuda, N., Sakagawa, E., Ohya, S., Gotoh, N., Tsujimoto, H. and Nishino, T. Contribution of the MexX-MexY-oprM efflux system to intrinsic resistance in *Pseudomonas aeruginosa. Antimicrob Agents Chemother.* 2000. 44(9):2242-6
141. Hill, I.T., Tallo, T., Dorman, M.J. and Dove, S.L. Loss of RNA Chaperone Hfq Unveils a Toxic Pathway in *Pseudomonas aeruginosa. J Bacteriol.* 2019. 201(20):e00232-19.
142. Wang, G., Huang, X., Li, S., Huang, J., Wei, X., Li, Y. and Xu, Y. The RNA chaperone Hfq regulates antibiotic biosynthesis in the rhizobacterium *Pseudomonas aeruginosa* M18. *J Bacteriol*. 2012. 194(10):2443-57.
143. Basta, D.W., Angeles-Albores, D., Spero, M.A., Ciemniecki, J.A. and Newman, D.K. Heat-shock proteases promote survival of *Pseudomonas aeruginosa* during growth arrest. *Proc Natl Acad Sci U S A*. 2020. 117(8):4358-4367.

144. Krajewski, S.S., Nagel, M. and Narberhaus, F. Short ROSE-like RNA thermometers control IbpA synthesis in *Pseudomonas species*. *PLoS One*. 2013. 8(5):e65168.
145. Llamas, M.A., Imperi, F., Visca, P. and Lamont, I.L. Cell-surface signaling in *Pseudomonas:* stress responses, iron transport, and pathogenicity. *FEMS Microbiol Rev*. 2014. 38(4):569-97.
146. Firoved, A.M. and Deretic, V. Microarray analysis of global gene expression in mucoid *Pseudomonas aeruginosa. J Bacteriol*. 2003. 185(3):1071-81.
147. Shiba, T., Ishiguro, K., Takemoto, N., Koibuchi, H. and Sugimoto, K. Purification and characterization of the *Pseudomonas aeruginosa* NfxB protein, the negative regulator of the *nfxB* gene. *J Bacteriol*. 1995. 177(20):5872-7.
148. Monti, M.R., Morero, N.R., Miguel, V., Argaraña, C.E.. nfxB as a novel target for analysis of mutation spectra in *Pseudomonas aeruginosa*. *PLoS One.* 2013. 8(6):e66236.
149. Chemotherapy, B.S.f.A. *BSAC to actively support the EUCAST Disc Diffusion Method for Antimicrobial Susceptibility Testing in preference to the current BSAC Disc Diffusion Method v 14*. [cited 2017 20/11/17]; Available from: http://bsac.org.uk/wp-content/uploads/2012/02/BSAC-Susceptibility-testing-version-14.pdf.
150. Mulet, X., Moyá, B., Juan, C., Macià, M.D., Pérez, J.L., Blázquez, J. and Oliver, A. Antagonistic interactions of *Pseudomonas aeruginosa* antibiotic resistance mechanisms in planktonic but not biofilm growth. *Antimicrob Agents Chemother*. 2011. 55(10):4560-8
151. Pryor, E.E. Jr, Waligora, E.A., Xu, B., Dellos-Nolan, S., Wozniak, D.J. and Hollis, T. The transcription factor AmrZ utilizes multiple DNA binding modes to recognize activator and repressor sequences of *Pseudomonas aeruginosa* virulence genes. *PLoS Pathog*. 2012. 8(4):e1002648.
152. Xu, B., Soukup, R.J., Jones, C.J., Fishel, R. and Wozniak, D.J. *Pseudomonas aeruginosa* AmrZ Binds to Four Sites in the algD Promoter, Inducing DNA-AmrZ Complex Formation and Transcriptional Activation. *J Bacteriol.* 2016. 198(19):2673-81
153. Jones, C.J., Ryder, C.R., Mann, E.E. and Wozniak, D.J. AmrZ modulates *Pseudomonas aeruginosa* biofilm architecture by directly repressing transcription of the psl operon. *J Bacteriol.* 2013. 195(8):1637-44.
154. Hou, L., Debru, A., Chen, Q., Bao, Q. and Li, K. AmrZ Regulates Swarming Motility Through Cyclic di-GMP-Dependent Motility Inhibition and Controlling Pel Polysaccharide Production *in Pseudomonas aeruginosa* PA14*. Front Microbiol*. 2019. 10:1847.
155. Tart, A.H., Blanks, M.J. and Wozniak, D.J. The AlgT-dependent transcriptional regulator AmrZ (AlgZ) inhibits flagellum biosynthesis in mucoid, nonmotile *Pseudomonas aeruginosa* cystic fibrosis isolates. *J Bacteriol.* 2006. 188(18):6483-9.
156. Adair, L., Borges, B.C., Govindarajan, S., Solvik, T., Escalante, V. and Bondy-Denomy, J. CRISPR-Cas immunity repressed by a biofilm-activating pathway in *Pseudomonas aeruginosa. bioRxiv*, 2019. 673095
157. Chambers, J.R., Liao, J., Schurr, M.J. and Sauer, K. BrlR from *Pseudomonas aeruginosa* is a c-di-GMP-responsive transcription factor. *Mol Microbiol*. 2014. 92(3):471-87.
158. Liao, J.L. and Sauer, K. The MerR-Like Transcriptional Regulator BrlR Contributes to *Pseudomonas aeruginosa* Biofilm Tolerance*. J. Bacteriol*, 2012. 194(18): 4823-36.
159. Wang, F., He, Q., Yin, J., Xu, S., Hu, W, and Gu, L. BrlR from *Pseudomonas aeruginosa* is a receptor for both cyclic di-GMP and pyocyanin. *Nat Commun*. 2018 . 9(1):2563.
160. Liao, J., M.J. Schurr, and K. Sauer, *The MerR-like regulator BrlR confers biofilm tolerance by activating multidrug efflux pumps in Pseudomonas aeruginosa biofilms.* J Bacteriol, 2013. **195**(15): p. 3352-63.
161. Poudyal, B. and Sauer, K. The ABC of Biofilm Drug Tolerance: the MerR-Like Regulator BrlR Is an Activator of ABC Transport Systems, with PA1874-77 Contributing to the

Tolerance of *Pseudomonas aeruginosa* Biofilms to Tobramycin. *Antimicrob Agents Chemother*. 2018. 62(2):e01981-17

162. Southey-Pillig, C.J., Davies, D.G.and Sauer, K. Characterization of temporal protein production in *Pseudomonas aeruginosa* biofilms. *J Bacteriol.* 2005. 187(23):8114-26.
163. Stewart, P.S., Franklin, M.J., Williamson, K.S., Folsom, J.P., Boegli, L. and James. G.A. Contribution of stress responses to antibiotic tolerance in *Pseudomonas aeruginosa* biofilms. *Antimicrob Agents Chemother*. 2015. 59(7):3838-47
164. Chambers, J.R. and Sauer, K. The MerR-Like Regulator BrlR Impairs *Pseudomonas aeruginosa* Biofilm Tolerance to Colistin by Repressing PhoPQ. *J Bacteriol*. 2013. 195(20):4678-88.
165. Souissi, I., Ladam, P., Cognet, J.A., Le Coquil, S., Varin-Blank, N., Baran-Marszak, F., Metelev, V. and Fagard, R. A STAT3-inhibitory hairpin decoy oligodeoxynucleotide discriminates between STAT1 and STAT3 and induces death in a human colon carcinoma cell line. *Mol Cancer.* 2012. 16;11:12.
166. Ye, J., Coulouris, G., Zaretskaya, I., Cutcutache, I., Rozen, S. and Madden, T.L. Primer-BLAST: a tool to design target-specific primers for polymerase chain reaction. *BMC Bioinform*. 2012. 18;13:134..
167. Riss, T.L., Moravec, R.A., Niles, A.L., Duellman, S., Benink, H.A., Worzella, T.J. and Minor, L. *Cell Viability Assays.*, in *Assay Guidance Manual [Internet]*. 2013 [Updated 2016], Eli Lilly & Company and the National Center for Advancing Translational Sciences.
168. Mamusa, M., Resta, C., Barbero, F., Carta, D., Codoni, D., Hatzixanthis, K., McArthur, M., and Berti, D. Interaction between a cationic bolaamphiphile and DNA: The route towards nanovectors for oligonucleotide antimicrobials. *Colloids Surf B Biointerfaces*. 2016. 1;143:139-147..
169. Hibbitts, A., Lucía, A., Serrano-Sevilla, I., De Matteis, L., McArthur, M., de la Fuente. J.M., Aínsa, J.A. and Navarro, F. Co-delivery of free vancomycin and transcription factor decoy-nanostructured lipid carriers can enhance inhibition of methicillin resistant *Staphylococcus aureus* (MRSA). *PLoS One.* 2019. 14(9):e0220684.
170. Shi, J., Zhao, D., Li, X., Ding, F., Tang, X., Liu, N., Huang, H. and Liu, C. The conjugation of rhodamine B enables carrier-free mitochondrial delivery of functional proteins. *Org Biomol Chem.* 2020. 18(35):6829-39.
171. Hodge, K., Have, S.T., Hutton, L., and Lamond, A.I. Cleaning up the masses: exclusion lists to reduce contamination with HPLC-MS/MS. *J Proteomics*. 2013. 88:92-103

Appendix

R Scripts Used in this Thesis

File paths have been edited in the scripts presented below for ease of reading. Programmer's comments present in the code are indicated by #.

Example of R Script Used for Transcription Factor Extraction from Proteomic Output

```
install.packages("Hmisc")
install.packages("gdata")
library(Hmisc)# Import the library

##need local files to import into R, does not seem to work from onedrive

dat<-read.csv("maxquant protein hits.csv")# Import maxquant output fractionated

#dat$Gene.names<-capitalize(as.character(dat$Gene.names)) use this if need to capitalize

length(unique(dat$Protein.names))

getwd()

tf_list<-read.csv("transcription factor gene list.csv")# Import tfd list
str(tf_list)
gene<-tf_list$Gene#creating the list of gene names to use in the comparison
levels(gene)
head(dat)

##tfd list for fractionated

gene  %in% dat$Gene.names #tells you if the gene is there or not in maxquant output as a true false
```

reg_pres<-gene[gene %in% dat$Gene.names]#tell you the transcription factors that are there or not in the maxquant output as saves it into reg_pres

table(reg_pres)#outputs reg_pres as a table into the console

write.csv(reg_pres,'tf hits.csv', col.names ='Gene')

#writes reg_pres into a csv file in project directory-gives the tf hits

##csv files needs to be closed will overwrite what is already written so be careful here!!!!!!!!!!

dat2<-read.csv("documents_name.csv") ##csv files are preferred as less likely to be corrupted

length(unique(dat$Protein.IDs)) #double check right amount of rows imported, checks if imported correctly

syn1=tf_list$synonym.1#to create var to do synonyms search with

gene_pres2=syn1[syn1 %in% dat$Gene.names]#assigns synonym search result to variable

table(gene_pres2)#outputs synonym search as a table

write.csv(gene_pres2,'tf difference.csv')#writes synonym search to a file

syn2=tf_list$synonym.2#creats var to do synonym search for the next set of synonyms, there are 9 columns in total, just change the number each time, most will be in syn1 unlikely to get hits in the other columns

###NB alsB is a synonym for lrp but is also the uniprot preferred name for another E. coli gene that is unrelated-yes stupidly confusing

gene_pres3=syn2[syn2 %in% dat$Gene.names]#asgins synonym hits to the variable

table(gene_pres3)#displasys the results in the console

write.csv(gene_pres3,'tf difference.csv')#writes results to a file--remember this overwrites whatever was previously outputted

gene %in% dat2$Gene.names##transcription factors in oxford output as true and false values outputs directly to console

gene_pres=gene[gene %in% dat2$Gene.names]#saves list of transcription factors into gene_pres variable as the gene names

table(gene_pres)#tabulates and outputs gene_pres into the console

write.csv(gene_pres,'tf hits oxford.csv')##writes gene_pres into a cvs file called tf hits oxford search in the working directory

reg_pres %in% gene_pres#what is in my maxquant search AND the oxford maxquant search

gene_pres %in% reg_pres#what is in the oxofrd maxquant search that is in my maxquant search, should give same output

compar=reg_pres[reg_pres %in% gene_pres]#asigns what TFs are in both searches to this variable using the variables

comparneg=reg_pres[!reg_pres %in% gene_pres]#asigns what TFs are NOT in the oxford search but are in my search to this varibale using the variable

inoxinmine=gene_pres[gene_pres %in% reg_pres]#asigns what TFS are in oxfords output and also mine using the variables

inoxnotmine=gene_pres[!gene_pres %in% reg_pres]###asigns the TFs that are in oxford's output but NOT MINE using the variables #####

table(compar)#outputs table of this var into console

table(comparneg)#outputs table of this var into console

table (inoxinmine)#outputs table of this var into console

write.csv(compar,'tf differences.csv', append=TRUE, sep = t)#outputs this var into csv file

write.csv(comparneg,'tf differences.csv', append = TRUE)#outputs this var into csv file==NOTE OVERWRITES WHAT WAS THERE FROM PREVISOUS LINE OF CODE

##how to append still working out

write.csv(inoxinmine,'tf difference.csv')#outputs this var into csv file

write.csv(inoxnotmine,'tf difference.csv')#outputs this var into csv file==NOTE OVERWRITES WHAT WAS THERE FROM PREVISOUS LINE OF CODE

##how to append still working out

###as there are synonyms to take into account, have manually combined the outputs and for both my results TF search and oxford's results TF search in a csv file, given the synonyms the preferred name therefore use this better way to compare, assign the two csv files with the preferred gene name to a var and uses these to compare

```
tfhits=read.csv('tf hits.csv')
tfhitsg=tfhits$gene.name
length(tfhitsg)

####################################
#output lfq results for tf hits
################################

tfhits=read.csv('tf hits mine.csv')##import tf hit list
tfhitsg=tfhits$gene.name#assign this var the gene names as a list
length(tfhitsg)#check number of entries is correct
lfq0v1=read.csv('maxquant lfq 0v1xmic.csv')#import lfq results for 0 v 0.1 xmic lfq results
length(unique(lfq0v1$Gene.names))#check number of entries is correct
head(lfq0v1)#check correct data set


lfq0v1=read.csv('maxquant lfq 0v1xmic.csv')#import lfq results for 0 v 0.1 x mic lfq results
length(unique(lfq0v1$Gene.names))#check number of entries is correct
head(lfq0v1)#check correct data set

##alt to dplyr which currently not working

subset(lfq0v1, Gene.names %in% tfhitsg)
hits=subset(lfq0v1, Gene.names %in% tfhitsg)
```

R Script Used for Transcription Factor Comparison in *E. coli* Proteomic Analysis

```
install.packages("Hmisc")

install.packages("gdata")

library(Hmisc)# Import the library


##for comparison of tf hits between submissions


#first import all the tf hit lists using my maxquant runs


tf1=read.csv("document_name.csv")#import tf hit list data set #1


tf2=read.csv("document_name.csv")#import tf hit list data set #2


tf3=read.csv("document_name.csv")#import tf hit list data set #3


tffull=read.csv("document_name.csv")#import tf hit list full proteome data set tpl


################

##set1vset2

################



in1and2=intersect(tf1$gene.name, tf2$x)


write.csv(in1and2, "tf1v2.csv")


in1not2=subset(tf1, !(gene.name %in% tf3$x))##what is in tf1 and not set 2 and extracts all the set 1 data that is not common


write.csv(in1not2, "tf1not2.csv")
```

```
in2not1=subset(tf2, !(x %in% tf1$gene.name))##what is in tf2 and not set 1 and extracts all the set 3 data that is not common


write.csv(in2not1, "tf3not1.csv")


################

##set1vset3

################



in1and3=intersect(tf1$gene.name, tf3$x)


write.csv(in1and3, "tf1v3.csv")


in1not3=subset(tf1, !(gene.name %in% tf3$x))##what is in tf1 and not set 3 and extracts all the set 1 data that is not common


write.csv(in1not4, "tf1not3.csv")


in3not1=subset(tf3, !(x %in% tf1$gene.name))##what is in tf3 and not set 1 and extracts all the set 3 data that is not common


write.csv(in3not1, "tf3not1.csv")


################

##set1vTPL

################



in1andf=intersect(tf1$gene.name, tffull$x)


write.csv(in1andf, "tf1vfull.csv")
```

```
in1notf=subset(tf1, !(gene.name %in% tffull$x))##what is in tf1 and not set full and extracts all the set 1 data that is not common


write.csv(in1notf, "tf1notfull.csv")


infnot1=subset(tffull, !(x %in% tf1$gene.name))##what is in tffull and not set 1 and extracts all the set full data that is not common


write.csv(infnot1, "tffullnot1.csv")

################

##set2vset3

################



In2and3=intersect(tf2$x, tf3$x)


write.csv(in3and5, "tf3v5.csv")


in3not2=subset(tf3, !(x%in% tf2$x))##what is in tf2 and not set 3 frac and extracts all the set 3 data that is not common


write.csv(in3not5, "tf3not5.csv")


in3not2=subset(tf3, !(x %in% tf2$x))##what is in tf5frac and not set 1 and extracts all the set 3 data that is not common


write.csv(in3not2, "tf2not3.csv")


################

##set2vsTPL

################
```

```
In2andf=intersect(tf2$x, tffull$x)

write.csv(in2andf, "tf3vfull.csv")

in2notf=subset(tf2, !(x%in% tffull$x))##what is in tf2 and not full and extracts all the set 2 data that is not common

write.csv(in3not5f, "tf3notfull.csv")

in2not3f=subset(tffull, !(x %in% tf3$x))##what is in tffull and not set 2 and extracts all the set full data that is not common

write.csv(in2not3f, "tf2not3full.csv")

################

##set3vsTPL

################



In3andf=intersect(tf3$x, tffull$x)

write.csv(in3andf, "tf3vfull.csv")

in3notf=subset(tf3, !(x%in% tffull$x))##what is in tf3 and not full and extracts all the set 2 data that is not common

write.csv(in2notf, "tf3notfull.csv")

in3notf=subset(tffull, !(x %in% tf3$x))##what is in tffull and not set 3 and extracts all the full data that is not common
```

```
write.csv(in3notf, "tfnot3full.csv")
```